Stockholm University

Topology in One-Dimensional Quantum Systems

Licentiate Thesis in Theoretical Physics

Christian Spånslätt

Akademisk avhandling för avläggande av licentiatexamen vid Stockholms universitet, Fysikum

June 2015

Abstract

States of matter which are described by concepts in topology are of great interest in the community of condensed matter physics. Both from a pure theoretical perspective, where many non-intuitive and mathematically rich results can be found from seemingly simple models, and also since recent experimental developments allows for explicit construction of devices where the underlying topology has observable consequences.

This thesis provides a conceptual introduction to the framework describing such topological states of matter (TSM). It starts by explaining ordinary band theory which is followed by a discussion of quantum mechanical symmetries. These two concepts provides a method of classifying all non-interacting fermionic TSM. Following are explicit applications to a few models in one spatial dimension.

In the accompanying paper, we study one-dimensional superconductors with Josephson-junctions allowing phase shifts of π. We make a detailed analysis of the junction bound states and their properties in some different settings and compare the behaviour of trivial and topological superconducting junctions. In addition, we provide a phenomenological topological field theory in the low energy limit.

Sammanfattning

De senaste åren har forskning rörande så kallad topologisk materia utgjort en huvudfåra inom teoretisk kondenserad materiefysik. Detta beror inte bara på en mycket rik och intressant matematisk struktur, utan också på en enorm utveckling inom den experimentella nanofysiken, vilken möjliggjort en intressant plattform för utveckling av nya konstruerade kvantmekaniska system och material.

I denna avhandling ges en introduktion till det vedertagna ramverket för att teoretiskt beskriva system med en sådan topologisk struktur. Därpå följer tillämpningar av detta ramverk på ett fåtal system i en rumsdimension.

I den medföljande artikeln behandlas en-dimensionella supraledare i fasvridna Josephson-övergångar. De topologiska egenskaperna hos supraledarna visas inverka på beteendet hos bundna tillstånd i sådana övergångar och vi visar även hur skillnader i detta beteende kan användas för att detektera topologisk supraledning.

Acknowledgements

It is my pleasure to thank those who have made this thesis possible. Foremost, I want to thank my supervisor Eddy Ardonne for his knowledge, friendlyness, open-door policy and encouragement. I also want to thank my co-supervisor Thors Hans Hansson for being engaged in my projects, sharing his wisdom and having an additional watching eye over me.

Besides my supervisors, I am also very thankful to Jan Carl Budich for helping me as a newcomer in this field by answering tons of questions and for guidance and advice.

My mentor Fawad Hassan also deserves a warm thank you for support and encouragement.

I also want to express my gratitude to people in the Lund physics department; Hongqi Xu, Martin Leijnse, Chunlin Yu and Simon Abay Gebrehiwot for hosting such a nice research stay for me.

My sincere thanks goes also to additional members of the (extended) Quantum matter group: Babak, Micke, Thomas, Fernanda, Emma & Emma, Supriyah, Sören, Jonas & Jonas, Astrid, Jonathan, Axel, Nick, Douglas, Anders and Ole. Thank you all for generating such a friendly and inspiring atmosphere!

Last but not the least, I want to tank those outside of the university that have made this thesis possible; my parents and brother for encouragement, the 031- and 08-Indians for being wonderful friends and especially my wife Elin for all love, encouragement and for us being “di go’aste vänner”!

Christian Spånslätt, Stockholm, May 19, 2015

Contents

1

Introduction

1.1 Condensed Matter Physics

The creation of quantum mechanics in the early twentieth century was a paradigmatic shift in how to describe nature. By applying quantum mechanics to systems of constant density, such as solids and liquids, in the energy range corresponding roughly to room temperature and below, one enters the realm of *condensed matter physics*.

This is one of the most successful branches in physics and has given us both mathematically interesting theoretical models and a huge number of hands-on applications such as the transistor [BB48], Magnetic Resonance Imaging (MRI) [Lau73], Nuclear Magnetic Resonance (NMR) for chemical analysis [RZMK38], superconducting magnets [Ynt55] and Light Emitting Diodes (LEDs) [Zhe07].

The unification of seemingless unrelated phenomena has paved the way for an accurate description of condensed matter in nature. This success can be attributed to the formulation of a couple of strong principles underlying most of condensed matter theory [AS10].

Emergence is the concept that knowledge of the constituents of a system by no means implies that the system behaviour itself is understood. A system can be, and usually is, more than stacked fundamental building blocks, meaning that on each level of complexity, new features in terms of new physical laws and behaviour arise. Therefore, there is hope that though given an underlying microscopic model that might be impossible to solve exactly (which is usually the case), it is still possible to formulate effective theories relevant for the level of study, and to reduce the system in question by ignoring effects that are beyond said level.

Symmetry is deeply rooted in the language of all physics and that a system is invariant under some manipulation or transformation. As such it is further typically related to some conserved quantity. As will be later explained in this thesis, symmetries can also be responsible for the stability of certain phases of matter and the exotic particles associated to them.

Adiabatic continuity states that given some fundamental symmetries, the theoretical description of interacting systems often can be viewed as emerging

by *adiabatically* (in this context meaning slowly) turning on interactions in the corresponding non-interacting system provided the symmetries remain intact. Related to this adiabatic continuity is the emergence of quasiparticles, weakly interacting particles "dressed" by effects from interactions. This principle is the reason why seemingly "wrong" theories of non-interacting systems accurately can describe systems where interactions are known to be strong.

Universality means that many microscopically different systems actually demonstrate common collective behaviour and are therefore describable with the same effective models. These are usually much simpler than any microscopic theory since many layers of complexity can be ignored at the scale of study.

One of the most successful results of condensed matter physics has been to identify all ways matter can organize itself, the so called *phases of matter*. Classically, we learn of phases such as solids, liquids and vapours, but quantum mechanics predicts a plethora of additional phases. The characterization of these phases has been extremely successful by the use of *Landau's theory of symmetry breaking* [Lan37, LL80].

Within this framework, a phase transition is described by the behaviour of a quantity called the *local order parameter*. This quantity takes a non-zero value only below some transition temperature and is associated with the breaking of some underlying symmetry of the system. For example, a ferromagnet exhibits a spontaneous magnetization at the Curie temperature, where rotational invariance is broken as the microscopic dipoles all align in a single random but fixed direction. One of the great strengths of Landau's theory is that it can be formulated on quite general premises, requiring only an expansion of the free energy in terms of the local order parameter.

This thesis discusses the combination of failure of Landau's theory and the mathematical branch of *topology*. Already in 1931, with Dirac's quantum mechanical treatment of the magnetic monopole [Dir31], the concept of topology seriously entered the realm of theoretical physics. But it was not until some 50 years later that it made its grand and physical appearance in condensed matter physics, progressively branching of into various different subfields.

Most interestingly, in the last couple of decades, condensed matter physics has seen a rapid development due to groundbreaking experimental developments including cold atom traps, fabrication of nano-scale devices with atom precision and superconducting circuits. These, in combination with new and exciting topological models pose a promising and exciting path for a fundamentally new generation of quantum devices and exotically engineered materials.

1.2 Topology in Condensed Matter

Topology made a distinct entry in condensed matter physics in the 1980's with the discovery of the Integer [vDP80] and Fractional Quantum Hall ef-

fects [TSG82, Lau83] (IQH and FQH respectively) which generated a paradigmatic change in how matter is described. These effects occur when a two-dimensional electron gas, trapped in a semiconducting heterostructure at low temperature, is exposed to a strong magnetic field, while a current is driven through it. The resulting Hall conductance as a function of magnetic field takes on integer (IQH) or fractional (FQH) multiples of e^2/h, regardless of any microscopical details, to nearly one part in a billion. This conductance is one of the most well measured numbers in nature.

The quantum Hall setup was the first experimental example of a state that was not describable with Landau's framework of symmetry breaking. Phases of matter that exhibit a quantized Hall conductance can not be assigned any local order parameter [TKND82,Koh85,NTY85]. Systems that have this property are usually said to be *topologically ordered* [Wen90], though a more accurate definition would be a phase whose low energy effective field theory is a *topological field theory*. These field theories, as the name suggests, depend on concepts from the mathematical field of *topology*. This topology is the origin of the exact quantization of the Hall conductance. But there is another but closely related amazing feature of the quantum Hall state. Namely that it is insulating in the interior but conducting on the edges. It is these edge states that transfer the current across the sample trough ideal conducting channels yielding the perfectly quantized Hall conductance. The state is said to be topologically insulating.

Though topologically ordered systems have been around for quite some time, theories describing them are usually extremely complicated involving strong interactions and correlations. But surprisingly, it was shown that states formed in free fermion systems, despite seeming trivial and being exactly solvable, also can show interesting properties rooted in topology. These states are called *Topological States of Matter* (TSM). The IQH state is actually the first example of such a TSM, while the FQH state can not be described by any free fermion model. It was also discovered that the theory of electronic band structure in solids, which had been around since the advent of quantum mechanics, turned out to have an underlying topological structure. This enhanced band theory is called *topological band theory* and lies at the heart of TSM.

In 1988, Haldane showed that in a graphene-like model with non-interacting spinless fermions, there could be a quantized Hall conductance although the net magnetic field was zero [Hal88]. This is remarkable, since the magnetic field was thought to be the crucial ingredient for topological properties in the IQH state. Haldane's model is called the Quantum Anomalous Hall Effect (QAHE) or the Chern Insulator and has recently been realized in cold atom traps [JMD+14].

Quite some years later, in 2005, Kane and Mele predicted that Graphene should exhibit the so called Quantum Spin Hall (QSH) effect [C.L05, KM05]. In their model, two copies of Haldane's model, one for each spin direction, were coupled via spin-orbit interactions. This leads to a zero Hall conductance, but

opposite spin currents along the edges, so called *helical* edge states, which are stable just because there is no magnetic field. The edge states are said to be protected by time reversal symmetry in the sense that the system looks the same if time would be reversed.

Unfortunately, the QSH effect turned out to be too small for detection in graphene. But one year leater, Bernevig, Hughes and Zhang (BHZ) developed another model of the QSH effect, which was appropriate for two-dimensional HgTe/CdTe quantum wells [BHZ06]. This time, the effect was measurable, and the QSH state was measured and verified as a symmetry protected topological state of matter [KWB$^+$07]. The QSH effect was later generalized to three dimensions where exotic surface states appear on slabs of certain heavy element materials [FKM07, HQW$^+$08].

Meanwhile, Kitaev presented in 2001 a paper where a model for a topological superconductor was constructed [Kit01]. This model featured so called Majorana Bound States (MBS) having the peculiar property of *non-Abelian statistics* which are of immense interest in the field of topological quantum computation. The Kitaev paper launched a huge effort in realizing MBS experimentally, culminating in ingenious devices where already existing building blocks of nanotechnology are combined into engineered versions of topological superconductivity. These quantum devices are theoretically predicted to host the exotic MBS. Though theoretically promising, it is fair to say that experimental results still are under debate.

A couple of years later, it was found that the models of the IQH effect, the QSH effect, topological superconductors and many other models could be collectively described by a general framework, the so called *The Ten-fold Way*, *The Periodic Table of Topological Insulators and Superconductors* or *The Cartan-Altland-Zirnbauer Classification Table* [SRFL08, RS$^+$10, A.Y09]. It describes a general setting where insulating and superconducting band structure, symmetry and topology lead to a classification of all possible non-interacting fermionic TSM.

In this thesis we shall be concerned with quantum mechanical systems exhibiting TSM which in addition are confined to one spatial dimension. This will be motivated as follows.

1.3 Systems Confined to One Dimension

The concept of a one-dimensional system may seem as only a theoretical approximation when two of the three dimensions of a system are much smaller than the third. But quantum mechanically, given a sufficiently low energy regime (for example in a low temperature environment), the energy for accessing excited states corresponding to the smaller dimensions is much higher than any relevant energy scale. Compare for instance with the level spacing, $\Delta E \sim 1/L$, where L is the box length, in the "particle in a box problem" of

elementary quantum mechanics (see for instance Ref. [Rob06]). This implies that the system for all practical purposes is constrained to one dimension since the smaller dimensional degrees of freedom are energetically "frozen out".

One-dimensional quantum physics is itself a vast area of research and is fundamentally different from higher dimensions (see [Gia03] for an introduction). There are many exotic phenomena that occur in one dimension such as spin-charge separation, Luttinger liquids or the absence of spontaneous symmetry breaking. In addition, as will be discussed below, the so called bulk-boundary principle implies that the edges of two-dimensional TSM can be described by a particular kind of one-dimensional models. These models can have many peculiar features, such as non-charge conservation, since they can not exist independently without the bulk system. Other prominent examples of existing one-dimensional systems are carbon nanotubes, quantum spin Hall edges, polymers such as polyacetylene and fabricated heavy element nano wires.

1.4 Goals and Outline

The main goal of this thesis is to provide a conceptual introduction to fermionic TSM and describe a specific application to one-dimensional systems. It is meant to be accessible for students entering this field of research and to provide a firm basis for reading more in depth research papers. Some emphasis has been given to explain the frequently used jargon which can, at least according to the author's experience, be frustrating and time consuming to understand for a newcomer. The thesis is organized as follows:

In the second chapter, the stage is set for analyzing TSM. A general discussion of important concepts is given together with a description of the tight-binding formulation which is a convenient language for describing topological band theory. Following is a discussion of quantum mechanical symmetries which are the basic ingredients for a classification of all non-interacting topological states of matter. This classification will be explained together with a discussion of it's limitations and applications.

In chapter three, a few one-dimensional models that exemplify the contents of chapter two will be presented. The two first models concern topological superconductivity and MBS. The first one is the Kitaev Wire which is a simple toy model realizing the concept of isolated MBS. The next one is a physical realization of Kitaev's model, which is the one mostly used for analyzing real experiments. It goes under various name, but in this thesis the Majorana Wire Model will be used. The last model is a toy model for the polymer polyacetylene which exhibits fractional charge states localized at deformations of the polymer chain. Together, these three models will hopefully clarify many concepts and concretize abstract notions of topology.

Chapter four gives an accessible introduction to the accompanying paper. Along the way, pointers to previous chapters will motivate the research.

The fifth, and final, chapter summarizes the thesis and points out some directions for future research.

2

Topological States of Matter

This chapter starts with an introduction to the field of topological insulators and superconductors, collectively called Topological States of Matter (TSM). Here the motivation of using the adjective *topological* will be explained. The chapter continues with an accessible introduction to the tight binding formalism, which will be used in the remainder of the thesis to describe various models exhibiting topological properties. Following is a brief description of the concept of quantum mechanical symmetries which are of paramount importance in the field of TSM. These symmetries will then be used as a basis for the classification of all non interacting TSM in different spatial dimensions. The chapter concludes with a discussion of the limitations of the presented framework and highlights some extensions which are focus of contemporary research. The chapter will be at an introductory level and references to more in-depth treatments will be given along the way.

2.1 Topological Insulators and Superconductors

The mathematical field of *topology* deals with how mathematical objects can be deformed into each other. These deformations include bending, stretching and twisting but not tearing, cutting or gluing. In addition, it investigates which global properties of the objects that are preserved in these deformation processes.

As an example, a ball can be continuously deformed into a cube but not into a torus because that would require cutting a hole which the rules do not allow. The ball and cube are then said to be topologically equivalent, or *homeomorphic*, while the ball and the torus are topologically distinct.

Applied to the setting of condensed matter physics, we may ask the question whether quantum systems, represented by their Hamiltonians, continuously can be transformed into each other given some constraint on the deformation [ASv$^+$15, HK10]. If this is possible, the systems are said to be topologically equivalent. The constraint is important, for without it the above notion would be meaningless as any Hamiltonian could in some way be deformed to any other. Compare with the rule of "no cutting" above. In this thesis we shall be concerned with the constraint of treating gapped Hamiltonians which

describe insulators and superconductors. Having a gapped fermionic Hamiltonian means that between occupied and unoccupied energy eigenstates, there is a finite energy region where no states exist. This gap must exist regardless of the system size.

Related to the deformation of Hamiltonians, is a quantity called the *topological invariant*. This invariant, as the name suggests, does not change under continuous transformations between two topologically equivalent Hamiltonians, but will generally do so whenever a deformation forces the energy gap to close. When this happens, the system is said to undergo a *topological phase transition*. To connect to the example of the ball-torus deformation, the number of holes, called the genus or the Euler characteristic, would be the relevant quantity for a topological invariant in this specific problem. In this thesis, however, we shall be concerned with slightly more complicated invariants expressed as *winding numbers* and *Pfaffian invariants*.

We shall also see that certain symmetries further constrain the allowed set of deformations between Hamiltonians. This leads naturally to the definition of a *symmetry protected topological state of matter* which can formulated as:

> *"As long as a certain symmetry is present, the state can not be deformed into a trivial state unless the gap closes."*

A *trivial state* is equivalent to an ordinary insulator or superconductor which will turn out to never have non-trivial topological invariants. A trivial insulator is such that it can be adiabatically (which is sufficiently slow so that the associated energy scale is far below that of the energy gap) deformed into a state of isolated atoms. A trivial superconductor is defined as one that has a trivial topological invariant. Symmetry protected TSM will be the main theme of this thesis and in particular how the topology of a system's band theory is manifested in its edge properties. This connection, that non-trivial bulk topology implies exotic edge modes, has a name, *The Bulk-Boundary Correspondence* and lies at the heart of topological states of matter and how to detect them in experiments.

2.2 Tight Binding and Bloch Hamiltonians

The tight binding description of quantum systems is a powerful method of modeling band structure of non-interacting electrons (see for instance [YC10, AM76]). It captures the lattice structure of the system while at the same time allowing for symmetry constraints, internal degrees of freedom, impurities and external fields. Additionally, the tight binding description contains a natural high energy cutoff which is crucial for a well behaved bulk topology of the system. For a model lacking this cutoff, various regularization and compactification schemes have to be implemented. The absence of need for

such schemes is again a powerful property of the tight binding description. Many models of TSM are in fact written in this language.
A general tight binding model has the form

$$\mathcal{H} = \sum_{ij\alpha\beta} c^\dagger_{i\alpha} H^{\alpha\beta}_{ij} c_{j\beta}, \tag{2.1}$$

where i,j denotes lattice sites in any dimension and α,β are any internal site degree of freedom, for example spin, orbitals or electron-hole properties. The second quantization operator $c^\dagger_{i\alpha}$ creates particles on site i and with internal degree of freedom α. The coefficients $H^{\alpha\beta}_{ij}$ capture any symmetries of the system.

By requiring translational invariance, the Hamiltonian can be Fourier transformed into the form

$$\mathcal{H} = \sum_{k\alpha\beta} c^\dagger_{k\alpha} h^{\alpha\beta}(k) c_{k\beta}, \tag{2.2}$$

where $h^{\alpha\beta}(k)$ is an element of the *Bloch* (or in the superconducting case, the Bogoliubov - deGennes or simply *BdG*) *Hamiltonian*. The quantity k is the Bloch, or crystal, momentum and takes values in the first Brillouin zone (BZ). In one dimension, the BZ is the interval $[-\pi,\pi]$ assuming a unit lattice constant.

The notion of the *bulk Hamiltonian*, in the sense that it describes a system without a border, is also frequently used. As will be shown, the topology of the bulk Hamiltonian is manifested by introducing edges in the system. This is called the bulk-boundary correspondence and is one of the key concepts of TSM.

Note that the Bloch Hamiltonian is a matrix in the internal degrees of freedom. The matrix elements $h^{\alpha\beta}(k)$ are related to $H^{\alpha\beta}_{ij}$ by

$$h^{\alpha\beta}(k) = \sum_{\delta} H^{\alpha\beta}_{\delta} e^{-i\delta\cdot k}, \tag{2.3}$$

where δ is a vector connecting the lattice sites. Frequently δ is restricted to the set of nearest neighbour vectors.

Another advantage of the tight binding model is that it can be straightforwardly implemented numerically. To see this, we recall the notion of matrix representation of quantum mechanics.

Assume there exists an orthonormal and complete basis set of the Hilbert space, $\{|i\rangle\}_i$ fulfilling $\sum_i |i\rangle\langle i| = \mathbb{1}$ with inner product $\langle i|j\rangle = \delta_{ij}$. Any operator, $\hat{\mathcal{A}}$, on the Hilbert space, can be written as

$$\hat{\mathcal{A}} = \mathbb{1}\cdot\hat{\mathcal{A}}\cdot\mathbb{1} = \Big[\sum_i |i\rangle\langle i|\Big]\cdot\hat{\mathcal{A}}\cdot\Big[\sum_j |j\rangle\langle j|\Big] = \sum_{ij} A_{ij}|i\rangle\langle j|, \tag{2.4}$$

with $A_{ij} = \langle i| \hat{\mathcal{A}} |j\rangle \in \mathbb{C}$, being an element of the matrix $\mathbf{A}$ which is a representation of the abstract operator $\hat{\mathcal{A}}$ in the given basis. This procedure can also be performed on a state vector yielding the representation

$$|\psi\rangle = \mathbb{1} |\psi\rangle = \sum_i |i\rangle \langle i|\psi\rangle = \sum_i \psi_i |i\rangle , \tag{2.5}$$

with $\psi_i = \langle i|\psi\rangle \in \mathbb{C}$, being the basis element of the vector $\vec{\boldsymbol{\psi}}$ which represents $|\psi\rangle$ in the given basis.

The abstract entities $\hat{\mathcal{A}}$ and $|\psi\rangle$ on the Hilbert space have thus been converted to the matrix $\mathbf{A}$ and the vector $\vec{\boldsymbol{\psi}}$ which are sets of complex numbers that can be calculated on a computer.

Consider now the time independent Schrödinger equation $\hat{\mathcal{H}} |\psi\rangle = E |\psi\rangle$. Using the representations (2.4) and (2.5) above gives

$$\begin{aligned} &\Big[\sum_{ij} H_{ij} |i\rangle \langle j| \Big] \Big[\sum_k \psi_k |k\rangle \Big] = E \Big[\sum_i \psi_i |i\rangle \Big] \\ &\Rightarrow \sum_{ij} H_{ij} \psi_j |i\rangle = E \sum_i \psi_i |i\rangle . \end{aligned} \tag{2.6}$$

Multiplying with $\langle k|$ from the left and using the orthonormality of the basis leads then to the equation

$$\sum_{kj} H_{kj} \psi_j = E \psi_k \quad \text{or} \quad \mathbf{H} \vec{\boldsymbol{\psi}} = E \vec{\boldsymbol{\psi}}, \tag{2.7}$$

which is just the eigenvalue equation of the matrix $\mathbf{H}$. Solving it will give the eigenvalues or eigenenergies $\{E_i\}$, and the eigenvectors $\{\vec{\boldsymbol{\psi}}_i\}$. The elements of the eigenvectors will be the coefficients of the basis expansion (2.5). The procedure above can be extended to time-dependent systems, but this is out of the scope of this thesis.

To clarify the concepts above, consider a one-dimensional chain of N sites with on-site chemical potential μ and nearest neighbouring hopping amplitude t. This model can be implemented by

$$\mathcal{H} = \sum_{i=1}^{N} \Big[-t(c_i^\dagger c_{i+1} + c_{i+1}^\dagger c_i) - \mu c_i^\dagger c_i \Big] . \tag{2.8}$$

This Hamiltonian can be implemented numerically by defining a sparse $N \times N$ matrix $\mathbf{H}$ with non-zero elements

$$H_{ii} = -\mu, \quad H_{i,i+1} = H_{i+1,i} = -t. \tag{2.9}$$

Here we have used the basis states $|i\rangle \equiv c_i^\dagger |0\rangle = (0, \ldots, 1, \ldots, 0)^T$, where $|0\rangle$ is the vacuum state containing no particles, the 1 is in the i:th position, and T

denotes transposition. Solving the eigenvalue equation for the matrix **H** gives the spectrum of the model and the eigenstates, where the latter will be linear combinations of the basis states, the so called Bloch states which will arise in any periodic crystal structure.

Imposing periodic boundary conditions, $c_{N+1} = c_1$, allows for a Fourier transform which in this problem directly yields the one-dimensional Bloch Hamiltonian and eigenenergies $h(k) = \epsilon(k) = -2t\cos(k) - \mu$ where we have assumed a unit lattice constant. The crystal momentum k takes the values $k = \frac{2\pi n}{L}$ where $n = 0,1,2,...,N-1$ and are of course exactly (or as far as machine precision allows) the same as the eigenvalues of the matrix **H** with periodic boundary conditions $H_{1N} = H_{N1} = -t$.

We shall now move on to discuss how symmetries of the bulk Hamiltonian is constructed and analyzed.

2.3 Symmetries

A physical system can posses various symmetries. These are quantum mechanically represented by unitary operators that commute or anti-commute with the Hamiltonian. An ordinary symmetry, U, is said to exist if the system Hamiltonian is such that it commutes with a unitary operator

$$[\mathcal{H},U] = 0 \Leftrightarrow U^\dagger \mathcal{H} U = \mathcal{H}. \tag{2.10}$$

Examples of such symmetries are the spin projection or linear momentum operators.

Any such unitary symmetry allows for a reduction of the Hamiltonian into symmetry-free blocks. As an example, a spin Hamiltonian commuting with σ_z can be written in separate spin-up and spin down-blocks. Due to the commutativity with the Hamiltonian and by the Heisenberg equation of motion, these spins are conserved and the blocks will therefore be completely disconnected. Each block on it's own will not posses the spin-symmetry since that degree of freedom has been eliminated.

Each sub-block may in turn be analyzed further until no symmetry is left and one has reached an *irreducible* representation of the full symmetry group of the Hamiltonian. But each sub-block can be classified further with a second kind of symmetry operators. These are the so called anti-unitary operators which work in a somewhat different way. They impose spectral constraints on the Hamiltonian which is of utter importance when topological band structure is concerned. Examples of such constraints will explicitly be given below.

For TSM there are two important anti-unitary symmetries [Ber13]. A Hamiltonian is defined to be time reversal symmetry (TRS) or particle-hole symmetry (PHS) invariant respectively if there can be found anti-unitary operators that commute respectively anti-commute with the Hamiltonian:

$$\mathcal{T}\mathcal{H}\mathcal{T}^{-1} = \mathcal{H}, \quad \mathcal{P}\mathcal{H}\mathcal{P}^{-1} = -\mathcal{H}. \tag{2.11}$$

TRS is present in any system that would look the same if time would be reversed. PHS is a little bit more subtle, since it in some situations, notably in mean field superconductivity, arises automatically from an artificial doubling of the degrees of freedom. For this reason we shall keep in mind that PHS is not always an actual symmetry, but we will treat it on the same footing as any other symmetry.

According to Wigner's theorem (see for instance [SN11]), every anti unitary operator can be written as the product of some unitary operator and the complex conjugation operator. For example, the TRS operator for a spin$-1/2$ system in the basis of σ^z-eigenstates, can be written as $\mathcal{T} = i\sigma_y\mathcal{K}$ with $i\sigma_y$ unitary and $\mathcal{K}$ the complex conjugation operator (it is important to note that the representation of any operator can depend on the choice of basis). Applying $\mathcal{T}$ on the spin operator flips all spin components,

$$\mathcal{T}\sigma_i\mathcal{T}^{-1} = -\sigma_i, \quad i = x,y,z \tag{2.12}$$

as time reversal intuitively should. By the virtue of Wigner's theorem we shall use the notational convention $\mathcal{T} = T\mathcal{K}$ and $\mathcal{P} = P\mathcal{K}$ with T and P being unitary operators.

TRS and PHS can each each come in two distinct classes. Squaring any of the operators we can have the possibilities $\mathcal{T}^2 = \pm 1$ and $\mathcal{P}^2 = \pm 1$. These different sides of the same symmetry coin may have drastical consequences on the energy spectrum. A well known example is the $\mathcal{T}^2 = -1$ operator for spin-$1/2$ particles which yields *Kramer's degeneracy*: all energy states are at least two-fold degenerate.

For Bloch or BdG Hamiltonians $h(k)$ (which usually are matrices) the TRS and PHS symmetries in Equation (2.11) translate into the the following spectral constraints

$$Th(k)^{\mathrm{T}}T^\dagger = h(-k), \quad Ph(k)^{\mathrm{T}}P^\dagger = -h(-k), \tag{2.13}$$

where the hermicity of $h(k)$ has been used and T denotes matrix transposition.

Furthermore, the combination of TRS and PHS yields the Chiral Symmetry (CS) which can be represented by the operator $\mathcal{C} = T\mathcal{K}P\mathcal{K} = TP^* \equiv C$ imposing the following Hamiltonian constraints:

$$\mathcal{C}\mathcal{H}\mathcal{C}^{-1} = -\mathcal{C} \tag{2.14}$$

and

$$Ch(k)C^\dagger = -h(k). \tag{2.15}$$

Thus, a CS is represented by a unitary operator that anti-commutes with the Hamiltonian and is sometimes called sub-lattice symmetry since the same type of symmetry operator arises in systems where one can make a division

between two sublattices, a and b. The Hamiltonian can then be written in a basis such that the Bloch Hamiltonian has the form

$$h(k) = \begin{pmatrix} 0 & h_{ab} \\ h_{ab}^{\dagger} & 0 \end{pmatrix}. \tag{2.16}$$

For such a Hamiltonian, it is straightforward to show that all eigenstates come in $\pm E$ pairs. As we shall see next, the analysis of TSM boils down to classifying Hamiltonians according to the symmetries mentioned in this section.

To summarize, in the field of TSM there are three important symmetries:

- TRS which is an anti-unitary symmetry that commutes with the Hamiltonian.
- PHS which is an anti-unitary symmetry that anti-commutes with the Hamiltonian.
- CS which is a unitary symmetry that anti-commutes with the Hamiltonian.

We shall now use these symmetries as a basis for classifying all non-interacting TSM.

2.4 Classification of Topological States of Matter

The topological classification of all non-interacting and gapped Hamiltonians boils down to two basic sets of problems.

1. Given a set of anti-unitary symmetries and some specified physical dimension, what is the group of topologically distinct Hamiltonians, how many different topological phases are there and what kind of object is the topological invariant?
2. Given a Hamiltonian with certain fixed parameters belonging to a certain class, which topological phase is the system in, and what is the value of the topological invariant?

The first of these problems is discussed at a conceptual level in this section, while the second, which is a bit more subtle, will be adressed in some specific examples in the next chapter.

2.4.1 Outline of Classification

The main idea behind the classification is that physical systems in any spatial dimension having an insulating bulk gap can be divided into different classes distinguished by their underlying symmetries, TRS, PHS and CS. Both TRS

and PHS can either be present, and can either square to ± 1, or be absent. This directly yields nine different possibilities. The CS is always fixed by the other two symmetries except for one specific case. When both TRS and PHS are absent, there is still the possibility of having the CS present anyway. This yields a grand total of ten distinct classes having various topological properties. We shall now roughly sketch the procedure of determining what kind of topological phases a certain class has.

The relevant quantity for the topological classification of an insulating band structure is the projection operator onto the subspace of occupied bands [SRFL08, QHZ08]. This operator can be written as

$$P(k) = \sum_{j=1}^{n} |u_j(k)\rangle \langle u_j(k)| , \tag{2.17}$$

where we have assumed that n out of $n+m$ bands are occupied.

Since it is only the global properties of the band structure that are relevant, we can deform the band structure as long as the gap separating occupied and empty bands is maintained. The insulator can therefore conveniently be deformed into a so called flat band insulator, where all occupied bands have energy $\epsilon_- = -1$ and all empty bands have energy $\epsilon_+ = +1$. The Hamiltonian $h(k)$ is then transformed into the corresponding flat Hamiltonian:

$$q(k) = (+1)(1 - P(k)) + (-1)P(k) = 1 - 2P(k). \tag{2.18}$$

We note that $q(k)^2 = 1$ due to the idempotence of projection operators and also that $\mathrm{Tr}\,[q(k)] = m - n$. Generally, $q(k)$ will be some $U(n+m)$ matrix defined up to a $U(n) \times U(m)$ "rotational" or gauge degree of freedom corresponding to basis rotations in the occupied and empty band subspaces. Then the flat band Hamiltonian, and the original Hamiltonian too as far as topology is concerned, belongs to the symmetric space

$$G_{n+m,m}(\mathbb{C}) = G_{n+m,n}(\mathbb{C}) = U(n+m)/(U(n) \times U(m)), \tag{2.19}$$

which is called the complex Grassmannian and is a generalization of the projective spaces.

The set of topologically distinct Hamiltonians is then determined by the homotopy classes of the mappings

$$\begin{aligned} q\colon T^d &\to G_{n+m,m}(\mathbb{C}) \\ k &\mapsto q(k). \end{aligned} \tag{2.20}$$

Here, T^d is the d-dimensional torus corresponding to the BZ in the case of lattice models. For a continuum model, T^d is replaced by S^d, the d-sphere, yielding by definition the first fundamental group

$$g = \pi_d(G_{n+m,m}(\mathbb{C})). \tag{2.21}$$

Class	**TRS**	**PHS**	**CS**	$d=0$	1	2	3	4	5	6	7
A	0	0	0	$\mathbb{Z}$	0	$\mathbb{Z}$	0	$\mathbb{Z}$	0	$\mathbb{Z}$	0
AIII	0	0	1	0	$\mathbb{Z}$	0	$\mathbb{Z}$	0	$\mathbb{Z}$	0	$\mathbb{Z}$
AI	+1	0	0	$\mathbb{Z}$	0	0	0	$2\mathbb{Z}$	0	$\mathbb{Z}_2$	$\mathbb{Z}_2$
BDI	+1	+1	1	$\mathbb{Z}_2$	$\mathbb{Z}$	0	0	0	$2\mathbb{Z}$	0	$\mathbb{Z}_2$
D	0	+1	0	$\mathbb{Z}_2$	$\mathbb{Z}_2$	$\mathbb{Z}$	0	0	0	$2\mathbb{Z}$	0
DIII	−1	+1	1	0	$\mathbb{Z}_2$	$\mathbb{Z}_2$	$\mathbb{Z}$	0	0	0	$2\mathbb{Z}$
AII	−1	0	0	$2\mathbb{Z}$	0	$\mathbb{Z}_2$	$\mathbb{Z}_2$	$\mathbb{Z}$	0	0	0
CII	−1	−1	1	0	$2\mathbb{Z}$	0	$\mathbb{Z}_2$	$\mathbb{Z}_2$	$\mathbb{Z}$	0	0
C	0	−1	0	0	0	$2\mathbb{Z}$	0	$\mathbb{Z}_2$	$\mathbb{Z}_2$	$\mathbb{Z}$	0
CI	+1	−1	1	0	0	0	$2\mathbb{Z}$	0	$\mathbb{Z}_2$	$\mathbb{Z}_2$	$\mathbb{Z}$

Table 2.1: The CAZ table. The classes are defined by their time reversal (TRS) particle-hole (PHS) and chiral (CS) symmetry properties. For TRS and PHS, $\pm$ describes whether the repeated action squares to $+1$ or -1. For CS, 1 means presence and 0 means absence. The two topmost classes are called complex while the remaining eight are called real. d denotes spatial dimension. For a certain class in a certain dimension, there is a topological invariant in the right section. For the meaning of the entries, see the main text.

Assigning additional symmetries to the Hamiltonian (2.18) changes the mapping target space in Equation (2.20) so that the homotopy group may change too. The mathematical depth of determining all homotopy classes for the mappings (2.20) is extremely complicated and describing the various methods used is out of the scope of this thesis. For more information, we refer to Refs. [SRFL08, A.Y09, RS$^+$10, QHZ08].

The classification of all TSM according to this scheme can be summed up in a table that goes under various names. The most commonly used are: *The Ten-fold Way*, *The Periodic Table of Topological Insulators and Superconductors* or *The Cartan-Altland-Zirnbauer Classification Table*. In this thesis we shall use the latter name using the abbreviation CAZ.

We shall now move on to in detail describe some of the features of the CAZ table and show some of the extraordinary explanatory power it has for studying TSM.

2.4.2 The CAZ table

Having outlined the method of topologically classifying all non-interacting gapped Hamiltonians, we are now ready to take a look at the resulting CAZ table.

The entries in the CAZ table tells what is the topological classification of a system with a given combination of TRS, PHS, CS in spatial dimension d. That is what possible values the topological invariant ν of such a system can take.

Entries in the first column are the somewhat cryptical names of the different classes. They originate from the fact that the corresponding Hamiltonian spaces turned out to be exactly those of Cartan's classification of symmetric spaces, performed in the early twentieth century [Car26]. They were later studied by Altland and Zirnbauer in the context of disordered mesoscopic hybrid structures [AZ97]. These three authors are honored in naming the classifying table. It is interesting to note that a seemingly abstract group theoretical concept finds is used as a description of nature almost 100 years later.

The next three columns describe the symmetries corresponding to the class. If TRS or PHS are present, it is marked by ± 1 referring to if the symmetry squares to $+1$ or -1. CS is denoted by 1 for presence and 0 for absence.

A $\mathbb{Z}$ invariant means that it takes values in the set of integers $\nu = 0, \pm 1, \pm 2, \ldots$. A system with this kind of invariant is for example the IQH effect belonging to the symmetry free class A in two dimensions.

A $2\mathbb{Z}$ entry in the table means that $\nu = 0, \pm 2, \pm 4, \ldots$ A spin-1/2 quantum dot with TRS and thereby Kramer's degeneracy would have an invariant equal to the number of filled levels which thereby is a $2\mathbb{Z}$ -invariant.

A $\mathbb{Z}_2$ invariant means that there are only two distinct topological phases: trivial or topological or $\nu = \pm 1$. One example of a system with such an invariant is the Kitaev Wire which is a topological superconductor belonging to class D with $d = 1$. This invariant will be derived explicitly in the next chapter.

A zero entry means that no topological invariant can be defined meaning that all gapped Hamiltonians with the given symmetries and dimensionality can be deformed into each other without closing the gap or breaking any symmetries. This means for example that there can be no IQH state in three dimensions.

The first two classes, A and AIII are called complex since they don't have any anti-unitary symmetry involving complex conjugation. The eight latter classes are called the real classes for the opposite reason.

Apart from the examples above, other notable examples of systems belonging to the CAZ table are the QSH effect in class AII with $d = 2$, The AQH effect in class A with $d = 2$ and the B-phase of Helium 3 in class DIII with $d = 3$.

2.4.3 Dimensional Extension and the Bott Clock

There is a periodicity in the occurrence of topological invariants in the CAZ table. This structure is quite subtle and requires advanced mathematics to

explain. We shall in this section briefly sketch the reason for this periodicity basing our discussion to large extent on Ref. [ASv$^+$15].

Starting with the complex classes, we note that we can either have chiral symmetry or not. Assume first that a Hamiltonian in dimension d, denoted by $\mathcal{H}_d$, has a chiral symmetry which is represented by the operator $\mathcal{C}$. We then have that $\mathcal{H}_d$ belongs to class AIII. The eigenenergies $\pm\epsilon_d^n$ are symmetrically distributed around zero energy and depends on d Bloch momenta. We then form the *extended Hamiltonian*

$$\mathcal{H}_{d+1} = \mathcal{H}_d \cos(k_{d+1}) + \mathcal{C} \sin(k_{d+1}), \tag{2.22}$$

which has eigenenergies

$$\epsilon_{d+1}^n = \pm \left[(\epsilon_d^n)^2 \cos^2(k_{d+1}) + \sin^2(k_{d+1}) \right]^{1/2}. \tag{2.23}$$

Here we have used the fact that $\mathcal{C}^2 = 1$ and we note that $\mathcal{H}_d$ and $\mathcal{H}_{d+1}$ has the same number of bands, though the latter depends on one more Bloch momentum. The expression (2.22) ensures, by construction, that the gap of $\mathcal{H}_{d+1}$ closes if and only if that of $\mathcal{H}_d$ closes. This means that their topological invariant must be the same. The construction further ensures that $\mathcal{H}_{d+1}$ breaks the CS since we have added a term with $\mathcal{C}$. Hence, we have proved that the topological classification of a class AIII Hamiltonian in dimension d is the same as that for a class A Hamiltonian in dimension $d+1$. We abbreviate this observation by AIII→A.

Let us now assume that $\mathcal{H}_d$ does not have any CS, thus being in class A. We then construct

$$\mathcal{H}_{d+1} = \mathcal{H}_d \cos(k_{d+1})\tau_x + \sin(k_{d+1})\tau_y, \tag{2.24}$$

having twice the number of bands compared to $\mathcal{H}_d$ and with eigenenergies given by Equation (2.23). By the same argument as above, $\mathcal{H}_{d+1}$ must have the same topological invariant as $\mathcal{H}_{d+1}$ but now has a CS given by $\mathcal{C} = \tau_z$. We can therefore state that A→AIII.

These two procedures, adding one extra dimension and breaking or assigning symmetry goes under the name of *dimensional extension*. We can see that this explains the staggered pattern in the upper section of the CAZ table: A→AIII→A. One physical consequence of this result is that there can be no IQH effect in odd dimensions.

It is possible to apply dimensional extension to the other classes too. The strategy is the same but it is a little bit more tricky and we shall here only state the result:

$$\text{AI} \to \text{BDI} \to \text{D} \to \text{DIII} \to \text{AII} \to \text{CII} \to \text{C} \to \text{CII} \to \text{C} \to \text{AI}. \tag{2.25}$$

We note here something interesting. The pattern for real classes repeats itself after 8 dimensional extensions. This is called *Bott periodicity* [Bot59] and is a property of the underlying mathematical structure of *K-theory* [RS$^+$10].

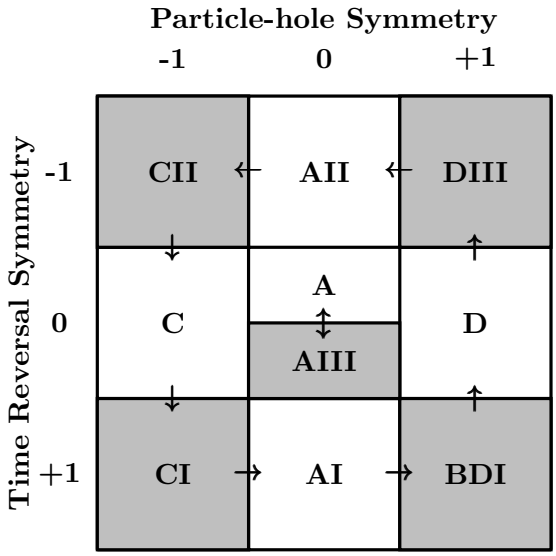

Figure 2.1: The Bott Clock which describes the periodicity upon dimensional extension of CAZ classes. Grey classes are chiral and arrows depicts the direction in which dimensional extension conserves the topological invariant. The periodicity is eight for the real, outer classes, but two for the inner complex classes.

We can visualize the Bott periodicity in the form of table named the *Bott clock* depicted in Fig.2.1. Here the different classes are arranged in a 3×3 grid according to their symmetries. Chiral classes are displayed in gray. The arrows tells which classes that have the same topological invariant when performing the dimensional extension $d \to d+1$. The two complex classes are situated in the middle and are isolated from the real classes positioned around the "clock". Going one revolution around the clock takes us back to the same class after 8 dimensional extensions.

There are many more interesting symmetry properties of the CAZ table, for instance the $\mathbb{Z}_2 \to \mathbb{Z}_2 \to \mathbb{Z}$ occurrence in all rows. The interested reader is referred to Refs. [SRFL08, A.Y09, RS$^+$10], for a more detailed discussion.

2.5 The Bulk-Boundary Correspondence

A question that naturally arises is how to identify which side of the topological phase transition that is the topological phase. In particular it would be preferable to observe this concretely in a lab and not through the mathematically abstract topological invariant. One answer to this question is *The Bulk-Boundary Correspondence* (or the bulk-edge correspondence) which is the topic of this section.

The essence of the bulk-boundary correspondence is that the topology of a closed bulk Hamiltonian will result in edge states for the corresponding open system. This principle can be understood in the following intuitive way.

Since a topological invariant only can change if the bulk gap closes, any region where some parameter changes such that it forces a topological phase transition will be accompanied with a local closing of the gap. This holds especially at an edge, which borders the (by definition) trivial vacuum. Edges of a topological insulator or superconductor will therefore generally host some exotic edge states which properties will depend on the symmetries of the bulk. As a rule of thumb, a system having TRS will generally host helical edge modes, meaning that opposite spins travel in opposite directions, PHS implies Majorana modes which are equally weighted superpositions of particles and holes and CS implies helical Majorana modes. Additionally, the edge states can be conducting since they will cross the Fermi level which in TSM always lies in the gap.

It shall be noted that edge and bulk dimensions do not always have to differ by only one (as the two-dimensional surface of a three-dimensional slab). An example of this is the Majorana bound states trapped in zero dimensional vortices penetrating a two dimensional topological superconductor.

The bulk-boundary principle was first used by Halperin [Hal82] to explain the *chiral* edge states of the IQH effect and was later formalized by many authors (see for example the book by Volovik [Vol03]). The mathematical foundation can be traced back to the Atiyah-Singer index theorem [AS68, Nak03]. Roughly speaking, this theorem relates the topology of a manifold $\mathcal{M}$ to the number of zero energy solutions (that is edge states) of differential operators acting on $\mathcal{M}$.

Being of paramount importance in the field of TSM, we shall use the bulk-boundary correspondence explicitly in Chapters 3 and 4.

As a final remark, we want to stress that the bulk-boundary correspondence is not the only way to determine if a phase is non-trivial or not. See for instance Refs. [Kit01, BA13].

2.6 Limitations and Applications

To round off this chapter, we discuss the limitations of the previously described framework. The perhaps most obvious objection is that it only treats single particle Hamiltonians describing non-interacting fermionic systems or, in the case of superconductivity, systems with non-self consistent mean field approximations. Electrons in real materials are subjected to interactions of various types and to realize the theoretical models there must be reasons for the topology to survive even in the presence of interactions. One way to overcome this limitation is to rely on the principle of adiabatic continuity, presented in the introduction. One then assumes that the gapped ground state of the non-

interacting system is adiabatically connected to the interacting ground state in a process which at all points maintain the gap. Interestingly, and mentioned in the introduction, interactions may in fact themselves generate new possible topological states which are not adiabatically connected to any non-interacting state. The FQHE is the prominent example of this phenomena.

Another objection would be that in real systems, the influence of decoherence or thermal fluctuations leads to mixed states and a density matrix formulation of TSM would be appropriate. Research in this direction is indeed ongoing and will hopefully shed some light on how the TSM classification can be extended to more complicated and realistic systems where the environment can not be ignored.

Moreover, the potential applications of TSM are many, but may in reality be hard to realize. One major incentive for the theoretical community is the possibility of using the exotic edge states associated with non-trivial bulk topology as building blocks of topological quantum computers [FKLW03]. These rely on the topological stability of such states and it has been shown that their interesting non-Abelian statistics can be used for quantum computational manipulations. From a more practical point of view, TSM might be exploited for energetically more effective devices where the absence of scattering processes, originating from topological protection, substantially reduces dissipation.

3

One-Dimensional Topological Models

Having reviewed the general framework of topological states of matter, we turn in this chapter our attention to a few models where it can explicitly be applied.

We will first look at the Kitaev Wire, which is a seminal toy-model of a topological superconductor hosting exotic Majorana excitations. Secondly, we shall study a more realistic incarnation of a Kitaev Wire, a model referred to as the Majorana Wire. The third, and final model we study is the so called SSH-model, describing the polymer polyacetylene which exhibits fractional charged states located at distortions of the underlying lattice.

3.1 The Kitaev Wire and Majorana Bound States

In this section we shall study a simple, but theoretically rich, toy-model of p-wave superconductivity. This model is often referred to as the *Kitaev Wire* [Kit01]. Though more than a thousand materials are known to be superconducting, there is only a single one, Sr_2RuO_4, that shows evidence of p-wave pairing [HKL$^+$10]. All superconducting states are believed to be described by condensation of *Cooper-pairs* but how these pairs connect in momentum-energy space can, at least theoretically, occur in various ways. In this thesis we shall refer to pairing of the type $\Delta(k) \sim \Delta k$ as p-wave pairing, the important property being here that the pairing potential is k-dependent.

The two main interesting features of the Kitaev wire is first of all that it hosts two phases distinguished by a $\mathbb{Z}_2$-invariant. Secondly, the edge states in the non-trivial phase are Majorana bound states. These states obey *non-Abelian statistics*, a property of great interest for topological quantum computation [FKLW03].

Following is a description of the Kitaev Wire Hamiltonian and a proof of the existence of Majorana bound states and their statistics. We then provide a derivation of the topological invariant together with the determination of the relevant CAZ-classes of the model. We shall also explicitly construct the real space tight-binding Hamiltonian and give the spectrum and position basis eigenstates.

3.1.1 Hamiltonian

The Kitaev Wire Hamiltonian can be written as [Kit01]

$$\mathcal{H} = \sum_{j\in[1,N]} \left[-tc_j^\dagger c_{j+1} - t^* c_{j+1}^\dagger c_j + \Delta c_j c_{j+1} + \Delta^* c_{j+1}^\dagger c_j^\dagger - \mu(c_j^\dagger c_j - \frac{1}{2}) \right]. \tag{3.1}$$

As such, it describes a one-dimensional electronic chain with $N \gg 1$ sites (for simplicity, we have set the lattice constant to unity) that can be empty or occupied by spinless fermions, created/annihilated by $c_i^\dagger / c_i$ operators. These operators fulfill the canonical fermionic commutation relations $\{c_i^\dagger, c_j\} = \delta_{i,j}$, all other anti-commutators being zero.

The hopping between neighboring sites is denoted by $t = |t|e^{i\phi}$, μ is the chemical potential and $\Delta = |\Delta|e^{i\theta}$ is the superconducting order parameter. The latter parameter is accompanied by two creation or annihilation operators, describing the creation or annihilation of electron pairs living on *neighbouring sites*. These terms will, as shown below, be responsible for the p-wave pairing of electrons. We note that ordinary on-site s-wave pairing is not possible for spinless fermions due to the Pauli principle.

We shall now use the framework of TSM to study this model and explore the underlying topology and the edge states manifesting the bulk-boundary correspondence.

3.1.2 Topological Invariants

We start our investigation by imposing periodic boundary conditions and write the Hamiltonian (3.1) in momentum space using Equation (2.2). We introduce the Nambu (or particle/hole) spinor $\Psi_k^\dagger = (c_k^\dagger, c_{-k})$, so that the Hamiltonian can be written as $\mathcal{H} = \frac{1}{2}\sum_k \Psi_k^\dagger h(k) \Psi_k$ with the two-dimensional BdG-Hamiltonian $h(k)$ given by

$$h(k) = \big(-\mu - 2|t|\cos(k+\phi)\big)\tau_z - 2\Re(\Delta)\sin(k)\tau_y + 2\Im(\Delta)\sin(k)\tau_x. \tag{3.2}$$

The Pauli-matrices τ_i act in particle-hole spinor space, and $\Re$ and $\Im$ denote the real and imaginary parts respectively. The energy bands are given by[§]

$$\epsilon_\pm(k) = \pm\left[\big(\mu + 2|t|\cos(k+\phi)\big)^2 + 4|\Delta|^2\sin^2(k)\right]^{1/2}. \tag{3.3}$$

These bands are plotted in Figure 3.1 for the choice $\phi = 0$, corresponding to taking t to be real which we shall do for the remainder of this section. A most notable feature of this band structure is that the effective gap, $\tilde{\Delta}(k) \equiv \epsilon_+(k) - \epsilon_-(k)$, depends on the Bloch momentum k and that the wire is *gapless*

[§]This is most easily derived by using the identity $h(k)^2 = \mathbb{1}\epsilon(k)^2$, holding for any Hamiltonian expressed as a linear combination of Pauli matrices.

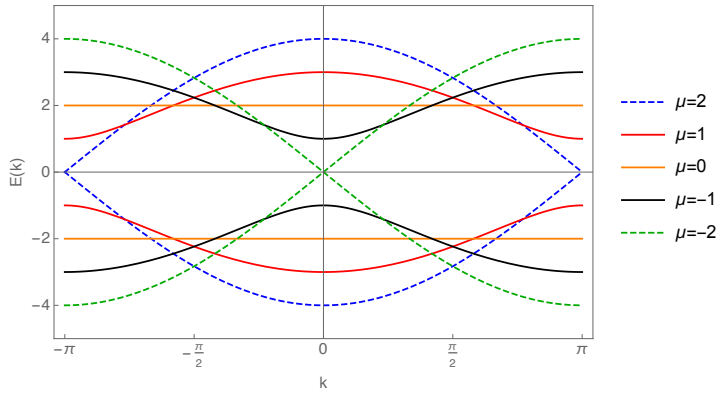

Figure 3.1: The spectrum of the bands in Equation (3.3) with $\phi = 0$. The chemical potential, μ, is varied while other parameters are fixed to $t = \Delta = 1$. The gap closes at $k = 0$ and $k = \pi$ for $\mu = -2$ and $\mu = 2$ respectively.

when $\mu = \pm 2t$. The gap closing points in the BZ are then at $k = 0$ or $k = \pi$ (we recall that $\pm\pi$ refers to the same point in the BZ). As we soon shall see, these two gap closing points constitute the topological phase transitions between two topologically distinct phases of matter.

Regarding symmetries, the Bloch Hamiltonian (3.2) admits generally only a single one, namely PHS which in the chosen basis is given by

$$\tau_x h(k)^T \tau_x = -h(-k), \tag{3.4}$$

where one needs to eliminate ϕ in favor for transforming θ with a gauge transformation. With this single symmetry, we note from Section 2.4 that the Kitaev Wire belongs to CAZ symmetry class D having a $\mathbb{Z}_2$-invariant distinguishing two topological regimes. We shall now explicitly construct this invariant.

Motivation of an Invariant

The physical motivation for finding an invariant can be thought of in the following way [ASv$^+$15]. The PHS of the BdG Hamiltonian enforces the spectral constraint that eigenstates come in pairs: Given an energy eigenstate $|\Psi\rangle$ with energy E, there will be another eigenstate $|\tilde{\Psi}\rangle = \mathcal{P}|\Psi\rangle$ with energy $-E$. This follows directly from Equation (2.11). Therefore, the spectrum of a general BdG-Hamiltonian is always mirror symmetric around $E = 0$.

We can now think of deforming two arbitrary BdG-Hamiltonians into each other and calculating the energy spectrum at all steps in the deformation. In this process, we may find that some energy levels cross at $E = 0$. In general, such an energy crossing is related to some conserved quantity. A general BdG Hamiltonian actually has a conserved quantity which is the parity. Remember that a superconductor does not conserve the particle number due to the

pairing terms, but provided that the superconductor is isolated, it conserves the particle number modulo two, which is the fermionic parity.

The parity is not a single particle property but one of the many body state. To relate the energy crossings to the parity we have to recall that the BdG-doubling we perform to extract the single particle spectrum is artificial and that the two $\pm E$ states actually refers to a *single* state. This state is a superposition of particles and holes, a so called Bogoliubov quasiparticle (sometimes the word Bogoliubon is used) state. An interpretation of the doubling is therefore that occupying a quasiparticle in the state $-E$ is the same as emptying the one with energy $+E$.

When a zero energy crossing occurs during the deformation, one energy state changes sign and it becomes energetically favorable to add or remove one quasiparticle. Thus, the ground state parity will change by one at a zero energy crossing. Therefore the crossings are sometimes called *fermion parity switches*.

It is thus natural to use the ground state parity as a topological invariant since it can not change unless some state crosses zero energy, that is the gap closes. The mathematical quantity appropriate to describe the parity switch is the Pfaffian which is introduced by the following argument.

Since the energy eigenvalues of the Hamiltonian $\mathcal{H}$ come in $\pm E_n$ pairs, the product of them, the determinant, can be written $\det(\mathcal{H}) = \prod_n (-E_n)^2$ being zero when the gap closes and some energy crosses zero. The Pfaffian is defined as the square root of the determinant $\mathrm{Pf}(H) = \pm i \prod_n E_n$ and is valid for any skew-symmetric matrix: $A^T = -A$. Any BdG-Hamiltonian can due to the PHS be written in such a way, see below.

At a zero energy crossing, a single state changes it's sign which in turn forces a sign change of the Pfaffian. The sign of the Pfaffian is therefore a topological invariant for a superconductor. As will be argued below, for a translationally invariant system, the Pfaffian of the Hamiltonian is actually only interesting at certain points in the BZ due to the PHS. We shall now use this idea to express the Kitaev Wire topological invariant in terms of it's parameters.

The Pfaffian Invariant

Our starting point is to formally re-write the Hamiltonian (3.1) in terms of Majorana operators: $c_j^\dagger = \exp(i\theta/2)(\gamma_{Aj} - i\gamma_{Bj})/2$. See also Ref. [Kit01] and Equations (3.9) and (3.11) below. The Hamiltonian is then on the general Majorana form which can be written for any translationally invariant quadratic Hamiltonian:

$$\mathcal{H} = \frac{i}{4} \sum_{ij} B_{\alpha\beta}(i-j)\gamma_{\alpha i}\gamma_{\beta j}. \tag{3.5}$$

Here $B_{\alpha\beta}$ are components of $\mathbf{B}$, a real and anti-symmetric matrix. For the Kitaev Wire, we have $i - j = +1, -1, 0$ due to the restriction to next nearest

hopping and on-site chemical potential. We can Fourier transform this matrix according to

$$\tilde{B}_{\alpha\beta}(q) = \sum_{\delta} e^{iq\delta} B_{\alpha\beta}(\delta), \tag{3.6}$$

where δ is a nearest neighbor vector, $\delta = +1, -1, 0$, and α,β labels the species of Majorana operators; in the present case α,$\beta = \{A,B\}$.

As has been argued by Kitaev [Kit01], the relevant quantity for a BdG topological invariant is $\nu = \mathrm{sgn}(\mathrm{Pf}(\tilde{\mathbf{B}}(0))\mathrm{Pf}(\tilde{\mathbf{B}}(\pi)))$ defined in terms of the Pfaffian of $\tilde{\mathbf{B}}(q)$. This is because the energies fulfill $\epsilon(k) = -\epsilon(-k)$ and Kitaev shows that only the points where $k = -k$ need to be considered since all other points together yields a unit contribution the Pfaffian. The remaining points are thus $k = 0$ and $k = \pi$ which happen to be the gap closing points.

Further, the Pfaffian is only defined for anti-symmetric matrices and takes a particularly simple form for 2×2 matrices: $\mathrm{Pf}[A] = A_{12}$, the upper right element.

Thus, the only quantities we have to calculate is $\tilde{B}_{A,B}(q)$ for $q = 0$ and $q = \pi$. This gives $\mathrm{Pf}(\mathbf{B}(0)) = 2\mu - 4t$ and $\mathrm{Pf}(\mathbf{B}(\pi)) = 2\mu + 4t$. Finally, this gives $\nu = \mathrm{sgn}(|\mu| - 2t)$ as the topological invariant for the Kitaev Wire, in agreement with the intuition that the parameters allowing the gap to close, $\mu = \pm 2t$, should yield an ill-defined invariant.

The Geometric Invariant

There is an easier and more visual way of determining the $\mathbb{Z}_2$-invariant [Ali12]. Consider Equation (3.2) but on the form $h(k) = \vec{d}(k) \cdot \vec{\tau}$, where $\vec{\tau}$ is the vector of Pauli matrices in particle-hole space. Since the basis spinors satisfy $\Psi_k = \tau_x \Psi^T_{-k}$, the vector $\vec{d}(k)$ must satisfy $d_{x,y}(k) = -d_{x,y}(-k)$ and $d_z(k) = d_z(-k)$ which can be straightforwardly checked. Thus, is suffices to investigate $\vec{d}$ on half the BZ ($0 \leq k \leq \pi$) since the other half follows from these constraints.

Suppose now that the Hamiltonian is gapped in the whole BZ. This sets the constraint $|\vec{d}(k)| \neq 0$, $\forall k$ and a unit vector $\hat{d}(k)$ can be defined. This unit vector now provides a map from half of the BZ to the unit sphere. See Figure 3.2. When sweeping k from 0 to π, $\hat{d}(k)$ starts from either the north or south pole, and ends up back at the same pole or at the opposite one depending on the sign of $-\mu - 2t$. Explicitly, $\hat{d}(0) = \mathrm{sgn}(-2t - \mu)\hat{z}$ and $\hat{d}(\pi) = \mathrm{sgn}(2t - \mu)\hat{z}$ so that the product $\nu = \mathrm{sgn}(|\mu| - 2t) = \pm 1$ defines a $\mathbb{Z}_2$-invariant which only can change when the bulk gap closes resulting in $\hat{d}(k)$ being ill-defined for some k. The signs corresponding to a specific pole on the sphere depends on the chosen spinor basis, but the product is invariant under any such choice.

We note that this geometric invariant is the same as the Pfaffian invariant, as it should be.

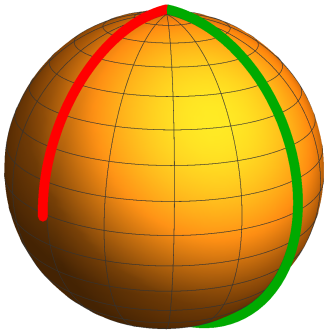

Figure 3.2: Two types of allowed trajectories of the vector $\hat{d}(k)$ when sweeping the BZ. The green curve goes from pole to pole resulting in a non-trivial phase. The red curve, on the other hand, goes from one pole back to the same, resulting in a trivial phase. These types of trajectories can not be deformed into each other without closing the gap.

The Winding Invariant

We shall also look at the topological invariant in a somewhat different setting. Consider a situation where Δ is real, or has a constant phase which can be globally gauged away.

It is then possible to choose $\vec{d}(k)$, defined in the previous section, to be two-dimensional. Without loss of generality, we make the choice $\vec{d}(k) = (0, -2\Delta\sin(k), -\mu - 2t\cos(k))^T$. We have that the gap is given by $|\vec{d}(k)|$. Consider now $\hat{d}(k)$ in the two dimensional $\tau_z - \tau_y$ plane. Fixing the values of μ and t and sweeping k from 0 to 2π, we can define a winding number equal to the number of revolutions $\hat{d}(k)$ makes around the origin. This winding can only take the values $1, -1, 0$ giving a $\mathbb{Z}$ invariant which will depend on the sign of Δ. The invariant can now be written as $\nu = \Theta(2t - |\mu|)\mathrm{sgn}(\Delta)$. See Figure 3.3.

The origin of this $\mathbb{Z}$ invariant can be understood from the classification table. Due to the constraint on Δ to be real, the Hamiltonian gains the additional PTRS, for spinless fermions equal to $\mathcal{T} = \mathcal{K}$ in our basis. This moves the Kitaev chain from class D to class BDI hosting the $\mathbb{Z}$ invariant. Out of these numbers only the set $\{+1, -1, 0\}$ is realized in the Kitaev Wire.

Due to this winding invariant, there is now a distinction between Kitaev Wires with opposite sign of the order parameter. We can then think of a situation where one half of a wire has a fixed zero superconducting phase, while the other has a phase of π, effectively yielding a negative value of Δ. The topological invariant is then different in these halves forcing the gap to

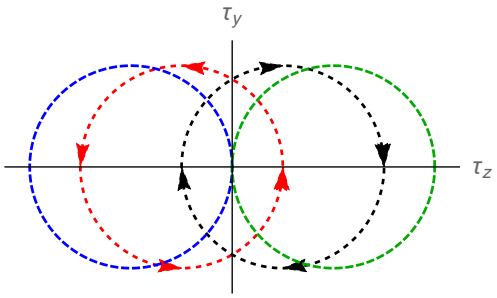

Figure 3.3: Winding around the origin of the vector $\vec{d}(k)$ as k goes from 0 to 2π. For the red curve $t = \Delta = \mu = 1$, the black has $t = -\Delta = \mu = 1$ and the blue and green curves correspond to gap closing points $t = \Delta = \pm\mu/2 = 1$. note that the gap closing curves correspond to ill-defined winding numbers as they cross the origin.

close. Due to the bulk-boundary correspondence, the gap has to close in this region, generating edge states. Exploring these edge states will be the topic of Chapter 4.

As a final remark we note that it is possible to write the winding invariant as

$$\nu = \frac{1}{2\pi i}\int_0^{2\pi} \partial_k \log\left[d_z(k) + i d_y(k)\right], \tag{3.7}$$

so that it properly counts the number of counter-clockwise revolutions $\vec{d}(k)$ performs as k sweeps through the BZ.

3.1.3 Appearance of Majorana Bound States

To see how Majorana Bound States (MBS) appear in this model we again follow Ref. [Kit01] and formally rewrite the fermionic operators on each site in terms of two *real* Majorana operators (Majoranas for short), A and B, defined by

$$\begin{aligned}\gamma_{Aj} &= \exp(+i\frac{\theta}{2})c_j + \exp(-i\frac{\theta}{2})c_j^\dagger \\ \gamma_{Bj} &= -i\exp(+i\frac{\theta}{2})c_j + i\exp(-i\frac{\theta}{2})c_j^\dagger.\end{aligned} \tag{3.8}$$

Here, θ is the superconducting phase $\Delta = |\Delta|e^{i\theta}$. We shall frequently also have use for the inverse relation

$$\begin{aligned}c_j &= \frac{\exp(-i\frac{\theta}{2})}{2}(\gamma_{Aj} + i\gamma_{Bj}) \\ c_j^\dagger &= \frac{\exp(+i\frac{\theta}{2})}{2}(\gamma_{Aj} - i\gamma_{Bj}).\end{aligned} \tag{3.9}$$

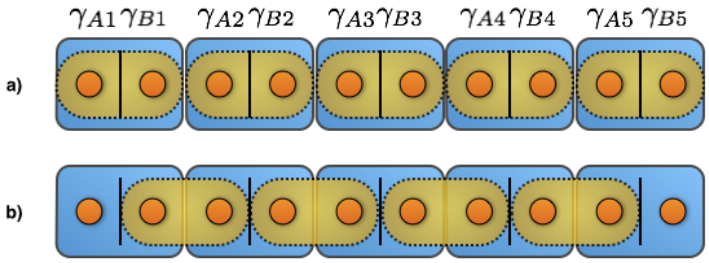

Figure 3.4: Two types of Majorana pairing in a wire with five electronic sites. In (a), the MBS are paired on the same site, while in (b), they couple from site to site, leaving two unpaired MBS, γ_1 and γ_{10}, at the edges.

The commutation relations for the Majoranas follows immediately from the fermionic ones, yielding

$$\{\gamma_{Ai},\gamma_{Bj}\} = 2\delta_{A,B}\delta_{i,j}. \tag{3.10}$$

In terms of Majorana operators, the Hamiltonian (3.1) becomes

$$\mathcal{H} = \frac{i}{2}\sum_j \left[-\mu\gamma_{Aj}\gamma_{Bj} + (|\Delta| + t)\gamma_{Bj}\gamma_{Aj+1} + (|\Delta| - t)\gamma_{Aj}\gamma_{Bj+1}\right]. \tag{3.11}$$

In this Majorana formulation, the interesting behaviour is revealed for two specific choices of parameters. We first make the choice $\Delta = t = 0$ and $\mu < 0$, yielding

$$\mathcal{H} = \frac{i|\mu|}{2}\sum_{j=1}^{N}\gamma_{Aj}\gamma_{Bj} = |\mu|\sum_{j=1}^{N}\left[c_j^\dagger c_j - \frac{1}{2}\right]. \tag{3.12}$$

We observe that the two Majoranas from the same site are coupled together forming an insulating system with a single gapped ground state with zero occupancy. See Figure 3.4a. As argued by Kitaev, this insulating behaviour extends to the whole parameter range $|\mu| > 2t$. This can be intuitively be understood by the following argument. With $\Delta = 0$, the band structure is simply $\epsilon(k) = -2t\cos(k) - \mu$ as shown in section 2.2. Realizing that $\mu < -2t$ is the region where no particles at all are present in the band, the chosen regime is definitely an insulator since pairing occur between empty levels. The region $\mu > 2t$ however corresponds to a completely full band, yielding a Pauli blockade which implies insulating behaviour as well.

The second choice we make is to put $\Delta = t$ and $\mu = 0$. In terms of Majorana operators we obtain the Hamiltonian

$$\mathcal{H} = it\sum_{j=1}^{N-1}\gamma_{Bj}\gamma_{Aj+1} = 2t\sum_{j=1}^{N-1}\left[\tilde{c}_j^\dagger\tilde{c}_j - \frac{1}{2}\right]. \tag{3.13}$$

We have in the second equality defined a new set of fermion operators by $\tilde{c}_j = \frac{1}{2}(\gamma_{Bj} + i\gamma_{Aj+1})$. Here, we note that for this parameter choice, the Majoranas are coupled between *neighbouring* sites. See Figure 3.4b.

Remarkably, the expression (3.13) does not include the two Majoranas γ_{A1} and γ_{BN}. These can be combined into a single fermionic operator $f = \frac{1}{2}(\gamma_{A1} + i\gamma_{BN})$, which has zero energy (being absent from the Hamiltonian) and is completely delocalized between the two edges of the system. Due to the zero energy of this fermionic state, there are two degenerate ground states differing in fermionic parity.

The situation of having a delocalized fermionic state, or equivalently two separately located MBS, extends to the parameter range $|\mu| < 2t$. Now the zero energy MBS are not given by γ_{A1} and γ_{BN} but rather by some complicated linear combination of Majorana operators. The corresponding wave functions now decay exponentially $e^{-L/\xi}$, where L is the wire length, into the wire bulk on a length scale given by the superconducting coherence length $\xi \propto t/\Delta$. The overlap of the wavefunctions then results in a splitting between the two degenerate ground states on the same length scale, effectively giving the edge states finite energy. This is usually referred to as *gapping out* the states. But if the wire is sufficiently long, the overlap is negligible and the states remain at zero energy.

As we shall see shortly, this is a manifestation of the bulk-boundary correspondence. But first, we shall look at the MBS explicitly.

3.1.4 Real Space Calculation

Using the formalism presented in Section 2.2 we write down an open Kitaev Wire with N unit cells as a $2N \times 2N$ matrix $\mathbf{H}$. We use the basis states $\{|i\rangle\}_i$, unit-vectors of length $2N$ where non-zero entries on even respectively odd positions corresponds to occupied holes and electrons respectively.

To clarify, an open system with 6 sites would in this basis explicitly be

$$\mathbf{H}_{6\times 6} = \begin{bmatrix} H_{\text{on}} & H_{\text{off}} & 0 & 0 & 0 & 0 \\ H_{\text{off}}^\dagger & H_{on} & H_{\text{off}} & 0 & 0 & 0 \\ 0 & H_{\text{off}}^\dagger & H_{\text{on}} & H_{\text{off}} & 0 & 0 \\ 0 & 0 & H_{\text{off}}^\dagger & H_{\text{on}} & H_{\text{off}} & 0 \\ 0 & 0 & 0 & H_{\text{off}}^\dagger & H_{\text{on}} & H_{\text{off}} \\ 0 & 0 & 0 & 0 & H_{\text{off}}^\dagger & H_{\text{on}} \end{bmatrix}. \tag{3.14}$$

Here $H_{\text{on}} = -\mu\tau_z$ and $H_{\text{off}} = -t\tau_z - i\Re(\Delta)\tau_y + i\Im(\Delta)\tau_x$, themselves being 2×2 matrices. They represent the internal particle-hole degree of freedom on each site. Such a Hamiltonian can be straightforwardly diagonalized on a computer, where the eigenstates are particle/hole occupations along the wire, and the eigenvalues are the single particle energies. The great advantage of this approach is that site dependent parameters can easily be implemented just by modifying $H_{\text{on/off}}$ for any site.

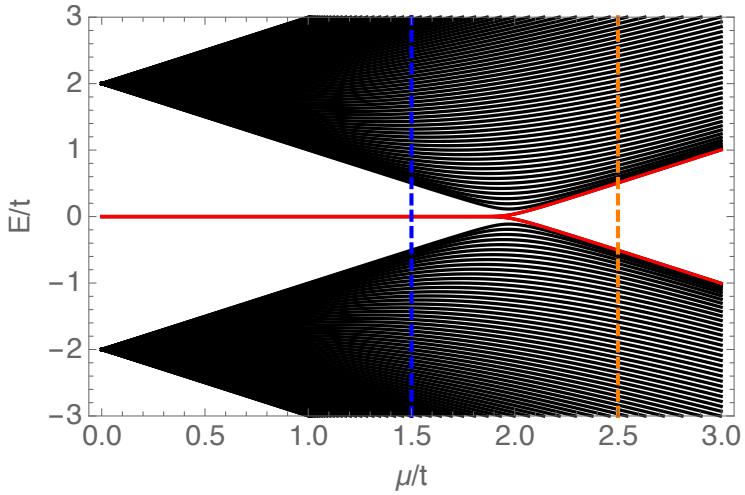

Figure 3.5: The energy spectrum of the Kitaev Wire as the chemical potential μ is varied. The superconducting gap $\Delta = 1$ and the number of sites $N = 80$. The lowest energy states are marked in red. The blue and orange lines marks parameter choices corresponding to the trivial and non-trivial phase respectively. Note that the gap closes at $\mu = 2t$.

In Figures 3.5 and 3.6 we show that the lowest energy states in the two distinct phases correspond to exponentially localized and delocalized states respectively.

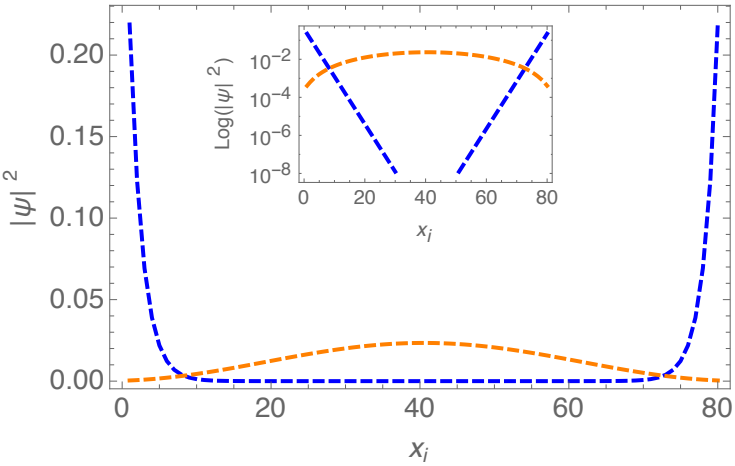

Figure 3.6: Lowest energy states of the Kitaev Wire for the two parameters choices in Figure 3.5. The inset shows the same states but on a logarithmic scale, showing that the non-trivial edge states are exponentially localized.

3.1.5 Non-Abelian Statistics

We have previously mentioned that the MBS fulfill *non-Abelian statistics*. We shall now give a brief explanation of what that means.

It is well known in quantum mechanics that the wave function of a system of bosons or fermions has to be symmetric or anti-symmetric respectively upon exchange of any two particles. The generated $\pm$-sign can be viewed as if the wave function acquires a phase of 0 or π.

This fact breaks down in spatial dimensions $d \leq 2$ [LM77]. In one dimension, the concept of bosons and fermions is not even meaningful, since particles can not be exchanged living on a line. This observation leads to the concepts of *bosonization* and the Luttinger Liquid [Hal81].

In two dimensions, it is possible for the wave function to pick up *any* phase resulting in so called *anyonic* statistics [Wil82]. Particles having this peculiar property are referred to as *anyons*.

For simplicity we shall now consider a system of four Majoranas made out of two fermionic states. We can for example think of a system of four vortices on a two-dimensional p-wave superconductor. We construct the fermionic creation operators

$$c_1^\dagger = \frac{1}{2}(\gamma_1 + i\gamma_2), \quad c_2^\dagger = \frac{1}{2}(\gamma_3 + i\gamma_4) \tag{3.15}$$

and their respective annihilation operators. We know that the Majoranas are midgap states at zero energy and we shall employ the adiabatic assumption – all involved energy scales are much smaller that the gap. The MBS then form a four-fold degenerate ground state manifold, since all fermionic states can be occupied or empty with the same energy cost. The four basis states of the manifold are

$$|00\rangle \quad |11\rangle \quad |10\rangle \quad |01\rangle\,, \tag{3.16}$$

where the three latter states are constructed by acting with the fermionic creation operators on the vacuum state $|00\rangle$, defined by $c_i\,|00\rangle$ for $i = 1{,}2$. For example, $|11\rangle = c_1^\dagger c_2^\dagger\,|00\rangle$.

It is crucial to understand that there never can be any single occupation of a Majorana state. There is not even a way of constructing a sensible number operator since $\gamma_j^\dagger \gamma_j = \gamma_j \gamma_j \equiv 1$.

The operator exchanging two Majoranas, m and n can be derived on quite general premises (see Refs. [Ali12, ASv$^+$15] for instance). Requiring parity conservation, locality (in the sense that only the exchanged Majorana operators should be involved) and unitarity yields the operator

$$B_{mn} = \frac{1}{\sqrt{2}}(1 \pm \gamma_m \gamma_n), \tag{3.17}$$

where the two signs correspond to clock- or anti-clockwise exchange. In the remainder of this section, we shall only use the clock-wise exchange operator.

The exchange operator acts on the Majoranas according to

$$\begin{aligned} B_{mn}\gamma_m B_{mn}^\dagger &= -\gamma_n \\ B_{mn}\gamma_n B_{mn}^\dagger &= +\gamma_m, \end{aligned} \tag{3.18}$$

which is verified using Equation (3.10). Let us now see what happens if we start from the state $|00\rangle$ and exchange Majorana number 1 and 3:

$$B_{13}\,|00\rangle = \frac{1}{\sqrt{2}}(1+\gamma_1\gamma_3)\,|00\rangle = \frac{1}{\sqrt{2}}(1+c_1^\dagger c_2^\dagger)\,|00\rangle = \frac{1}{\sqrt{2}}(|00\rangle + |11\rangle). \tag{3.19}$$

We note that by exchanging two of the Majoranas, we have obtained a superposition of states. This is fundamentally different from just picking up an overall phase. It is also clear that this exchange is interesting for constructing qubits, the cornerstone of a potential quantum computer.

If we perform two exchanges in a row, something interesting occurs. The order of exchange matters. For instance we can check that

$$B_{12}B_{23} \neq B_{23}B_{12} \Leftrightarrow [B_{12},B_{23}] \neq 0, \tag{3.20}$$

independently of the starting state. With some further analysis, one can show that the exchange operators B_{mn} form a representation of a group called the *Braid group*. If the group elements in a group fail to commute like in Equation (3.20), the corresponding group is said to be non-Abelian. This is the reason for calling MBS non-Abelian particles.

This calculation was done in two dimensions while the MBS we have considered previously exist in a one-dimensional setting. It is then natural to ask if the concept of braiding or exchange is meaningful in the Kitaev Wire. The answer to this question is yes. In Ref. [AOR$^+$11] it is reported that non-Abelian exchange can be performed in a setup where the MBS are moved around using electronic gates in T-junction networks of Kitaev Wires.

3.2 The Majorana Wire Model

Although the Kitaev wire is just a toy model, it can actually be realized as the low energy regime of more realistic setups. Two prominent directions of research are magnetic impurity chains on top of superconducting slabs [CEAB11,NPDBY13,NPDL$^+$14,PGv14] and superconducting nanowires with strong spin orbit coupling in external magnetic fields [LSDS10, ORv10]. In this section we shall focus on the latter setup which can be motivated as follows.

Since no p-wave superconductor candidates have been found in nature, the idea is to engineer one by combining simple and existing building blocks [ASv$^+$15]. To start with, we want to have a one-dimensional system with a "tweakable" band structure. For this purpose, semiconducting nano wires are useful, since the chemical potential can be manipulated by doping or external gate electrodes. Our starting Hamiltonian is then

$$\mathcal{H}_0 = (-\frac{\partial_x^2}{2m} - \mu)\sigma^0, \tag{3.21}$$

where m is the effective mass, μ the chemical potential and σ^0 the unit matrix in spin space, reflecting the spin degeneracy of the bare Hamiltonian. The band structure then has four Fermi points, due to right-left movers and spin degeneracy, and any superconducting pairing would be s-wave. To get spinless fermions with p-wave pairing, as in the Kitaev Wire, we need to isolate one of the spin components.

For this purpose Rashba spin-orbit coupling (SOC) is useful. This term can be written as

$$\mathcal{H}_\alpha = -i\alpha\sigma^y\partial_x, \tag{3.22}$$

and can be viewed as a "magnetic field" with momentum dependence. We have chosen the SOC to favor spin alignment in the y-direction. So far, we still have four Fermi points.

By also adding a magnetic field we can reduce the number of Fermi points to two, since a magnetic field shifts the spin components oppositely in energy. A term modeling this is

$$\mathcal{H}_Z = h\sigma^z, \tag{3.23}$$

and leads to a spinless regime, if the chemical potential, μ, is chosen to lie in the induced Zeeman gap at $k = 0$. It is important that the magnetic field is not parallel to the SOC in Equation (3.22) since they would just reinforce each other in a momentum dependent way and the number of Fermi points would remain four.

Finally, we can add superconductivity. Placing a one-dimensional wire close to an ordinary s-wave superconductor will induce superconducting correlations into the wire by Andreev reflection. We crudely model this by

$$\mathcal{H}_\Delta = \Re(\Delta)\tau^y\sigma^y - \Im(\Delta)\tau^x\sigma^y, \tag{3.24}$$

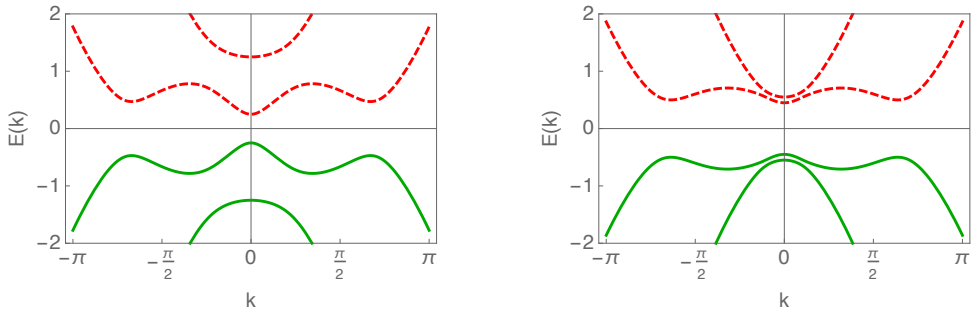

Figure 3.7: The spectrum of the Hamiltonian (3.28) for the topological phase (left) and trivial phase (right). Parameters used are $m = 0.5$, $\mu = 0.0$, $\alpha = 1.0$ and $\Delta = 0.5$ and $h = 0.75$(left) and $h = 0.05$ (right). Green, filled lines are occupied states and red, dashed lines are empty states. There is no concrete way of distinguishing topological from trivial phase from analyzing the spectrum.

where we have extended the spinor basis states to the Nambu-spin space by introducing additional Pauli-matrices τ^i by BdG-doubling.

All together, the terms we have introduced generate the spectrum shown in Figure 3.7, where we have plotted the spectra for the topological and trivial phases which will be derived below. Note that the spectrum itself does not allow for any distinction between topological and trivial phases. In summary, the Kitaev Wire can be realized in an ordinary mesoscopic setting consisting of a spin-orbit coupled wire in proximity to an ordinary s-wave superconductor both exposed to an external magnetic field. For certain values of the external parameters, the superconducting wire will enter a topological superconducting phase hosting MBS.

In the remainder of this section, we shall study the model describing this setup. To start with, we shall write down the total real-space Hamiltonian, both in the continuum limit and and on a lattice. Next, we derive the corresponding BdG-Hamiltonians and explore their bulk topology proving that they indeed have a non-trivial phase. Then we derive the topological invariants and explore the phase diagrams. The section concludes with a brief discussion of recent experimental progress to detect topological superconductivity.

3.2.1 Hamiltonians

Our starting point is a one-dimensional nanowire lying in the x direction. There is a strong spin orbit coupling favoring spin alignment in the y direction and also an external magnetic field in the z direction. The precise spin-orbit and magnetic field directions are not important as long as they are

perpendicular. In addition, the wire lies close to an ordinary s-wave superconductor inducing superconducting correlations in the wire by the proximity effect. As motivated above, this setup can be modeled by

$$\mathcal{H} = \mathcal{H}_{\text{wire}} + \mathcal{H}_{\Delta}, \tag{3.25}$$

$$\mathcal{H}_{\text{wire}} = \int dx\ \psi^{\dagger}_{\sigma}\left(-\frac{\partial_x^2}{2m} - \mu - i\alpha\sigma^{y}_{\sigma\sigma'}\partial_x + h\sigma^{z}_{\sigma\sigma'}\right)\psi_{\sigma'}, \tag{3.26}$$

$$\mathcal{H}_{\Delta} = \int dx\left(\Delta\psi_{\uparrow}\psi_{\downarrow} + \Delta^{*}\psi^{\dagger}_{\downarrow}\psi^{\dagger}_{\uparrow}\right). \tag{3.27}$$

Here $\psi^{\dagger}_{\sigma}$ is the creation operator of an electron with effective mass m and spin σ, the chemical potential is denoted μ (measured from the bottom of the band) and the spin orbit coupling, magnetic field strength and superconducting paring are given by α, h and Δ respectively. Repeated spin indices are implicitly summed over and any position dependence has been suppressed.

To explore the band structure of this system, we close the wire into a ring and write the Hamiltonian for a translationally invariant system as $\mathcal{H} = \frac{1}{2}\int dk\ \Psi^{\dagger}h(k)\Psi$ with

$$h(k) = \left[(\frac{k^2}{2m} - \mu)\tau^{z}\sigma^{0} + h\tau^{z}\sigma^{z} + \alpha\tau^{z}\sigma^{y}k + \Re(\Delta)\tau^{y}\sigma^{y} - \Im(\Delta)\tau^{x}\sigma^{y}\right], \tag{3.28}$$

where τ^i and σ^i are Pauli matrices for particle-hole and spin space respectively. We have in this expression used the basis $\Psi = (\psi_{\uparrow},\psi_{\downarrow},\psi^{\dagger}_{\uparrow},\psi^{\dagger}_{\downarrow})^{T}$. The symbols $\Re$ and $\Im$ denotes real and imaginary parts respectively.

For numerical calculations it is useful to discretize the Hamiltonian (3.25) on a lattice[§] which yields the following tight binding Hamiltonian:

$$\begin{aligned}
\mathcal{H}_{TB} = &\frac{1}{2}\sum_{i=1}^{N-1}\left[\Psi^{\dagger}_{i}(-t\tau^{z}\sigma^{0})\Psi_{i+1} + h.c.\right] \\
&+ \frac{1}{2}\sum_{i=1}^{N}\left[\Psi^{\dagger}_{i}(-\mu - 2t)\tau^{z}\sigma^{0}\Psi_{i}\right] \\
&+ \frac{1}{2}\sum_{i=1}^{N}\left[\Psi^{\dagger}_{i}(h\tau^{z}\sigma^{z})\Psi_{i}\right] \\
&+ \frac{1}{2}\sum_{i=1}^{N}\left[\Psi^{\dagger}_{i}(\Re(\Delta)\tau^{y}\sigma^{y} - \Im(\Delta)\tau^{x}\sigma^{y})\Psi_{i}\right] \\
&+ \frac{1}{2}\sum_{i=1}^{N-1}\left[\Psi^{\dagger}_{i}(-\frac{i\alpha}{2}\tau^{z}\sigma^{y})\Psi_{i+1} + h.c.\right].
\end{aligned} \tag{3.29}$$

[§]This is most conveniently done by approximating derivatives with finite differences: $\partial_x f(x) \approx \frac{1}{2a}(f_{i+1} - f_{i-1})$, where f is any function and a is the lattice constant.

The terms represent in order: nearest neighbor hopping, chemical potential, magnetic Zeeman splitting, proximity superconductivity and spin orbit coupling (spin flip hopping). We set the lattice constant to unity and the hopping amplitude $t \equiv 1/(2m)$. Note that the chemical potential μ still is measured from the bottom of the (normal state) band.

The Bloch Hamiltonian corresponding to Equation (3.29) with imposed periodic boundary conditions is given by

$$h_{TB}(k) = \Big[(-2t\cos(k) + 2t - \mu)\tau^z\sigma^0 + h\tau^z\sigma^z \\ - i\alpha\tau^z\sigma^y\sin(k) + \Re(\Delta)\tau^y\sigma^y - \Im(\Delta)\tau^x\sigma^y\Big], \tag{3.30}$$

where now $k = \frac{2\pi n}{N}$, $n = 0,..., N-1$. The models (3.28) and (3.30) can be seen to agree for $k \ll 1$.

As we shall now show, the Hamiltonians in this section are characterized by a bulk topological invariant. The non-trivial phase is characterized by MBS on interfaces between topologically distinct sections of finite systems. So in essence, this setup is a physical realization of the Kitaev Wire in section 3.1. In the remainder of this section, we shall use the discretized version of the setup.

3.2.2 Symmetry Classes and Topological Invariants

The Hamiltonian (3.30) has PHS given by the operator $P = \tau^x\sigma^0$ in our chosen basis. We see that $P^2 = +1$ so the Hamiltonian belongs to symmetry class D which is characterized by a $\mathbb{Z}_2$ topological invariant.

The spectrum is most easily derivied by squaring the Hamiltonian and the class D invariant can be obtained with the same method as in section 3.1. It is given by

$$\nu_{\mathbb{Z}_2} = \mathrm{sgn}(h^2 - |\Delta|^2 - \mu^2)\cdot\mathrm{sgn}(h^2 - |\Delta|^2 - (4t-\mu)^2), \tag{3.31}$$

where $\nu_{\mathbb{Z}_2} = -1$ and $\nu_{\mathbb{Z}_2} = +1$ is the topological and trivial phase respectively. The formula is valid whenever the spectrum is gapped, requiring a non-zero SOC strength α. We note further that there are two critical magnetic fields

$$h_{c1} = \sqrt{|\Delta|^2 + \mu^2}, \quad \text{and} \quad h_{c2} = \sqrt{|\Delta|^2 + (4t-\mu)^2}, \tag{3.32}$$

where the gap closes. Between these critical fields, the wire will reside in the topological phase. In Figure 3.8, we have plotted the energy spectrum of the Hamiltonian (3.29) as a function of the magnetic field to observe the gap closing points and the zero modes related to the topological phase.

Enforcing the additional constraint on the superconducting order parameter $\Delta = \Delta^*$ (which is equivalent to a global choice of phase) introduces an additional pseudo time reversal symmetry (PTRS) through the operator

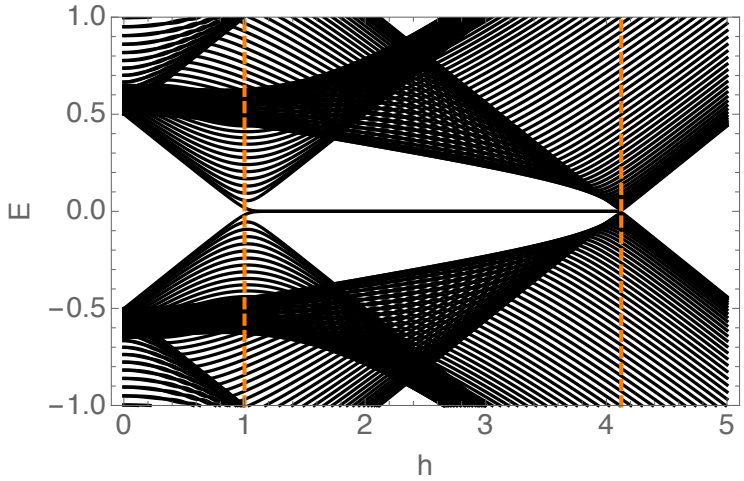

Figure 3.8: The energy spectrum of the nanowire in Equation 3.29 with length $N = 80$ as a function of magnetic field. Parameters used are: $t = \Delta = 1$, $\mu = 0$, $\alpha = 2$. The two critical fields $h_{c1} = 1$ and $h_{c2} = \sqrt{17}$, depicted in orange, are clearly seen to close the gap. In between the gap closing points lies the topological phase hosting Majorana zero modes.

$\mathcal{T} = \tau^0\sigma^0\mathcal{K}$ which fulfills $\mathcal{T}^2 = +1$. With this additional symmetry the Hamiltonian moves to class BDI which according to the CAZ table has a $\mathbb{Z}$ invariant.

To derive this invariant, we shall use a method described in Ref. [TS12]. We start with the Hamiltonian (3.30) and put it on the form

$$h_{TB}(k) = \hat{h}_0(k)\tau_z + i\hat{\Delta}\tau_y, \tag{3.33}$$

where, the hat denotes a 2×2 matrix in spin-space. We next perform a unitary transformation with the matrix $\mathrm{U} = \exp(-i\frac{\pi}{4}\tau_y)$ yielding

$$h_{TB}(k) \to U h_{TB}(k) U^\dagger = \begin{pmatrix} 0 & \hat{A}(k) \\ \hat{A}^T(-k) & 0 \end{pmatrix}, \tag{3.34}$$

with $A(k) = \hat{h}_0(k) + \hat{\Delta}$. We now have that

$$\mathrm{Det}(h_{TB}(k)) = \mathrm{Det}(U h_{TB}(k) U^\dagger) = \mathrm{Det}(A(k))\mathrm{Det}(A^T(-k)), \tag{3.35}$$

so that $\mathrm{Det}(A(k))$ can only vanish if $\mathrm{Det}(h_{TB}(k))$ does, which in turn requires a zero eigenvalue, or equivalently a closing of the gap. Explicitly, we have that

$$\mathrm{Det}(A(k)) = (-2t\cos(k) - \mu - 2t)^2 - h^2 + \Delta^2 - \alpha^2\sin^2(k) - 2i\alpha\Delta\sin(k). \tag{3.36}$$

We now consider the phase of $\mathrm{Det}(A(k))$, written as $z(k) = \exp(i\theta(k)) = \mathrm{Det}(A(k))/|\mathrm{Det}(A(k))|$ and count how many times it rotates around the origin

in the complex plane by writing

$$\nu_{\mathbb{Z}} = \frac{1}{\pi i} \int_{k=0}^{k=\pi} \frac{dz(k)}{z(k)}, \tag{3.37}$$

where we have used the property $A(k) = A^*(-k)$ to reduce the integral to half the BZ. We note further that a non-zero winding only occurs if the phase crosses the real axis at points on opposite sides of the origin. Additionally, the sign of the product $\alpha\Delta$ will determine the direction of the winding. With these observations we can finally write the BDI invariant for the nanowire as

$$\begin{aligned}\nu_{\mathbb{Z}} = \operatorname{sgn}(\alpha\Delta) \cdot \Theta(8t(2t-\mu) - (h^2 - \Delta^2 - \mu^2)) \\ \cdot \Theta(h^2 - \Delta^2 - \mu^2),\end{aligned} \tag{3.38}$$

which yields three different phases $\nu_{\mathbb{Z}} = \pm 1, 0$. Here, Θ denotes the Heaviside step function and we have assumed t, α, h and μ to be real. The $\nu_{\mathbb{Z}} = 0$ case, corresponding to no winding and therefore a trivial phase, can be identified with the trivial phase $\nu_{\mathbb{Z}_2} = +1$ in class D. For the invariant to be valid, the system is required to be gapped at all points in the BZ.

3.2.3 Phase Diagrams and Zero modes

Having derived the topological invariants, we are ready to investigate the consequences of the non-trivial phase. In Figures 3.9 and 3.10 , we have plotted the invariants as functions of the superconducting gap and the magnetic field. And as a comparison, from Figure 3.11, it is clear that the trivial phase is a gapped phase just as the non-trivial one, while the latter hosts zero energy modes, in correspondence with the bulk-boundary-correspondence. These states can be shown to be Majorana fermions by investigating the corresponding eigenvectors. We note further that the gap closes (resulting in an ill-defined invariant) at every transition between topologically distinct phases.

3.2.4 Discussion

In practice, it is not obvious how the parameters should be tuned to optimize the topological phase of the Majorana Wire. There are many subtle issues regarding the interplay between competing mechanisms that complicate the picture considerably.

First of all, the proximity coupling in the wire must not be too large, since a large inflow of particles from the underlying superconductor can push the Fermi level above the induced Zeeman gap.

Secondly, a large external field yields a larger freedom to place the chemical potential, while at the same time suppresses the induced superconductivity.

Another crucial issue is to assure that the nano-wire used is at least close to being one-dimensional, that is only one or a few transverse channels may be

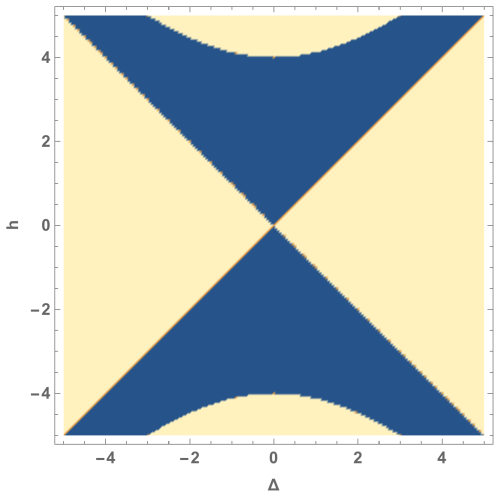

Figure 3.9: The topological invariant in Equation (3.31) for $\mu = 0$ and $\alpha = 1$. Blue means a value of -1 while light yellow means $+1$. Orange, seen at the transitions means an undefined invariant and corresponds to a closing of the gap.

occupied. For disordered wires, the detection of how many transverse channels that are occupied is a complicated task and the influence of more than one channel may affect the topological properties.

So while being ingenious and simple in theory, the realistic Majorana Wire described in this section is far from trivial, resulting in experiments that are hard to evaluate properly. The results of some of these experiments are discussed next.

3.2.5 Experimental Signatures of Majorana Bound States

In this section we comment briefly on some of the experimental developments in detecting MBS in nanoscale devices.

One conceptually simple method of detecting Majorana modes was reported in Refs. [LLN09, Fle10, J.L12]. The authors suggested that electron tunneling into the edge of a topological superconductor such as in section 3.2 would reveal the existence of a localized Majorana mode trough the quantized tunneling conductance at zero bias voltage.

Due to being perfectly particle-hole symmetric and being located at zero energy, the Majorana mode restricts the scattering matrix at the interface to yield perfect Andreev or normal reflection for any incoming electron state with subgap energy. Hence, the tunneling conductance can only be non-zero for perfect Andreev reflection and is therefore quantized to $2e^2/h$. This conductance can be shown to survive in the whole topological phase of the wire.

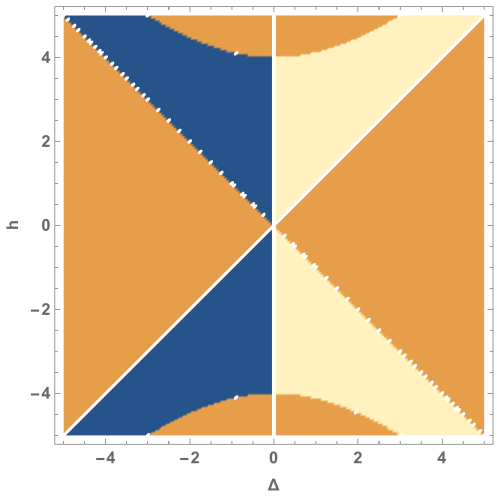

Figure 3.10: The topological invariant of Equation (3.38) for $\mu = 0$ and $\alpha = 1$. Blue means a value of -1 while light yellow means $+1$. Orange means a value of 0. At the transitions, the invariant is ill-defined, corresponding to a closing of the gap.

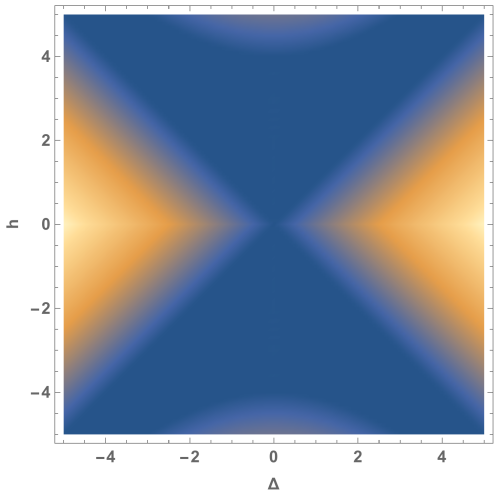

Figure 3.11: The lowest single particle energy of the Hamiltonian (3.29) with $N = 100$, $t = 1$, $\alpha = 1$, $\mu = 0$. Blue means zero energy.

Subsequent experiments [MZF+12,DYH+12,DRM+12], have generated results consistent with predictions, though alternative non-topological explanations of zero bias peaks have been provided. For example, Ref. [BA12] reports zero bias peaks due to disorder, and finite temperature has been shown to also influence the zero bias conductance [LPLL12].

Another proposed signature of MBS is the so called Fractional- or 4π-

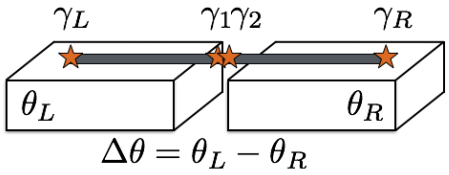

Figure 3.12: A setup for the Fractional or 4π Josephson effect. The two Majoranas in the center region couple via a tunneling junction. The outer Majoranas are localized far away and does not overlap with the central ones . The resulting single particle current is driven by the phase difference $\Delta\theta$ and is 4π-periodic.

Josephson Effect. Already in Ref. [Kit01] it was pointed out that the Majorana operators are 4π-periodic in the superconducting order parameter, see Equation (3.8). By placing two non-trivial wires in a Josephson junction setup, a measurement of the Josephson current would contain a topological contribution which is 4π-periodic in the phase difference of the order parameter.

We shall here present an explanation of this phenomenon closely following Ref. [Ali12]. The Kitaev Hamiltonian 3.1 is indeed 2π-periodic in the phase, true for any superconductor, but the physical states are not, which we now show.

The system can be modeled by coupling two MBS, γ_1 and γ_2, across a Josephson junction with a subgap effective Hamiltonian written as

$$\mathcal{H}_0 = -\frac{\Gamma}{2}\cos(\frac{\Delta\phi}{2})i\gamma_1\gamma_2 = -\Gamma\cos(\frac{\Delta\phi}{2})(n_0 - 1/2). \tag{3.39}$$

Here $\Gamma > 0$ is the coupling strength assumed to be small, $\Delta\phi$ is the phase difference across the junction and n_0 is the number operator corresponding to the formed fermion state in the junction region. See Figure 3.12.

Most importantly, since the Hamiltonian commutes with n_0, the occupation number is conserved. Starting in a state with $n_0 = \tilde{n}_0$ the corresponding Josephson current is

$$I_\gamma = \frac{2e}{\hbar}\frac{d\langle\mathcal{H}_0\rangle}{d\Delta\phi} = \frac{e\Gamma}{2\hbar}\sin(\frac{\Delta\phi}{2})(2\tilde{n}_0 - 1). \tag{3.40}$$

As seen from this expression the current is mediated by single electron tunneling and is 4π-periodic in $\Delta\phi$. In trivial superconductors, only Cooper pair tunneling can mediate any Josephson current for subgap voltages, but in this setup single electron tunneling is allowed since the weak coupling between MBS allows the fermionic state to be located in the gap.

Starting for example with $\Delta\phi = 0$ and $\tilde{n}_0 = 1$, the Hamiltonian (3.39) is in the ground state with energy $-\Gamma/2$. Tuning $\Delta\phi$ to 2π adiabatically yields

now an excited state with energy $+\Gamma/2$. But since the fermion occupancy is conserved, this means that one finite energy quasiparticle must have been added to the junction region. Now, due to the outer Majorana states, γ_L and γ_R, there is always a degeneracy between odd and even parity ground states, but since fermion occupancy at the junction region is conserved due to the gap, the ground state parity can not switch. The system can decay back into the ground state only if the fermionic state corresponding to the unpaired outer MBS can tunnel into the junction region but this mechanism is suppressed if the wires are long compared to the coherence length. Tuning $\Delta\phi$ further from 2π to 4π gets us back to the same state again yielding the 4π-periodicity. So far, no experimental evidence of the 4π Josephson effect has been reported.

More recently, a conceptually different approach using magnetic atom arrays on bulk superconductors has been show to generate the Kitaev Wire model in the low energy limit. The interested reader is referred to Ref. [NPDL$^+$14] for more information.

To conclude, MBS are fundamentally interesting particles due to their non-abelian statistics. But it would also be of great interest if the experimental progress in the hunt for MBS could point the way towards other devices with engineered species of quasiparticles, both Abelian and non-Abelian, perhaps culminating in a topological quantum computer. Though it might not be possible at all to construct one, the emergent field of topological quantum devices is indeed a small step towards finding that out.

3.3 Polyacetylene and Fractional Charge

The final model we shall take a look at is the Su–Schrieffer–Heeger-model (SSH-model) [SSH79, WSH80]. It describes the polymer polyacetylene which is a simple carbon chain consisting of coupled $C-H$ units in a quasi one-dimensional lattice. Evey carbon atom has four valence electrons of which three form the bonds to neighbouring carbon atoms and the hydrogen atom. The remaining electron is weakly occupying a single π-orbital perpendicular to the chain and can be treated in a simple tight binding model description. One might then suspect that the weakly overlapping π-orbitals form a band leading to polyacetylene being in a metallic state, but this is not the case. Due to phonon interactions, the system can lower its energy by distorting the lattice resulting in the opening of a gap in the spectrum. This mechanism is known as *Peierls distortion* and has as a result that polacetylene forms an insulating state.

In the remainder of this section, we shall give the Hamiltonian for this model, deduce the spectrum and its topological properties. In addition, we discuss some of the peculiar predictions of this model, including zero energy states having fractional charge and derive their wave function.

3.3.1 The SSH-Hamiltonian

The SSH Hamiltonian can most easily can be formulated as

$$\mathcal{H} = \sum_{n=1}^{N/2} \left[-t_1 (a_n^\dagger b_n + \text{H.c.}) - t_2 (b_n^\dagger a_{n+1} + \text{H.c.}) \right], \tag{3.41}$$

which describes spinless electrons hopping on a one-dimensional lattice with staggered amplitudes, t_1 and t_2, taken to be real. We allow $t_1 \neq t_2$ due to the Peierls distortion described above. Next, we define the unit cell to consist of two sites denoted A and B and to have a length equal to unity. Operators creating electrons on these sites are given by $a^\dagger$ and $b^\dagger$ respectively. The on-site energy on each site is crucially taken to be zero, resulting in one particle per unit cell and, as we shall see, imposes a symmetry in the model. In addition, we assume local charge neutrality, meaning that an empty unit cell must have charge $+e$. See Figure 3.13(a).

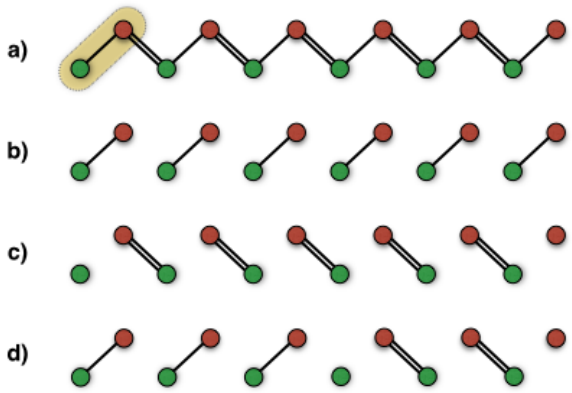

Figure 3.13: The SSH model. (a) depicts a staggered lattice with t_1 (single line) and t_2 (double line) hopping. (b) shows the chain in the limit $t_1 \gg t_2$ dimerizing the chain. (c) shows the limit $t_2 \gg t_1$ also dimerizing the chain but leaving two isolated lattice sites. (d) depicts a frustrated lattice with a domain wall hosting a fractionally charged state at the kink.

The Bloch Hamiltonian for the translationally invariant system is derived by the methods in Section 2.2 and is given by

$$h(k) = -\left[t_1 + t_2 \cos(2k)\right] \tau_x - \left[t_2 \sin(2k)\right] \tau_y, \tag{3.42}$$

with energy bands

$$\epsilon_\pm(k) = \pm \left[t_1^2 + t_2^2 + 2 t_1 t_2 \cos(2k) \right]^{1/2}. \tag{3.43}$$

Here, τ_i are Pauli matrices acting in sublattice space. Let us now analyze Equation (3.43) in more detail. We first note that there is a gap in the spectrum with size $\Delta_0 = |t_1 - t_2|$ which occurs for $k = \pi/2$ and $k = 0$ for $t_1 > t_2$

and $t_1 < t_2$ respectively. There are also two interesting parameter limits. In the limit $t_1 \gg t_2$ we obtain a staggered system isolating every unit cell from another since only couplings of the type $A - B$ remain. See Figure 3.13(b). In each cell the two sites hybridize yielding a two level system with energies $E = \pm t_1$. Let us denote this configuration the AB phase. In the other limit, see Figure 3.13(c), $t_1 \ll t_2$, only $B - A$ couplings remain, pairing the unit cells into separated two level systems with energies $E = \pm t_2$. For an open chain, this BA-phase isolates the first A-atom and the last B-atom which remain at zero energy due to the zero chemical potential. We note also that which of the phases AB or BA that has zero energy edge states depend on if the lattice starts with an A or B site. So one can say that both phases are topologically distinct from one another.

It is now natural to imagine connecting one open chain of each phase, leaving an isolated A or B site between. See Figure 3.13(d). This frustration of the lattice is referred to as a *domain wall*, *soliton* or a *kink*. We can deduce that the state localized in the kink region actually has *fractional charge* from the following argument. Since the chemical potential is zero, resulting in one electron per unit cell, charge neutrality requires that a single electronic state on a single site (that is half a unit cell) will contribute with charge $-e/2$ if it is full and $+e/2$ if it is empty. Note however that a kink-state never can exist on its own, but must have a kink-partner somewhere else in the lattice. Nevertheless, situated far apart, the kink state can be viewed as an independent and movable excitation. These peculiar states are of topological origin and we shall now explore how they appear from the underlying topology of the system.

3.3.2 Topological invariant

To derive the topological invariant, we first observe that the Hamiltonian in Equation (3.42) has all three symmetries which are given by $T = \mathbb{1}$, $P = \tau_z$ and $C = \tau_z$ so that the model belongs to class BDI and has a $\mathbb{Z}$-invariant. We can save ourselves some work by noting that the discussion of the winding invariant of the Kitaev Wire in Section 3.1.2 is applicable here as well. We can then immediately state that the winding invariant is given by

$$\nu = \frac{1}{2\pi i} \int_{-\pi/2}^{\pi/2} \partial_k \log \left[d_x(k) + i d_y(k) \right] = \theta(|t_2| - |t_1|) \tag{3.44}$$

when the Hamiltonian (3.42) is written as $h(k) = \vec{d}(k) \cdot \vec{\sigma}$. The invariant takes the values $\nu = +1$, or 0 depending on whether the vector $\vec{d}(k)$ winds counter-clockwise or not at all around the origin. when $t_1 = \pm t_2$, the winding is ill-defined since then the gap gloses for some k. The winding number $\nu = -1$ can be acquired in a setting where a $B - A$ instead of an $A - B$ group is chosen as the unit cell, effectively changing the how the lattice is terminated.

We can now understand the kink state as a consequence of the bulk-boundary correspondence. A kink is a domain wall between two topologically distinct regions and is associated with a closing of the gap resulting in zero energy states which outlive the specific parameter choice presented above. We shall now derive the wave function for such a state.

3.3.3 The Dirac Equation and Localized Kink States

The Dirac equation plays a very important role in various TSM (see for instance Ref. [WBSB14] for a review). The original equation can be written

$$(\gamma^\mu k_\mu + m)\psi = 0, \tag{3.45}$$

with γ^μ being matrices representing the Lorentz group, k the four-momentum, m the mass and ψ a four-component spinor. The equation was formulated as a relativistic description of the free electron and is one of the greatest achievements in theoretical physics. Solely based on Lorentz-invariance and symmetries, Dirac managed to deduce that the electron has an anti-particle, later named the positron, which was subsequently found. In condensed matter, with Graphene being the most famous example, the Dirac equation arises as a low energy effective theory of some linearized Bloch or BdG spectrum.

As we have seen previously, many Hamiltonians are written on the form

$$h(k) = \vec{d}(k) \cdot \vec{\sigma}, \tag{3.46}$$

where $\vec{d}(k)$ usually depends on $\cos(k)$ and $\sin(k)$. We can now expand these to lowest order in k around any gap closing point. This will capture the behaviour close to these points which is where the low energy behaviour occurs. The resulting linear equation

$$h(k) \sim \alpha k \sigma_z + \beta \sigma_x, \tag{3.47}$$

with α and β some constants, is up to a basis rotation on the form of a Dirac Equation, hence the name.

Consider now Equation (3.42) and linearize around $k = 0$. We can write this low energy Dirac Hamiltonian as

$$h(k) = \Delta(x)\tau_x + v_F k \tau_y, \tag{3.48}$$

with $v_F = 2t_2$ and $\Delta = t_1 + t_2$, the latter term given a spatial dependence due to two spatially separated regimes with different staggered hopping.

Let us find a zero energy solution by solving $h(k \to -i\partial_x)\psi(x) = 0$ when $\Delta(x) = -\Delta_0$ for $x < 0$ and $\Delta(x) = +\Delta_0$ when $x > 0$ effectively modeling a kink. The precise form of the spatial dependence is not important as long as it asymptotically approaches a different topological phase in each direction.

The solution is most easily found by multiplying the equation from the left by τ_y and trying the ansatz $\psi(x) = \phi(x)\,|\pm\rangle$, where $|\pm\rangle$ are the eigenvectors of τ_x. This approach results in

$$\phi(x) = Ne^{\pm\frac{1}{v_F}\int_0^x \Delta(x')dx'}, \tag{3.49}$$

with N some normalization constant. If we assume the boundary condition that $\phi \xrightarrow{x\to\pm\infty} 0$, we see that only one of the solutions satisfy these, depending on the sign of $\frac{\Delta_0}{v_F}$. Assuming a positive sign we obtain the solution

$$\psi(x) = \sqrt{\frac{\Delta_0}{v_F}} e^{\frac{-\Delta_0|x|}{v_F}} |-\rangle\,. \tag{3.50}$$

A system with this kind of Dirac equation having a sign-changing term like above (often called a *mass-term* as it resembles the mass in the original Dirac equation) was first studied in Ref. [JR76], where it was pointed out that it results in a fractionally charged state. In the context of polyacetylene, the low energy physics of the SSH-model was first described in Ref. [TLLM80].

The procedure we have used for solving for zero energy solutions is not applicable only to the SSH-model. In fact, it can be generally used to derive the form of edge states between topological sectors, hence being in close connection to the bulk-boundary principle. We shall have further use for this method in Chapter 4.

Before closing this section, we point out that no indication of fractional charge can be observed in polyacetylene. This is because we have neglected spin degeneracy which effectively muliplies the fractional charge by two. Nevertheless, the inclusion of spin allows for another interesting behaviour called *spin-charge separation*. With spin included, there are three types of kink states in the model. One with charge $q = 0$ and spin $\sigma = 1/2$ and two with $q = \pm e$ and $\sigma = 0$. These states can in some situations dominate the transport properties of the polymer. The interested reader is encouraged to see the review by Heeger [HKSS88].

4

Introduction to Accompanying Paper

4.1 The π-shifted Josephson Junction

In the paper [SABH15], we study various one-dimensional superconductors with two kinds of Josephson Junctions. It is based on the observation that one can form so called π-junctions by varying the superconducting order parameter continuously across some region. This type of junction can be formed either by constraining the order parameter to be real and changing sign, or by keeping the amplitude fixed and "winding" the phase from 0 to π. It turns out that the properties of any such junction is dependent on the topological properties of the superconductor. By studying these properties one can probe the nature of topological superconductivity.

In addition, we propose a topological field theory that gives a minimal description of a superconducting wire with π-junction defects. This effective theory is a one-dimensional version of higher dimensional theories describing trapped Majorana bound states in superconducting vortices.

In the remainder, we shall briefly review the different steps in the paper in some more detail and refer back to the previous sections of this thesis.

4.1.1 Superconducting Models

In order to explore topological superconductivity, we want to construct various one-dimensional models describing superconductivity. Our starting point is a field theoretical model of a p-wave superconductor with Hamiltonian

$$\mathcal{H}_p = \int dx \left[(\psi^\dagger(-\frac{\partial_x^2}{2m} - \bar{\mu})\psi + \Delta_p(x)\psi(-i\partial_x)\psi + \Delta_p^*(x)\psi^\dagger(-i\partial_x)\psi^\dagger \right] \quad (4.1)$$

where ψ is a fermionic field, $\bar{\mu}$ is the chemical potential measured from the band bottom and $\Delta_p(x) = \Delta(x)/k_F$ is the dimensionless p-wave superconducting order parameter. We have here defined the order parameter, $\Delta(x)$ such that, for constant Δ, the induced energy gap is 2Δ. It can be shown that this model is the same as the Kitaev Wire model in Equation (3.1) up to a global gauge transformation.

In addition, we define an ordinary s-wave superconductor with the Hamiltonian

$$\mathcal{H}_s = \sum_{\sigma=\uparrow,\downarrow} \int dx (\psi_\sigma^\dagger (-\frac{\partial_x^2}{2m} - \bar{\mu})\psi_\sigma + \int dx \left[\Delta_s(x)\psi_\uparrow^\dagger \psi_\downarrow^\dagger + \Delta_s^*(x)\psi_\downarrow \psi_\uparrow\right], \quad (4.2)$$

where σ is the spin index, $\psi_\uparrow$, $\psi_\downarrow$ are fermionic fields, $\bar{\mu}$ is the chemical potential and $\Delta_s(x)$ is the, position dependent, s-wave order parameter. When put on a lattice, the resulting tight binding model is given by Equation (3.29) when taking $\alpha = h = 0$ up to a shift in the chemical potential.

The models (3.1) and (3.29) are used for all numerical calculations in the paper using methods discussed in Section 2.2.

4.1.2 Linearization Schemes

To analyze the low energy behaviour, we linarize the model (4.1) in two different ways which are equal with respect to energy behaviour, but differ in their topological properties. The first method is similar to the standard linearization scheme of the Luttinger liquid, where the parabolic dispersion is replaced by a Dirac-like dispersion at the two Fermi points by adding unphysical "positron states". We show that this procedure reproduces the low energy model considered in the TLM-model [TLLM80], given by

$$h_{Lin}(k) = \frac{1}{2}\left[v_F \tau_z k - 2(\Re\big(\Delta(x)\big)\tau_y - \Im\big(\Delta(x)\big)\tau_x)\right]. \quad (4.3)$$

This model properly describes the low energy behaviour of the Kitaev Wire model, but has some drawbacks. First, it is hard to define any k-space topology since the limits for $k \to \pm\infty$ are different, which in turn complicates the concept of winding numbers. Secondly, the PHS is not a redundancy resulting from a BdG-doubling, but follows instead from the extension of the spectrum to negative energies. To remedy this, we define another linearization scheme where the artificial doubling is explicit and the k-space topology can be properly defined by regularization. In essence, we replace k^2 by $|k|$ such that the slopes at the Fermi points are preserved. This results in the Hamiltonian

$$h_v(k) = \frac{1}{2}\left[(-\bar{\mu} + v_F|k|)\tau_z + \Delta \mathrm{sign}(k)\tau_y\right]. \quad (4.4)$$

We show with this Hamiltonian that it is possible to make a linearization that is consistent with the topology in the corresponding full model.

4.1.3 Numerical Analysis of Junction States

We look at the subgap states in both the real π-junction and the phase winding junctions. In the real case, we show that our low energy theory is described

by Equation (4.3). By using a soliton profile $\Delta(x) = \Delta_0 \tanh(x/\xi)$, we then derive using methods described in Section 3.3.3 that the junction zero energy bound state is given by [TLLM80]

$$\psi(x) = N_0 \operatorname{sech}(x/\xi)^{\xi/\xi_0}, \tag{4.5}$$

where $\xi_0 \equiv v_F/(2\Delta_0)$, the effective coherence length of the problem and N_0 is a normalization constant. With convincing numerical evidence, we confirm that these states indeed describes the low energy section of the Kitaev Wire in a real π-junction setup. This is done in the following way.

We take $\Delta_j = \Delta_0 \tanh(j/\xi)$, a discretized version of the profile used by TLM. By choosing the width ξ not too large, this determines the order parameter to $-\Delta_0$ at one end of the wire and $+\Delta_0$ at the other end, generating a domain wall (between sectors with different winding numbers) at the center of the wire. The topological properties of the full Kitaev Wire then ensures the existence of localized zero modes between these sectors in addition to the MBS localized at the boundaries between the topological phases and the topologically trivial vacuum.

The Kitaev chain can be diagonalized as

$$H_K = \sum_i \epsilon_i (A_i^\dagger A_i - 1/2), \tag{4.6}$$

where $A_i = \alpha_{ij} a_j + \beta_{ij} a_j^\dagger \equiv \vec{\alpha}_i \cdot \vec{a} + \vec{\beta}_i \cdot \vec{a}^\dagger$, and $\{A_i, A_j^\dagger\} = \delta_{ij}$. When the wire is in the topological phase, there are pairs of self-conjugate zero energy modes, with coefficients that can chosen to be real and satisfying $\vec{\alpha}_m = \pm\vec{\beta}_m$, We define the Majorana operators $\gamma_m/\sqrt{2} \equiv A_m = A_m^\dagger$ in the case $\vec{\alpha}_m = \vec{\beta}_m$, and $\gamma_m/\sqrt{2} = -iA_m = iA_m^\dagger$ if $\vec{\alpha}_m = -\vec{\beta}_m$, and refer to these as symmetric and anti-symmetric MBS respectively. In both cases the operators satisfy the Majorana conditions $\gamma_m = \gamma_m^\dagger$ and $\{\gamma_n, \gamma_m\} = 2\delta_{m,n}$.

In our case we have four MBS of which two symmetric ones form a Dirac zero mode (DZM) at the π-junction, while the remaining two, which are anti-symmetric, are localized at the edges of the wire. The probability distribution for the DZM mode is given by α_{ni}^2, which can be compared to the corresponding distribution for the zero mode solution localized on a soliton in the TLM-model. For example, choosing $\xi = \xi_0$ should generate a zero mode probability distribution given by $|\psi(x)|^2 \sim \operatorname{sech}(x/\xi_0)^2$, and we compare the solution obtained from our tight binding model with this function as follows. We define

$$g_i(\lambda) = \int_{i-0.5}^{i+0.5} \frac{1}{\lambda} \operatorname{sech}\left(\frac{x - N/2}{\lambda}\right)^2 \, \mathrm{d}x\,, \tag{4.7}$$

where N is the number of sites in the wire. This function integrates the TLM-given probability distribution over small intervals centered around the lattices sites, numbered by i. The parameter λ is chosen to minimize $G(\lambda) = \sum_i (\alpha_{ni}^2 - g_i(\lambda))^2$, where the α_{ni} are obtained from the tight binding model. If

the models are similar, the value of λ should be close to the value ξ_0 determined from the input parameters of the model.

The results is that the TLM model captures the the properties of the DZM in the junction region of the Kitaev Wire very well [SABH15]. In general, our matching is more accurate for parameter choices given broader probability distributions where the lattice effects are expected to be small. The condition for this is that $v_F \gg 2\Delta_0$ or equivalently that $t \gg \Delta_0$. The agreement between the full and the linearized model persists also when $\xi \neq \xi_0$.

The analysis is repeated for complex π-junction where there are no symmetry protected zero energy bound states. First we perform analytical calculations for a simple type of phase winding junction and show that these agree well with the numerics. Then we contrast the behaviour between topological and trivial junctions in the short junction limit. This results in the conclusion that topological junctions has bound states with asymtotically zero energy as the junction shrinks, while this is not happening for trivial junctions. This can be explained by noting that the topological junction moves from class D to BDI in the short junction limit.

4.1.4 Topological Field Theory

In the last section, we define an effective field theory in a phenomenological manner describing Dirac zero modes bound to order parameter phase junctions. With certain approximations and in specific but motivated limits, the topological field theory is consistent with the theory in the previous sections of the paper. It should be noted however that the derivation of the topological field theory is not rigorous but some speculations on how to properly arrive at the model are given. We also relate our theory to already existing topological field theories describing Majoranas trapped in vortices in two-dimensional topological superconductors.

4.1.5 Results and Conclusions

The main results of the paper is to give a detailed description of the states in a π phase winding junction, a junction which breaks the underlying PTRS protecting the zero energy states that exist in a π-junction with a real order parameter. We show that although no zero energy states can be expected on general grounds, it is possible to tune states to arbitrarily low energies. Furthermore, we speculate loosely on how this might be used as a bulk (in contrast to edge) probe of topological superconductivity in an experimental setup. As our final result, we construct an effective topological field theory, capturing the behaviour of movable phase winding junctions.

5

Summary and Outlook

In this thesis we have discussed the general framework of topological states of matter. It is fair to say that our focus has been from a practical point of view rather than presenting mathematical rigour, mostly due to the interests of the author but also for the sake of the newcomer in this field.

We have only explored a minor region of the vast landscape of topological states of matter. Specifically we have considered one-dimensional topological states of matter in Cartan-Altland-Zirnbauer classes D and BDI. The reason for choosing one-dimensional models is at least three-fold. Most importantly, when only one k-momentum is required, many concepts and invariants become quite simple to calculate without loosing the conceptual importance. Further, many computer simulations can be done for quite large systems within reasonable time on an ordinary desktop computer. Finally, one-dimensional and two dimensional models are the ones that are mostly used when designing devices out of topological states of matter so studying one-dimensional systems is indeed of experimental relevance.

Some obvious directions for further research would be to explore models in higher dimensions, to add interactions or to include thermal environments by introducing mixed states in a density matrix formulation.

Another interesting option is to apply the framework of quantum transport to topological states of matter. For this purpose, the Non-Equilibrium Green's Function (NEGF) or Keldysh approach to quantum transport is well suited for these type of tight binding systems. It is also suitable for including interactions, disorder or phase decoherence. This direction would also be more experimentally oriented and opens up the possibility of collaboration with experimental groups. As a bonus, learning this framework is useful in most experimentally connected theoretical research fields.

There is also the possibility to dive into a quantum field theoretical description of topological states of matter which would be a slightly more analytical path than the previously mentioned ones, but would probably be both challenging and rewarding.

Having topological phases is an experimental reality, due to observation of the IQH effect, the FQH effect, the QSH effect, 3D-topological insulators, the Chern insulator and many more exotic states of matter. Theory and

experiment are to large extent consistent, but it still remains unsettled whether particles with non-Abelian statistics, for example Majorana bound states, exist and if topological quantum computation ever can be realized in laboratories. The next years will hopefully generate some answers to these questions and pave the way for new exciting models and devices.

Bibliography

[Ali12] J. Alicea, *New directions in the pursuit of majorana fermions in solid state systems*, Reports on Progress in Physics **75** (2012), no. 7, 076501.

[AM76] N.W. Ashcroft and N.D. Mermin, *Solid state physics*, Brooks Cole, 1976.

[AOR+11] J. Alicea, Y. Oreg, G. Refael, F. von Oppen, and M.P.A. Fisher, *Non-abelian statistics and topological quantum information processing in 1d wire networks*, Nature Physics **7** (2011), no. 5, 412–417.

[AS68] M. F. Atiyah and I. M. Singer, *The index of elliptic operators: I*, Annals of Mathematics **87** (1968), no. 3, pp. 484–530.

[AS10] A. Altland and B.D. Simons, *Condensed matter field theory*, 2nd ed., Cambridge University Press, 2010.

[ASv+15] A. Ahkmerov, J. Sau, B. van Heck, R. Skolasinski, and S. Rubbert, *Topology in condensed matter: Tying quantum knots*, TU Delft TOPOCMx, 2015.

[A.Y09] A.Y.Kitaev, *Periodic table for topological insulators and superconductors*, AIP Conference Proceedings **1134** (2009), no. 1, 22.

[AZ97] A. Altland and M.R. Zirnbauer, *Nonstandard symmetry classes in mesoscopic normal-superconducting hybrid structures*, Phys. Rev. B **55** (1997), no. 2, 1142.

[BA12] D. Bagrets and A. Altland, *Class D spectral peak in Majorana quantum wires*, Phys. Rev. Lett. **109** (2012), 227005.

[BA13] J. C. Budich and E. Ardonne, *Equivalent topological invariants for one-dimensional majorana wires in symmetry class d*, Phys. Rev. B **88** (2013), 075419.

[BB48] J. Bardeen and W.H. Brattain, *The transistor, a semi-conductor triode*, Phys. Rev. **74** (1948), 230.

[Ber13] B.A Bernevig, *Topological insulators and topological superconductors*, Princeton University Press, 2013.

[BHZ06] B.A. Bernevig, T.L. Hughes, and S.C. Zhang, *Quantum spin hall effect and topological phase transition in hgte quantum wells*, Science **314** (2006), no. 5806, 1757–1761.

[Bot59] R. Bott, *The stable homotopy of the classical groups*, Annals of Mathematics (1959), 313–337.

[Car26] É. Cartan, *Sur une classe remarquable d'espaces de riemann.*, Bull. Soc. Math. France **54** (1926), 214–264.

[CEAB11] T.P. Choy, J. M. Edge, A. R. Akhmerov, and C. W. J. Beenakker, *Majorana fermions emerging from magnetic nanoparticles on a superconductor without spin-orbit coupling*, Phys. Rev. B **84** (2011), 195442.

[C.L05] C.L. Kane and E.J. Mele, *Quantum spin hall effect in graphene*, Phys. Rev. Lett. **95** (2005), no. 22, 226801.

[Dir31] P.A.M. Dirac, *Quantised singularities in the electromagnetic field*, Proc. Roy. Soc. (London). Series A **A 133** (1931), 60.

[DRM+12] A. Das, Y. Ronen, Y. Most, Y. Oreg, M. Heiblum, and H. Shtrikman, *Evidence of majorana fermions in an al - inas nanowire topological superconductor*, Nature Physics **8** (2012), 887.

[DYH+12] M.T. Deng, C.L. Yu, G.Y. Huang, M. Larsson, P. Caroff, and H.Q. Xu, *Observation of Majorana Fermions in a Nb-InSb Nanowire-Nb Hybrid Quantum Device*, Nano Lett. **12** (2012), 6414.

[FKLW03] M. Freedman, A.Y. Kitaev, M. Larsen, and Z. Wang, *Topological quantum computation*, Bulletin of the American Mathematical Society **40** (2003), no. 1, 31–38.

[FKM07] L. Fu, C. L Kane, and E.J. Mele, *Topological insulators in three dimensions*, Phys.Rev. Lett. **98** (2007), no. 10, 106803.

[Fle10] K. Flensberg, *Tunneling characteristics of a chain of majorana bound states*, Phys. Rev. B **82** (2010), no. 18, 180516.

[Gia03] T. Giamarchi, *Quantum physics in one dimension*, Oxford University Press, 2003.

[Hal81] F.D.M. Haldane, *"Luttinger liquid theory" of one-dimensional quantum fluids. I. properties of the luttinger model and their extension to the general 1d interacting spinless fermi gas*, Journal of Physics C: Solid State Physics **14** (1981), no. 19, 2585.

[Hal82] B.I. Halperin, *Quantized hall conductance, current-carrying edge states, and the existence of extended states in a two-dimensional disordered potential*, Phys.Rev.B **25** (1982), no. 4, 2185.

[Hal88] F.D.M. Haldane, *Model for a quantum hall effect without landau levels: Condensed-matter realization of the "parity anomaly"*, Phys. Rev. Lett. **61** (1988), no. 18, 2015.

[HK10] M.Z. Hasan and C.L. Kane, *Colloquium: topological insulators*, Reviews of Modern Physics **82** (2010), no. 4, 3045.

[HKL+10] C. W. Hicks, J.R. Kirtley, T.M. Lippman, N.C. Koshnick, M.E. Huber, Y. Maeno, W.M. Yuhasz, M. B. Maple, and K.A. Moler, *Limits on superconductivity-related magnetization in Sr_2RuO_4 and $PrOs_4Sb_{12}$ from scanning squid microscopy*, Phys. Rev. B **81** (2010), 214501.

[HKSS88] A.J. Heeger, S. Kivelson, J.R. Schrieffer, and W.P. Su, *Solitons in conducting polymers*, Rev. Mod. Phys. **60** (1988), no. 3, 781.

[HQW+08] D. Hsieh, D. Qian, L. Wray, Y.Q. Xia, Y.S. Hor, R.J. Cava, and M.Z. Hasan, *A topological dirac insulator in a quantum spin hall phase*, Nature **452** (2008), no. 7190, 970–974.

[J.L12] J.Liu, A.C. Potter, K.T. Law and P.A. Lee, *Zero-bias peaks in the tunneling conductance of spin-orbit-coupled superconducting wires with and without majorana end-states*, Phys. Rev. Lett. **109** (2012), no. 26, 267002.

[JMD+14] G. Jotzu, M. Messer, R. Desbuquois, M. Lebrat, T. Uehlinger, D. Greif, and T. Esslinger, *Experimental realization of the topological haldane model with ultracold fermions*, Nature **515** (2014), no. 7526, 237–240.

[JR76] R. Jackiw and C. Rebbi, *Solitons with fermion number 1/2*, Phys. Rev. D **13** (1976), no. 12, 3398–3409.

[Kit01] A.Y. Kitaev, *Unpaired majorana fermions in quantum wires*, Physics-Uspekhi **44** (2001), no. 10S, 131.

[KM05] C.L Kane and E.J. Mele, $\mathbb{Z}_2$ *topological order and the quantum spin hall effect*, Phys. Rev. Lett. **95** (2005), no. 14, 146802.

[Koh85] M. Kohmoto, *Topological invariant and the quantization of the hall conductance*, Annals of Physics **160** (1985), no. 2, 343–354.

[KWB+07] M. König, S. Wiedmann, C. Brüne, A. Roth, H. Buhmann, L.W. Molenkamp, X.L. Qi, and S.C. Zhang, *Quantum spin hall insulator state in hgte quantum wells*, Science **318** (2007), no. 5851, 766–770.

[Lan37] L.D. Landau, *Zur theorie der phasenumwandlungen ii*, Phys. Z. Sowjetunion **11** (1937), 26–35.

[Lau73] P.C. Lauterbur, *Image formation by induced local interactions: examples employing nuclear magnetic resonance*, Nature **242** (1973), 190–191.

[Lau83] R.B. Laughlin, *Anomalous quantum hall effect: An incompressible quantum fluid with fractionally charged excitations*, Phys. Rev. Lett. **50** (1983), 1395–1398.

[LL80] L.D. Landau and E.M. Lifshitz, *Statistical physics, vol. 5*, vol. 30, Butterworth–Heineman, 1980.

[LLN09] K. T. Law, P.A. Lee, and T. K. Ng, *Majorana fermion induced resonant andreev reflection*, Phys. Rev. Lett. **103** (2009), 237001.

[LM77] J.M. Leinaas and J. Myrheim, *On the theory of identical particles*, Il Nuovo Cimento B Series 11 **37** (1977), no. 1, 1–23.

[LPLL12] J. Liu, A.C. Potter, K.T. Law, and P.A. Lee, *Zero-bias peaks in spin-orbit coupled superconducting wires with and without majorana end-states*, Phys. Rev. Lett. **109** (2012), 267002.

[LSDS10] R. M. Lutchyn, J.D. Sau, and S. Das Sarma, *Majorana Fermions and a Topological Phase Transition in Semiconductor-Superconductor Heterostructures*, Phys. Rev. Lett. **105** (2010), 077001.

[MZF+12] V. Mourik, K. Zuo, S. M. Frolov, S. R. Plissard, E. P. A. M. Bakkers, and L. P. Kouwenhoven, *Signatures of majorana fermions in hybrid superconductor-semiconductor nanowire devices*, Science **336** (2012), no. 6084, 1003–1007.

[Nak03] M. Nakahara, *Geometry, topology and physics*, CRC Press, 2003.

[NPDBY13] S. Nadj-Perge, I. K. Drozdov, B. A. Bernevig, and A. Yazdani, *Proposal for realizing majorana fermions in chains of magnetic atoms on a superconductor*, Phys. Rev. B **88** (2013), 020407.

[NPDL+14] S. Nadj-Perge, I.K. Drozdov, J. Li, H. Chen, S. Jeon, J.l Seo, A.H. MacDonald, B. A. Bernevig, and A. Yazdani, *Observation of majorana fermions in ferromagnetic atomic chains on a superconductor*, Science **346** (2014), no. 6209, 602–607.

[NTY85] Q. Niu, D.J. Thouless, and Wu Y.S., *Quantized hall conductance as a topological invariant*, Phys.Rev. B **31** (1985), no. 6, 3372.

[ORv10] Y. Oreg, G. Refael, and F. von Oppen, *Helical liquids and majorana bound states in quantum wires*, Phys. Rev. Lett. **105** (2010), 177002.

[PGv14] F. Pientka, L.I. Glazman, and F. von Oppen, *Unconventional topological phase transitions in helical shiba chains*, Phys. Rev. B **89** (2014), 180505.

[QHZ08] X.L. Qi, T.L. Hughes, and S.C. Zhang, *Topological field theory of time-reversal invariant insulators*, Phys.Rev. B **78** (2008), no. 19, 195424.

[Rob06] R. Robinett, *Quantum mechanics: Classical results, modern systems, and visualized examples*, 2nd ed., Oxford University Press, 2006.

[RS+10] S. Ryu, A.P. Schnyder, , A. Furusaki, and A.W.W. Ludwig, *Topological insulators and superconductors: tenfold way and dimensional hierarchy*, New Journal of Physics **12** (2010), no. 6, 065010.

[RZMK38] I. I. Rabi, J. R. Zacharias, S. Millman, and P. Kusch, *A new method of measuring nuclear magnetic moment*, Phys. Rev. **53** (1938), 318–318.

[SABH15] C. Spånslätt, E. Ardonne, J. C. Budich, and T. H. Hansson, *Topological aspects of π phase winding junctions in superconducting wires*, arXiv preprint arXiv:1501.03413v2 (2015).

[SN11] J.J Sakurai and J. Napolitano, *Modern quantum mechanics*, Addison-Wesley, 2011.

[SRFL08] A.P. Schnyder, S. Ryu, A. Furusaki, and A.W.W. Ludwig, *Classification of topological insulators and superconductors in three spatial dimensions*, Phys. Rev. B **78** (2008), 195125.

[SSH79] W.P. Su, J.R. Schrieffer, and A.J. Heeger, *Solitons in polyacetylene*, Phys. Rev. Lett. **42** (1979), no. 25, 1698.

[TKND82] D.J. Thouless, M. Kohmoto, M.P. Nightingale, and M. Den Nijs, *Quantized hall conductance in a two-dimensional periodic potential*, Phys.Rev. Lett. **49** (1982), no. 6, 405.

[TLLM80] H. Takayama, Y.R. Lin-Liu, and K. Maki, *Continuum model for solitons in polyacetylene*, Phys. Rev. B **21** (1980), no. 6, 2388.

[TS12] S. Tewari and J.D. Sau, *Topological invariants for spin-orbit coupled superconductor nanowires*, Phys. Rev. Lett. **109** (2012), no. 15, 150408.

[TSG82] D. C. Tsui, H. L. Stormer, and A. C. Gossard, *Two-dimensional magnetotransport in the extreme quantum limit*, Phys. Rev. Lett. **48** (1982), 1559–1562.

[vDP80] K. von Klitzing, G. Dorda, and M. Pepper, *New method for high-accuracy determination of the fine-structure constant based on quantized Hall resistance*, Phys.Rev.Lett. **45** (1980), 494–497.

[Vol03] G.E. Volovik, *The universe in a helium droplet*, Clarendon Press, 2003.

[WBSB14] T.O. Wehling, A.M. Black-Schaffer, and A.V. Balatsky, *Dirac materials*, Advances in Physics **63** (2014), no. 1, 1–76.

[Wen90] X.G. Wen, *Topological orders in rigid states*, International Journal of Modern Physics B **4** (1990), no. 02, 239–271.

[Wil82] F. Wilczek, *Quantum mechanics of fractional-spin particles*, Phys. Rev. Lett. **49** (1982), no. 14, 957.

[WSH80] J.R. Schrieffer W.P. Su and A.J. Heeger, *Soliton excitations in polyacetylene*, Phys. Rev. B **22** (1980), no. 4, 2099.

[YC10] P. Y. Yu and M. Cardona, *Fundamentals of semiconductors*, Springer, 2010.

[Ynt55] G.B. Yntema, *Superconducting winding for electromagnets*, Phys. Rev. **98** (1955), 1144–1209.

[Zhe07] N. Zheludev, *The life and times of the LED—a 100-year history*, Nature Photonics **1** (2007), 189–192.

A

Dictionary

In this appendix we have collected some frequently used concepts, which are usually assumed to be common knowledge in the field of TSM. The author hopes that a newcomer in this field will benefit from the dictionary below. Note however, that some words might be used differently in other fields.

Abelian statistics: Exchange operations commute
Adiabatic: Slow *w.r.t* to some corresponding energy
Bulk: Interior, but also trans.inv. system lacking edge
Bosonization: The fine art of turning fermions into bosons in 1D
Chiral state: One directional state
Domain wall: Interface between topologically distinct systems
Edge: Termination of lattice. Dim. smaller than corresponding bulk
Gapless: Not having a gap. Or situated at zero energy
Gap out: A state can gap out if it loses zero energy symmetry protection
Gapped: Having a forbidden energy region between occupied and empty states. Or having non-zero energy
Helical state: Directional state with a time reversed partner
Homeomorphic: Continous with continous inverse
Mode: Wave-like excitation. Often used interchangeably with state
Non-trivial: Can not be deformed into a trivial state w.o. closing the gap. Usually related to non-zero invariant
Non-Abelian statistics: Exchange operations don't commute
Parity: Property related to even-ness or odd-ness in terms of occupation number
Soliton: Equation solution with global properties that persists any local perturbations
State: Single particle quantum state
Topological invariant: Quantity that won't change unless a symmetry is broken or the gap closes
Topological field theory: Metric independent field theory with global properties
Topological order: Property of zero temperature state resulting in ground state degeneracy and long range entanglement. Phase transitions can not be descibed by symmetry breaking
Topological phase transition: The change of top. phase. Accompanied by gap closing and change in top. inv.
Trivial: Can be smoothly deformed into *some* vacuum state w.o. closing the gap

Accompanying Paper

Topological aspects of π phase winding junctions in superconducting wires

Christian Spånslätt[1], Eddy Ardonne[1], Jan Carl Budich[2,3], and T.H. Hansson[1]
[1] *Department of Physics, Stockholm University, SE-106 91 Stockholm, Sweden*
[2] *Institute for Theoretical Physics, University of Innsbruck, 6020 Innsbruck, Austria and*
[3] *Institute for Quantum Optics and Quantum Information, Austrian Academy of Sciences, 6020 Innsbruck, Austria*

(Dated: May 15, 2015)

We theoretically investigate Josephson junctions with a phase shift of π in various proximity induced one-dimensional superconductor models. One of the salient experimental signatures of topological superconductors, namely the fractionalized 4π periodic Josephson effect, is closely related to the occurrence of a characteristic zero energy bound state in such junctions. We make a detailed analysis of a more general type of π-junctions coined "phase winding junctions" where the phase of the order parameter rotates by an angle π while its absolute value is kept finite. Such junctions have different properties, also from a topological viewpoint, and there are no protected zero energy modes. We compare the phenomenology of such junctions in topological (p-wave) and trivial (s-wave) superconducting wires, and briefly discuss possible experimental probes. Furthermore, we propose a topological field theory that gives a minimal description of a wire with defects corresponding to π-junctions. This effective theory is a one-dimensional version of similar theories describing Majorana bound states in half-vortices of two-dimensional topological superconductors.

PACS numbers: 03.65.Vf, 72.15.Nj

I. INTRODUCTION

In a 2001 paper, Kitaev predicted the existence of unpaired Majorana zero modes (MZM) localized at the ends of a proximity effect induced one dimensional (1D) p-wave superconductor[1]. The Bogoliubov deGennes (BdG) mean field Hamiltonian of this "Kitaev chain" is distinguished from a trivial gapped 1D system by a $\mathbb{Z}_2$-invariant. This topological invariant can be expressed in terms of the Pfaffian of the Bloch-Hamiltonian in the Majorana representation. In the more recently established periodic table of topological states[2–4], this invariant is located in the column for dimension $d = 1$ in the row for symmetry class D , *i.e.* the class of superconductors without any additional symmetries[5].

A single channel nanowire with Rashba spin orbit coupling, in proximity to a bulk s-wave superconductor, and subject to an external magnetic field, has been one proposal for an experimentally viable realization of the Kitaev chain[6,7]. A different approach taken is a magnetic impurity chain on top of a superconductor[8–11].

Due to their charge-neutrality and non-magnetic nature, the unpaired MZMs are not easy to detect. The two main proposed signatures are a zero bias anomaly when the wire is coupled to a normal metal lead, and an anomalous 4π-periodic Josephson effect. Experimental evidence for the zero bias anomaly has been reported by several experimental groups[12–14]. However, it is fair to say that alternative explanations for robust zero bias resonances, not related to MZMs, have also been proposed[15,16]. So, in spite of a huge experimental effort, there is still no uncontested experimental realization of a 1D topological superconductor. The search for alternative observable signatures of this state thus remains a key challenge.

In this paper we investigate the spectroscopy of sub-gap modes in different types of Josephson junctions in some detail, and ask to what extent this might provide such an alternative signature. Apart from the frequently considered junctions, in which the order parameter changes sign by going through zero, we also consider junctions for which the phase of the order parameter winds, while the amplitude stays constant. The sub-gap modes in these junctions can, at least in principle, be detected by standard probes sensitive to the density of states, and in particular scanning tunneling spectroscopy. Since ordinary s-wave superconductors can also have sub-gap modes in Josephson junctions, we want to identify spectral features that are specific to the Kitaev chain.

We note that several other studies, complementary to ours, have investigated various aspects of Josephson junctions in topological wires[17–19].

The 4π-periodicity of the Josephson effect occurring in a junction between two Kitaev chains was pointed out already in Ref. 1 (see, e.g. Ref. 20 for a detailed discussion). Closely related to this 4π-Josephson effect is a characteristic level crossing between two sub-gap states associated with a change in the fermion parity of the many body ground state. This level crossing is accompanied with a fermionic zero energy state localized in the junction region. Here, we study the physics of such junctions in both s- and p-wave paired wires from a topological perspective, focusing in particular on the nature of the previously mentioned (Dirac) zero mode located at a π-junction. We recall how the level crossing at phase π is protected by an additional pseudo time reversal symmetry (PTRS) which is present in Kitaev's minimal model[1] for the Majorana wire if the pairing field is real (up to a constant phase). This additional symmetry, which is well known to refine the $\mathbb{Z}_2$ parity to an integer winding number[21,22], also protects the localized zero mode in the junction region. A major part of our present work is de-

voted to the study of the more general case where the phase of the superconducting order parameter is allowed to wind in the complex plane in the junction region, thus locally breaking the PTRS. We compare the properties of the π-junction in the topologically non-trivial p-wave case with those in the trivial s-wave case. Even in s-wave superconductors, there can still be localized sub-gap modes at a Josephson junction, but there is no protected zero mode.

Although Kitaev's original lattice model can be solved numerically for rather large systems and arbitrary junction profiles, it is nevertheless interesting to verify the presence of the sub-gap modes, and in particular the zero mode, in the junction by analytical means. To achieve this, we linearize the spectrum around the Fermi points to obtain a Luttinger model, augmented with anomalous, charge non-conserving terms, which is essentially equivalent to the Su-Schrieffer-Heeger model for polyacetylene[23], with the Josephson junction playing the role of the famous domain wall soliton[24]. This allows us to find an analytical solution for the zero mode, and also, for a special order parameter profile, for the full sub-gap spectrum. Although the topological properties of this linearized model differ from those of the original Kitaev chain, we present both theoretical and numerical arguments for them describing the same physics. First we compare with an alternative linearized model (called below the "V-shape model") which *does* have the same topology as the Kitaev chain. Since this model differs from the first linearized model only at high ($\sim \Delta$) energies it gives theoretical support for our claim that the extended Luttinger model indeed describes the low energy features of the Kitaev chain. Secondly, the analytical results from this model agrees extremely well with the numerical results obtained by directly diagonalizing the Kitaev chain.

Experimentally, the most obvious way to induce a junction in the wire such that the order parameter changes sign, is by proximity effect from a bulk superconductor with a real, sign changing order parameter already present - this is the original scenario considered by Kitaev. In such a junction, it is natural to assume that the induced order parameter in the wire remains real also in the junction region, and thus has to vanish at some point. An alternative way to introduce a junction is to place the wire on top of a bulk superconductor through which a current is flowing between two external leads placed below the wire. The resulting phase gradient is, by proximity, also present in the wire. The resulting "phase winding junction" violates the PTRS, and the zero energy state is transformed into a finite energy sub-gap state.

When discussing topological phases, it is interesting to ask what is the minimal model that will encapsulate the topological properties of the phase, and in particular those of the elementary excitations. Important examples are the Chern-Simons theories describing various Quantum Hall liquids[25], and the BF theories describing superconductors and topological insulators[26–28]. In the present case, the elementary excitations carrying topological charge are widely separated π-junctions at fixed positions, and we show that the linearized model, in the background of these π-junctions can be mapped onto a Dirac equation with a Goldstone-Wilczek type mass term[29]. We take this as a starting point for constructing an effective topological field theory describing the solitons and their associated zero modes, and comment on similar attempts in the case of the 2D topological superconductor.

This article is organized as follows: In the next section we first define the models that we shall study. In section III we study junctions with a real order parameter for the different models and with both analytical and numerical approaches. Section IV contains a similar analysis for the phase winding junctions with constant absolute value of the order parameter, but in this case we have to rely more heavily on numerics. Section V briefly discusses possible experimental configurations to study the physics of topological π-junctions, and finally, in section VI we construct the topological field theory referred to above. We end with a few concluding remarks. Some technical points, and in particular a discussion of the rather subtle k-space topology of the linearized models, are put in appendices.

II. MODELS

To set the stage for our analysis, we here first define the various models for the superconducting wires studied below.

A. The p-wave wire

The Hamiltonian for a spinless (or spin polarized) 1D p-wave superconductor can be written as

$$H_p = \int dx\, \mathcal{H}_p = \int dx\, [(\psi^\dagger(-\frac{\partial_x^2}{2m} - \bar{\mu})\psi + \Delta_p(x)\psi(-i\partial_x)\psi + \Delta_p^*(x)\psi^\dagger(-i\partial_x)\psi^\dagger]\,, \quad (1)$$

where ψ is a fermionic field (for simplicity we sometimes suppress the x-dependence), $\bar{\mu}$ is the chemical potential and $\Delta_p(x) = \Delta(x)/k_F$ is the dimensionless p-wave superconducting order parameter. The order parameter, $\Delta(x)$ is defined such that, for constant Δ, the energy gap is 2Δ.

By discretizing the Hamiltonian (1) we get the Kitaev chain model[1]

$$H_K = \sum_{j=0}^{N-1}(-t(a_j^\dagger a_{j+1} + a_{j+1}^\dagger a_j) + \Delta_j a_j a_{j+1} + \Delta_j^* a_{j+1}^\dagger a_j^\dagger - \mu(a_j^\dagger a_j - \frac{1}{2}))\,. \quad (2)$$

Here, the a_i are (spin polarized) fermion operators, and we have set the lattice parameter to unity for simplicity. The hopping parameter is denoted by t, μ is the chemical potential and Δ_j is the superconducting order parameter which can be position dependent. These parameters are related to those in the continuum model by $t = 1/(2m)$, and $\mu = \bar{\mu} - 2t$.

To write the H_K in momentum space (assuming constant Δ), we introduce the Nambu spinor $\Psi_k^\dagger = (a_k^\dagger, a_{-k})$, in terms of which,

$$H_K = \sum_k \Psi_k^\dagger \mathcal{H}_K(k) \Psi_k,$$

with $\mathcal{H}_K(k)$ given by

$$\begin{aligned}\mathcal{H}_K(k) =& \big(-\mu/2 - t\cos(k)\big)\tau_z - \mathrm{Re}(\Delta)\sin(k)\tau_y \\ &+ \mathrm{Im}(\Delta)\sin(k)\tau_x,\end{aligned} \tag{3}$$

where the Pauli-matrices τ_i act in the particle-hole spinor space. It is known[1], that for a constant order parameter, *i.e.* $\Delta_j = \Delta$, the Kitaev chain resides in a topological phase when $\Delta \neq 0$ and $|\mu| < 2|t|$.

B. The *s*-wave wire

As discussed in the introduction, we will compare the results for the topological wires with their topologically trivial, s-wave paired, counterparts. These trivial wires are described by the continuum Hamiltonian,

$$\begin{aligned}H_s = &\sum_{\sigma=\uparrow,\downarrow} \int dx (\psi_\sigma^\dagger (-\frac{\partial_x^2}{2m} - \bar{\mu})\psi_\sigma \\ &+ \int dx (\Delta_s(x)\psi_\uparrow^\dagger \psi_\downarrow^\dagger + \Delta_s^*(x)\psi_\downarrow \psi_\uparrow)),\end{aligned} \tag{4}$$

where σ is the spin index, $\psi_\uparrow$, $\psi_\downarrow$ are fermionic fields, $\bar{\mu}$ is the chemical potential and $\Delta_s(x)$ is the position dependent s-wave order parameter.

C. Two linearized models

To capture the behavior of the above models close to the Fermi energy, we expand ψ into fields containing only low energy degrees of freedom. We consider two different ways of doing this, which give the same low-energy physics, but differ in their topological properties.

1. *Luttinger like model*

There is a standard way to linearize that is illustrated in Fig. 1(c), where the parabolic band is replaced by a Dirac like dispersion relation. Just as in the Luttinger model, we have extended the spectrum by adding unphysical "positron" states. In the Luttinger model, a gap can be opened by $2k_F$ processes that scatter electrons between the two Fermi points. In our case a gap is opened by charge non-conserving processes that creates or destroys a Cooper pair formed by two electrons at different Fermi points.

Formalizing this argument we first define,

$$\psi = \frac{1}{\sqrt{2}}(e^{ik_F x}\varphi_+ + e^{-ik_F x}\varphi_-)\,,$$

where, $k_F \equiv \sqrt{2m\bar{\mu}}$ is the Fermi momentum, and φ_+ and φ_- are right and left moving fermion fields respectively. Inserting this expression into (1), neglecting terms $\sim e^{\pm 2ik_F}$, we obtain

$$\begin{aligned}H_{\mathrm{Lin}} = \frac{1}{2}\int dx (&-iv_F\varphi_+^\dagger \partial_x \varphi_+ + iv_F \varphi_-^\dagger \partial_x \varphi_- + \\ &+ 2(\Delta(x)\varphi_-\varphi_+ + \Delta^*(x)\varphi_+^\dagger \varphi_-^\dagger))\,,\end{aligned} \tag{5}$$

where the Fermi velocity is $v_F = k_F/m$. The quadratic dispersion, $\epsilon(k) = \frac{k^2}{2m} - \bar{\mu}$, is thus effectively replaced by two bands, corresponding to the right and left moving linearized fermionic fields, with dispersion relations $\epsilon_\pm(k) = \pm v_F k - \bar{\mu}$. In terms of the momentum q relative to the respective Fermi momenta, this reads $\epsilon_\pm(q) = \pm v_F q$. The superconducting order parameter couples these right and left moving fermions. By introducing the spinor $\Psi^\dagger = (\varphi_+^\dagger, i\varphi_-)$ (the factor i is for notational convenience) we get, after integration by parts, the linear Hamiltonian

$$H_{\mathrm{Lin}} = \int dx \Psi^\dagger \mathcal{H}_{\mathrm{Lin}}(x) \Psi$$

with

$$\mathcal{H}_{\mathrm{Lin}} = \frac{1}{2}(-iv_F\tau_z\partial_x - 2(\mathrm{Re}\big(\Delta(x)\big)\tau_y - \mathrm{Im}\big(\Delta(x)\big)\tau_x))\,, \tag{6}$$

where the Pauli matrices now act in right-left spinor-space. The pairing term is taken so that the gap for constant Δ coincides with that in the previous models.

In the following it will be important that, after rescaling v_F by $1/2$, the Hamiltonian (6) is identical to the one used by Takayama, Lin-Liu and Maki (TLM)[24], to describe the zero energy soliton solutions of the polyacetylene chain model introduced by Su, Schrieffer and Heeger (SSH)[23]. We shall therefore refer to it as the TLM model.

A linearized version of the trivial wire described by (4) can be constructed in a similar fashion, but with a four spinor containing the left and right components of the two spin polarizations. For details, see Appendix B.

At this point we should point out that the Hamiltonian H_{Lin} presents conceptual problems, and does not fit easily into the usual topological classification. The reasons are as follows: In Appendix A we show that as a consequence of the spectrum in Fig. 1(c) extending from plus to minus infinity, the k-space topology is not well

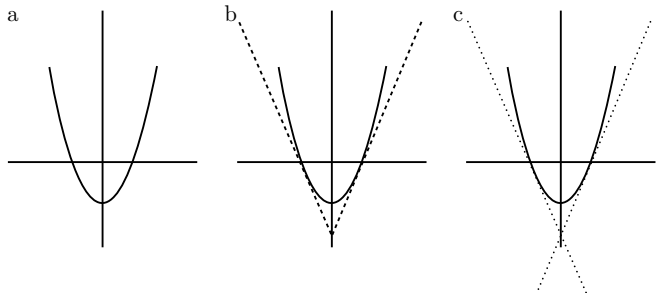

FIG. 1: Schematic dispersion relations for the free fermion models corresponding putting $\Delta = 0$ in (a) $\mathcal{H}_p$ solid line, (b) $\mathcal{H}_{\rm v}$ dashed line, and (c) $\mathcal{H}_{\rm Lin}$ dotted lines.

defined. Also, the particle-hole symmetry is not a consequence of a redundancy due to an artificial doubling of a band. Rather it follows from extending the linear dispersion to arbitrary large negative energies. If we were to add band bending corrections to this model we would break the particle-symmetry which again would change the topological classification of the model. This situation is unsatisfactory since it raises questions about the validity of linear approximations, and in particular the use of the TLM model, for analyzing the Kitaev chain. To resolve this we shall now present an alternative model that resolves the problems related to topology and doubling, while retaining a linear spectrum. Having shown the existence of such a model, we can safely continue to use $H_{\rm Lin}$ in the subsequent discussion.

2. V-shape model

First we replace the parabolic band in Fig. 1(a) with a V-shaped band, with dispersion $\epsilon_{\rm v}(k) = |k|v_F - \bar{\mu}$, as shown in Fig. 1(b).

Next we express the full field $\psi(k)$ in terms of the low momentum fermion fields $\varphi_\pm(k)$

$$\psi(k) = \frac{1}{\sqrt{2}}(e^{ik_F x}\varphi_+(k)\vartheta(k) + e^{-ik_F x}\varphi_-(k)\vartheta(-k))\,, \quad (7)$$

where $\vartheta(k)$ is the step function. In order to write a BdG Hamiltonian, we first define

$$\chi(k) = \frac{1}{\sqrt{2}}(e^{ik_F x}\varphi_+(k)\vartheta(-k) + e^{-ik_F x}\varphi_-(k)\vartheta(k))\,, \quad (8)$$

and the Nambu spinor $\Phi^\dagger = (\psi^\dagger, -i\chi)$. Next we substitute (7) and (8) in the expression for H_p, and disregard the rapidly oscillating terms $\sim e^{\pm 2ik_F}$ to get

$$\mathcal{H}_{\rm v}(k) = \frac{1}{2}\Phi^\dagger\big[(-\bar{\mu} + v_F|k|)\tau_z + \Delta\,\mathrm{sgn}(k)\tau_y\big]\Phi\,, \quad (9)$$

where again the Pauli matrices τ_i act in the Nambu space. As usual, this amounts to a doubling of the spectrum, and this redundancy is manifested in the particle-hole symmetry of $\mathcal{H}_{\rm v}$ which cannot be broken. The pairing term $\sim \Delta$ (which is assumed to be real) is such that it gives rise to the same gap as the original Hamiltonian H_p for constant Δ.

By inspection, we see that the dispersion relation for $\mathcal{H}_{\rm v}(k)$ has an unphysical 2Δ jump at $k = 0$. This discontinuity can be regularized by smoothening the tip of the V-shaped band, and this will in fact be necessary when we analyze the topological properties in Appendix A. Such a regularization will however necessarily yield a more complicated model, that is only amenable to numerical solutions, in spite of having a very simple low energy limit. We will not pursue this since, this model is of interest only to demonstrate the existence of a consistent model with a linear spectrum, and good topological properties.

III. JUNCTIONS AND SOLITONS

A. Topological properties

We start our discussion of π-junctions in 1D superconductors, by reminding the reader about which different topological superconductors are possible in 1D systems. To do this, we recall the topological classification of non-interacting fermion systems[2–4], where the possible topological phases are classified according to their non-unitary symmetries, *viz.* time-reversal symmetry (TRS) $\mathcal{T}$ and particle-hole symmetry (PHS) $\mathcal{C}$ (we note that the PHS is technically a spectral constraint rather than a physical symmetry. However, we here chose to follow the widely adopted terminology of Ref. 2).

In this paper, we consider superconductors in one dimension without spin rotation symmetry. The BdG structure of the Hamiltonian entails a built in algebraic constraint rooted in the fermionic algebra of the field operators that can formally be viewed as a PHS with $\mathcal{C}^2 = +1$. In the absence of time-reversal symmetry, *i.e.* for class D, the superconductor is either topologically trivial, or non-trivial, depending on the value of the $\mathbb{Z}_2$ invariant. In the latter case the wire supports MZMs at both ends[1]. In the case of time-reversal symmetric superconductors, with $\mathcal{T}^2 = -1$, *i.e.* in class DIII, the situation is similar, but in this case, the topological phase exhibits a Kramers-degenerate pair of MZMs at both edges, see, e.g., Refs. 30,31.) Finally, if the system respects the PTRS $\mathcal{T}^2 = +1$, *i.e.* for class BDI, the different topological phases are distinguished by an integer winding number, giving an infinite set of different topological non-trivial phases.

The p-wave wire, (1) or (2), will in general, *i.e.* when we allow both the hopping and the order parameter to be complex, belong to symmetry class D, which means that it can either be in a trivial phase, or in a topological phase. In the lattice model, the former happens for $|\mu| > 2|t|$, while the latter occurs for $|\mu| < 2|t|$, with $|\Delta| \neq 0$.

If both t and Δ are real, the Hamiltonian (2) is also pseudo time-reversal symmetric (here $\mathcal{T}$ is simply com-

plex conjugation, so trivially $\mathcal{T}^2 = 1$), and in this case, the possible topological phases are labeled by an integer, corresponding to a winding number (see Appendix A). Kitaev's model with a constant order parameter exhibits three of these phases, namely the trivial one (when $|\mu| > 2|t|$), as well as two non-trivial ones, both occurring for $|\mu| < 2|t|$, one with $\Delta > 0$, the other with $\Delta < 0$.

This means that for real t and Δ, the Kitaev chain can harbor an interesting junction, by allowing the order parameter to change from $-\Delta$ to $+\Delta$ in a finite region, corresponding to a π-junction. Just as the edge of a Majorana wire hosts a MZM, because it constitutes the boundary between a topological phase and the trivial vacuum, the π-junction we consider here will also support zero modes. Since the difference in winding number between the two neighboring topological phases is two, we expect twice as many zero modes in comparison to the edge of the Kitaev chain. Below we show that this is indeed the case, irrespective of the precise x-dependence of the order parameter.

We already mentioned the problems related to properly define the k-space topology for the TLM model, and how they are resolved by an alternative linearization scheme. The details are given in Appendix A, but we should here again stress that the outcome of this analysis is that we can safely use the TLM model to discuss the topological properties of the Kitaev chain.

B. The π-junction as a soliton

Although the k space argument for topology of the linearized model $\mathcal{H}_{\rm Lin}$ given in Appendix A is compelling, it is important to find out how well the TLM model (6) really captures the topological properties of the full model (2). To do this, we first briefly recall how a Dirac Zero Mode (DZM) arises in the TLM model[24], and then compare it with the zero mode arising in the full model (2), in the presence of a junction, at which the real order parameter Δ changes sign.

The presence of the DZM in the case of a real order parameter is most easily demonstrated in the TLM model, and from $\mathcal{H}_{\rm Lin}$ we get the BdG equations

$$\begin{aligned} \frac{1}{2}(-iv_F\partial_x u(x) + 2i\Delta^*(x)v^*(x)) &= \epsilon u(x) \\ \frac{1}{2}(iv_F\partial_x v^*(x) - 2i\Delta(x)u(x)) &= \epsilon v^*(x)\ . \end{aligned} \qquad (10)$$

For real $\Delta(x)$, and taking $\epsilon = 0$ since we are interested in the zero modes, these equations are easily decoupled by introducing $f_\pm(x) = u(x) \pm v^*(x)$. For a π-junction that interpolates between a negative constant Δ_- for $x \ll 0$ to a positive constant Δ_+ for $x \gg 0$, one finds the solution $f_+(x) = Ne^{-\frac{2k_F}{v_F}\int^x \Delta(x')dx'}$, $f_-(x) = 0$. Here, we will consider the special profile $\Delta(x) = \Delta_0 \tanh(x/\xi)$, that gives rise to the analytical solution[24]

$$f_+(x) = N_0\,\mathrm{sech}(x/\xi)^{\xi/\xi_0} \qquad f_-(x) = 0\ , \qquad (11)$$

where $\xi_0 \equiv v_F/(2\Delta_0)$ and N_0 a normalization constant.

We compare the DZM of the TLM model to the full model, by considering the discretized version $\Delta_j = \Delta_0 \tanh(j/\xi)$ of the TLM profile $\Delta(x) = \Delta_0 \tanh(x/\xi)$ in (2). By choosing the width ξ not too large, this determines the order parameter to $-\Delta_0$ at one end of the chain and $+\Delta_0$ at the other end, generating a domain wall (between sectors with different winding numbers) at the center of the chain. We set the junction parameter $\xi = \xi_0$, and fit the resulting zero mode to the TLM solution $g(x) = \mathrm{sech}(x/\lambda)$, with λ used as a fitting parameter. In Tab. I we show some representative results and in Fig. 2, we display a typical result for the probability density of the DZM located in the junction, as obtained from the Kitaev chain. Evidently, the TLM model captures the the properties of the DZM in the junction region of the Kitaev chain very well.

t	Δ_0	μ	λ/ξ_0	MLS Error
10.0	1.0	0.0	0.999418	$2.2002 \cdot 10^{-8}$
8.0	1.0	0.0	0.999098	$6.7994 \cdot 10^{-8}$
5.0	1.0	0.0	0.997777	$7.5333 \cdot 10^{-7}$
2.0	1.0	0.0	0.991853	$1.2267 \cdot 10^{-4}$
1.0	1.0	0.0	1.071428	$6.8020 \cdot 10^{-3}$

TABLE I: The fitting parameter λ, compared to its analytic value in the TLM model ξ_0, as well as the error of the fit (using the Method of Least Squares), for a system with $N = 1001$ sites and various values of t.

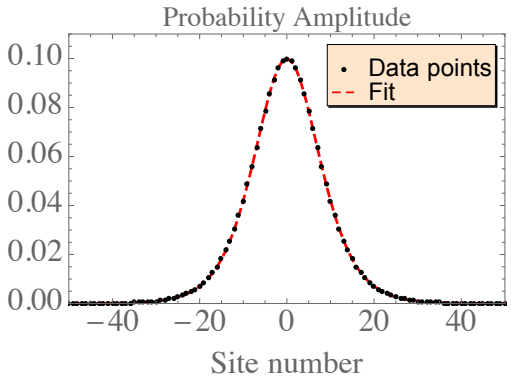

FIG. 2: The probability distribution (black dots) of the zero energy mode located in the junction region of the Kitaev chain with order parameter profile $\sim \tanh(x/\xi_0)$. The parameters used are: $t = 10.0$, $\Delta_0 = 1.0$ and $\mu = 0.0$ yielding $\xi_0 = 10$. The fit (red, dashed line) is made by the method of least squares, and resulted in $\lambda = 9.994$, in good agreement with the value of ξ_0. The number of sites is $N = 1001$; the figure only shows the central region.

IV. PHASE WINDING JUNCTIONS

In this section, we extend the previous discussion to the case of junctions with a complex order parameter where the phase winds in a finite segment of the wire. For simplicity we shall assume that the absolute value $|\Delta|$ remains constant. In this case we can find an analytical solution in the linearized model by taking a simple winding profile, while our numerical analysis easily generalizes to more general profiles.

Although a complex order parameter breaks the PTRS and with that the chiral symmetry that protects the DZMs in the junctions with real profiles, one would still expect that the low energy theory should not differentiate a rapid winding of the phase from 0 to π from a sharp step in the magnitude of Δ. We now demonstrate that this intuition is correct, and that low energy modes persist even in the case of phase winding junctions. Again it is easiest to start from the linearized model.

A. sub-gap states in the linearized model

We consider an order parameter with an x-dependent phase

$$\Delta = \Delta_0 e^{i\theta(x)} \qquad \theta(-\infty) = 0 \qquad \theta(\infty) = f\pi, \tag{12}$$

where Δ_0 is a positive constant, $\theta(x)$ is continuous and f is some real number. The BdG equations (10) then become,

$$\begin{aligned} -i\partial_x u(x) + i/\xi_0 e^{-i\theta(x)} v^*(x) &= \tilde{\epsilon} u(x) \\ i\partial_x v^*(x) - i/\xi_0 e^{i\theta(x)} u(x) &= \tilde{\epsilon} v^*(x)\,, \end{aligned} \tag{13}$$

where $\xi_0 = v_F/(2\Delta_0)$ and $\tilde{\epsilon} = 2\epsilon/v_F$. From the first equation we have

$$v^*(x) = -i\xi_0 e^{i\theta(x)}(\tilde{\epsilon} + i\partial_x) u(x) \tag{14}$$

and substituting this into the second, we get

$$\left[\partial_x^2 + i(\partial_x\theta)\partial_x + \tilde{\epsilon}(\partial_x\theta) + (\tilde{\epsilon}^2 - \xi_0^{-2})\right] u(x) = 0\,. \tag{15}$$

This equation cannot be solved analytically for a general profile, but for the case of

$$\theta_k(x) = \begin{cases} 0 & x < -a \\ \left(\frac{x+a}{2a}\right) f\pi & |x| \le a \\ f\pi & x > a \end{cases} \tag{16}$$

we can solve (15) in the three regions and then match the solutions. Just as in an 1D Schrödinger problem in a piece-wise constant potential, this is done by matching the function and its (logarithmic) derivative. We focus on the case $f = 1$, which corresponds to a π-junction where Δ changes sign, but the analysis below can easily be extended to junctions with arbitrary phase winding.

The piecewise solutions are given by

$$u(x) = \begin{cases} \alpha_1 e^{\kappa x} & x < -a \\ e^{-i\frac{\pi}{4a}x}\left(\alpha_2^+ e^{\tilde{\kappa}x} + \alpha_2^- e^{-\tilde{\kappa}x}\right) & |x| \le a \\ \alpha_3 e^{-\kappa x} & x > a \end{cases} \tag{17}$$

where $\kappa = \sqrt{\xi_0^{-2} - \tilde{\epsilon}^2}$ and $\tilde{\kappa} = \sqrt{\xi_0^{-2} - (\tilde{\epsilon} + \pi/(4a))^2}$. To obtain a normalizable solution, we must take $\kappa < 0$, or $|\tilde{\epsilon}| < 1/\xi_0$, implying that the (sub-gap) solution is localized in the junction region. From the matching conditions for the wave function and its derivative, one can infer that there is no solution when $\tilde{\kappa}$ is real. An imaginary $\tilde{\kappa}$ requires that $\tilde{\epsilon} > 1/\xi_0 - \pi/(4a)$, so localized sub-gap modes are possible in the energy range $1/\xi_0 - \pi/(4a) < \tilde{\epsilon} < 1/\xi_0$ if $a > \xi_0\pi/8$, or in the whole gap region $-1/\xi_0 < \tilde{\epsilon} < 1/\xi_0$ if $a < \xi_0\pi/8$.

For imaginary $\tilde{\kappa}$, the matching conditions have a solution if the following constraint is satisfied

$$\tan\left(2a\sqrt{(\tilde{\epsilon} + \frac{\pi}{4a})^2 - \xi_0^{-2}}\right) = \frac{\sqrt{\xi_0^{-2} - \tilde{\epsilon}^2}\sqrt{(\tilde{\epsilon} + \frac{\pi}{4a})^2 - \xi_0^{-2}}}{\tilde{\epsilon}^2 + \frac{\tilde{\epsilon}\pi}{4a} - \xi_0^{-2}}. \tag{18}$$

Upon analyzing this equation, one finds that even for arbitrary small a, there is always at least one solution. The energy of the associated bound state is always positive, but approaches zero in the limit of small a. Upon increasing a, more and more bound state solutions appear. In order to have at least $p+1$ bound states, a should satisfy $a \ge \frac{(4p^2-1)\pi\xi_0}{8}$.

Before turning to the numerical results, we briefly discuss the case of general phase winding, *i.e.*, we allow f in (16) to be arbitrary. For f arbitrary small, one finds a bound state, with an energy slightly below the band gap, $\tilde{\epsilon} \lesssim 1/\xi_0$. Upon increasing f, the energy of this bound state decreases towards $\tilde{\epsilon} = -1/\xi_0$. In the mean time, more bound states appear at the gap edge $\tilde{\epsilon} = 1/\xi_0$. In the limit of large f, the energies of the bound states become periodic in f, with a period of 2, *i.e.*, a period of 2π in the winding angle. Finally, in the limit of a very short junction, we find that for f an odd integer, there is a bound state at $\tilde{\epsilon} \approx 0$, while for f an even integer, there are two bound states with energy $\tilde{\epsilon} \approx \pm 1/\xi_0$. In the former case, the junction behaves as a π junction with a real order parameter, while the second case is equivalent to not having a junction at all. This is consistent with the topological discussion above, although we should point out that there are no topological reasons why the phase junction should behave as a real junction in the short junction limit. We next compare some of the results of this section with numerical simulations in the Kitaev chain and in the full s-wave model.

Analytic sol.	Linear model	Full model
0.940199	0.940201	0.940156
0.956549	0.956556	0.956385
0.981316	0.981324	0.981002

TABLE II: The energies of the first three bound states in a p-wave π phase winding junction. The parameters used for these calculations are: $t = 10.0$, $\Delta = 1.0$, $\mu = 0.0$, $a = 120$, $N = 800$. Analytical, linear model and full model refer to the equations (18), (10) and (2) respectively. Note that the linear model values are just a measure of how well analytic solution describes the discretized linear model, while the full model values describe how well the linearization captures the low energy degrees of freedom.

B. Comparison with the Kitaev chain

Starting with the Kitaev chain model given in (2), we take the profile $\Delta_j = |\Delta_0| e^{i\pi \frac{(j+a)}{2a}}$, so that over a segment of length $2a$, the phase increases linearly from 0 to π. Effectively, this amounts to changing the sign of Δ just as in the previous section. Using this profile, we numerically calculated the energy of the low lying fermion states both for the Kitaev chain and the linearized model, using a range of parameters. Typical results are shown in Tab. II, where the agreement between the first two columns is a measure of the precision of our numerics, and the good agreement with the third column again confirms that the linearized model faithfully describes the full Kitaev chain. We have also compared the numerical wave functions for the low lying states in the Kitaev chain, with the analytical expressions (17) and again found excellent agreement.

Next we studied what happens when the length of the phase winding π-junction shrinks. In Fig. 3, which shows our result for the p-wave case, we see clearly how a state that is close to the gap for large junctions comes down, and becomes a zero mode for the shortest junctions (which essentially amounts to a sign change between two lattice points). This supports the heuristic argument, given earlier, that a short phase winding π-junction should have properties very similar to the one where Δ remains real but changes sign. The corresponding s-wave setup is depicted in Fig.4, where no zero modes need to be formed in the short junction limit.

These results give additional confirmation that the low energy properties of junctions made by Kitaev chains can be captured by the linearized model in (5), and in the Section VI we construct a topological field theory, which captures the same physics.

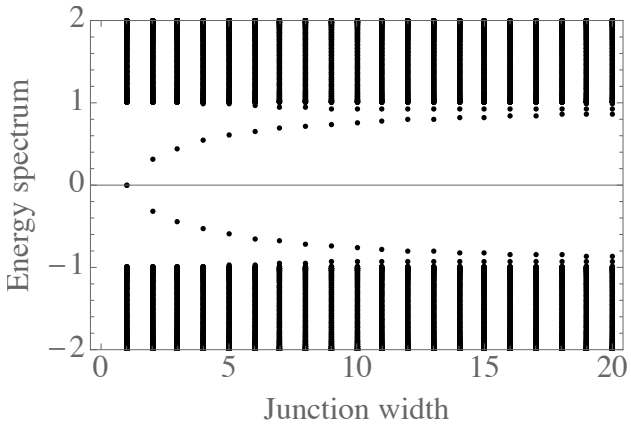

FIG. 3: The energy spectrum of the Kitaev chain as a function of its π phase junction length (in units of the lattice parameter).. A junction length of 1 means that the phase jumps from 0 to π from one site to another. Note that the zero energy states that represent MZMs located at the end points of the chain have been omitted. In addition, two new zero modes are formed as the junction length shrinks, effectively imitating a real π-junction. The parameters used are $t = 2.0$, $\Delta_0 = 1.0$, $\mu = 0.0$ and $N = 200$. The spectrum is displayed in a low energy regime.

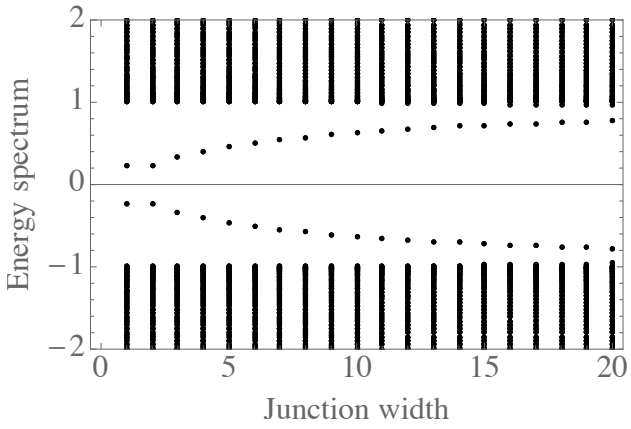

FIG. 4: The energy spectrum of the s-wave wire as a function of the length of its π phase junction (in units of the lattice parameter). A junction length of 1 means that the phase jumps from 0 to π from one site to another. Because the s-wave wire is topologically trivial, no zero modes form, even in the limit of a short junction. The parameters used are $t = 2.0$, $\Delta_0 = 1.0$, $\mu = 0.0$ and $N = 200$. The spectrum is displayed in a low energy regime.

V. HOW TO EXPERIMENTALLY PROBE TOPOLOGY BY A π-JUNCTION

Most of the experimental effort in studying the topological wires has been aimed at detecting the MZM at the edges. But as mentioned in the introduction, the proposed signatures for these modes can also be emulated by other effects. It is thus interesting to consider other signatures for the wire being in the topological phase,

and here we suggest the possibility of using the DZMs at π-junctions as such a probe. For this idea to be useful, we not only need a way to experimentally realize such a junction and detect the associated fermionic zero modes, but also a clear signature for the topological phase. We shall consider both junctions with topologically protected zero modes, and phase winding junctions. We begin with the latter.

A. Phase winding π-junction

One way to make a phase winding junction is to put a wire of the type used in previous experiments on top of a s-wave superconductor through which a current is driven between external leads placed close to the wire. By the the relation $\nabla\phi \sim J$, where ϕ is the superconducting phase and J is the current, one can arrange for a π phase difference between the leads, which will, by proximity, be imprinted on the wire. An experimentally more challenging task is to probe the fermion spectrum at the junction. An obvious possibility is to use a tunneling contact weakly coupled to the wire, or a scanning tunneling microscope.

From the previous section it would appear that a good signature for the p-wave pairing phase would be the presence of an almost zero mode in the junction region. Unfortunately, the situation is not very clear since an s-wave pairing would have a similar signature. Fig. 4 is similar to Fig. 3, but for s-wave pairing. Also here we find a low-lying sub-gap state for short junctions, and although it does not come all the way to zero, it is not clear that it could be distinguished from the p-wave case. Clearly one would need much more detailed studies of more realistic microscopic models in order to resolve this question.

B. Real π-junction

As already pointed out, in a π-junction with a real order parameter (that must go through zero) the zero energy Dirac mode is always present when the superconductor is in the topological phase. For the trivial s-wave case, there is no such protected zero mode, but the spectrum of the subgap modes does depend on the profile of the order parameter at the junction (and on the other parameters, such as the chemical potential). Importantly, there can be junction modes with zero energy, that can be described by the TLM model we studied above, for certain choices of parameters. For example, putting the chemical potential in the band middle ($\mu = 0$ or equivalently $\bar{\mu} = 2t$ as measured from the bottom of the band), there are localized modes with zero energy, regardless of the junction length. But these states can be gapped out in the short junction limit by lowering the chemical potential to the vicinity of the band bottom. This feature is demonstrated in Fig. 5 and contrasted with the corresponding p-wave system in Fig. 6. In the latter case, the topology protects the zero mode, regardless of the junction length, as long as the chemical potential lies in the band, so that the system is in the topological phase.

We note that for wide p-wave junctions, $\xi \gtrsim 30$, there are additional subgap modes with finite energy which are not in the range of ξ-values in Fig. 6.

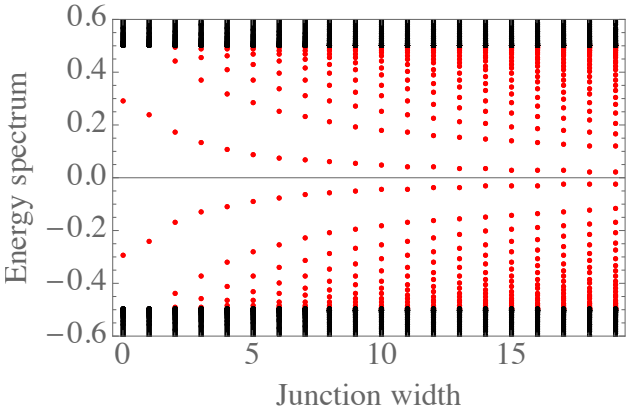

FIG. 5: The energy spectrum (bulk states in black and subgap states in red) of the s-wave wire (a discrete version of Eq. (4)) as a function of the width of its real π-junction (in units of the lattice parameter). Modes with zero energy exist only in the limit of a wide junction, and are gapped out in the short junction region due to the low chemical potential. The parameters used are $t = 1.0$, $\Delta_0 = 1.0$, $\mu = 1.9$ ($\bar{\mu} = 0.1$) and $N = 200$. The spectrum is displayed in a low energy regime.

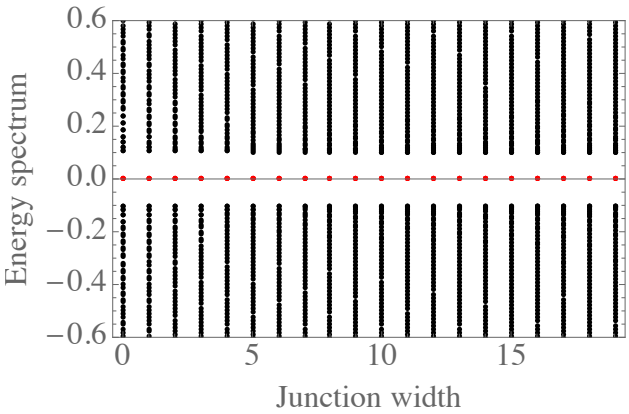

FIG. 6: The energy spectrum (bulk states in black and subgap states in red) of the p-wave wire (Eq. (2)) as a function of the width of its real π-junction (in units of the lattice parameter). The Dirac zero mode is topologically protected and exists for short and long junctions since the wire is in its topological phase. Subgap modes with finite energy are not present in the junction length regime displayed here. The parameters used are $t = 1.0$, $\Delta_0 = 1.0$, $\mu = 1.9$ ($\bar{\mu} = 0.1$) and $N = 200$. The spectrum is displayed in a low energy regime.

There are at least two possible ways to experimentally realize a junction of this type. The most direct would be to implement a π-junction in the underlying s-wave superconductor, but the problem here is that it is not easy to determine the Δ profile in the junction. An alternative way is to put the wire as a bridge connecting two different s-wave superconductors that are held at different values of θ, for instance by a SQUID geometry. In this case one might calculate the Δ profile by a realistic modeling of the wire.

Clearly both options need to be studied in more detail before any definite conclusion can be made about the feasibility of using sub-gap junction spectroscopy for probing the topological nature of the wire.

VI. A TOPOLOGICAL FIELD THEORY FOR π PHASE WINDING JUNCTIONS

As in the previous sections we consider Δ as given by the background s-wave superconductor by proximity. We generalize the previous discussion somewhat by considering a wire with many widely separated π-junctions of the phase winding type. Since the bound states are exponentially localized, such configurations will support subgap modes at each junction. We stress that we consider a fixed junction configuration, given by the background s-wave order parameter, and derive an effective theory for the fermions. We can, using the same formalism, also describe adiabatic motion of the junctions, but they cannot be considered as *bona fide* itinerant particles.

Our starting point is the Lagrangian formulation of the linearized version of the p-wave superconductor (6), which is given by

$$\mathcal{L} = \bar{\psi}\left(i\partial\!\!\!/ - g(x)e^{i\vartheta(x)\gamma_5}\right)\psi\ , \tag{19}$$

where the functions ϑ and g are related to the superconducting order parameter by $\Delta = ge^{i(\vartheta+\pi/2)}$, and where the Dirac matrices are related to the Pauli matrices by $(\gamma_0, \gamma_x) = (\sigma^x, -i\sigma^y)$ so $\gamma_5 = \sigma^z$. We have in our derivation relabeled the spinor Ψ to ψ, in accordance with standard notation. Furthermore, we have put $v_F = 2$, consistent with the linearization of (1). Note that for real Δ, the energy gap Δ is nothing but the mass in the Dirac equation.

The aim here is first to derive a bosonic form of the Lagrangian (19), and then to extract an effective action that describes the physics of the bound states on the solitons. This theory is topological in the sense that it does not have any bulk degrees of freedom, but only describes the quantum mechanics of the bound states residing on the solitons. Before embarking on this exercise, we will put it in context, and view it as part of the more challenging problem to formulate topological theories in the presence of fermionic zero modes.

As mentioned in the introduction, the Kitaev chain is a one-dimensional cousin of the two-dimensional (2D) p-wave superconductor, and the Majorana states located on the interfaces between the normal and topological phase of the model can, by employing geometries with junctions, be used for quantum computing. In this context the quantum mechanics of the zero modes is clearly very interesting. In the 2D case, there are two candidates for a topological field theory that describes the braiding of vortices with Majorana zero modes. One is based on a $SU(2)$ Chern-Simons theory[32], while the other employs an abelian BF theory coupled to a single Majorana field[33]. In this 2D case, the vortices are in principle itinerant, but are in practice often pinned to impurities. In this latter case there is a close analogy with our system of fixed, or adiabatically moving, π-junctions.

None of these effective theories just mentioned has been derived from a microscopic description, but are obtained from general principles based on symmetry and scaling. The effective topological theory for the fermionic bound states on solitons that we shall describe shortly, is closely related to the second of the 2D topological theories that we just mentioned. An obvious, and important, difference is that the fermionic modes on the solitons are of Dirac type, so, even if fine tuned to zero energy, they can not be used for topological quantum computing. The advantage with the present case is that it is more amenable to analytical treatment. Still we have not managed to obtain the topological theory directly from the microscopic model in a controlled fashion. The derivation presented below is therefore phenomenological and again based on symmetry considerations and scaling arguments. In Appendix C we do offer a microscopic derivation which however involves several unproven, and admittedly questionable, assumptions.

A. Symmetries

We now discuss the symmetries of (19). From this Lagrangian we can immediately get the vector and axial charge densities,

$$\rho_V = \psi^\dagger\psi = \varphi_+^\dagger\varphi_+ - \varphi_-^\dagger\varphi_- \tag{20}$$

$$\rho_A = \psi^\dagger\gamma_5\psi = \varphi_+^\dagger\varphi_+ + \varphi_-^\dagger\varphi_- \tag{21}$$

which shows that the electric charge $Q_{em} \equiv Q_A = \int dx\, \rho_A(x)$ in the superconductor is given by the *axial* charge (21) in the Dirac theory (19), and is thus not conserved, as appropriate for a superconductor. Note, however that (19) *is* invariant under the combined global transformation

$$\begin{aligned} \psi &\to e^{i\beta\gamma_5}\psi \\ \theta &\to \theta - 2\beta\,. \end{aligned} \tag{22}$$

In a BdG description this corresponds to a simultaneous global phase change of the electron field and the superconducting condensate $\langle\psi\psi\rangle$. Also note that the transformation,

$$\psi \to e^{i\pi\gamma_5}\psi = -\psi \tag{23}$$

is indeed a symmetry. As expected, this is a manifestation of the the conservation of electric charge modulo two, which is most easily seen by noting that the transformation (23) leaves the pairing terms $\varphi_+^\dagger\varphi_-^\dagger$ and $\varphi_+\varphi_-$ invariant. It will be important later that the vector charge $Q_V = \int dx\, \rho_V(x)$ in the Dirac theory is indeed conserved. Physically this is a consequence of the Cooper pairs having zero momentum, so adding or subtracting a pair will give identical changes at the two Fermi points[34]. In the following we shall give a bosonized version of the theory where it will be important to keep the correct symmetry pattern.

B. Bosonization

It will be advantageous to rewrite (19) in bosonic variables using the bosonization "translation table", (see for instance Ref. 35),

$$\begin{aligned} \bar\psi\psi &\to \kappa\cos\varphi \\ \bar\psi\, i\gamma_5\psi &\to \kappa\sin\varphi \\ \bar\psi\gamma_\mu\psi &\to \frac{1}{2\pi}\epsilon^{\mu\nu}\partial_\nu\varphi \end{aligned} \tag{24}$$

where the dimension-full parameter κ depends on the short distance cutoff, and the scalar field φ is normalized so that the bosonic version of (19) is

$$\mathcal{L} = \frac{1}{8\pi}(\partial_\mu\varphi)^2 - g\cos(\varphi-\vartheta) \tag{25}$$

where we have rescaled g with κ. The minima of the potential are at

$$\varphi_n = \vartheta + \pi + n2\pi = \theta - \frac{\pi}{2} + n2\pi\,, \tag{26}$$

so for large g, $\vartheta = \theta - \pi/2$ will make small fluctuations around one of these (equivalent) minima. In particular, if θ winds, then φ follows. From the work of Jackiw and Rebbi[36], and Goldstone and Wilczek[29], we know that windings in the scalar field φ will describe solitons carrying (in general fractional) fermion number. For simplicity we neglect 2π windings, and taking $n = 0$ in (26) we define the kink current as

$$j_\mu^k = \frac{1}{2\pi}\epsilon^{\mu\nu}\partial_\nu\theta\ , \tag{27}$$

so the charge of the soliton that interpolates $\theta(x)$ from φ_L to φ_R is given by,

$$Q_s = \frac{1}{2\pi}(\varphi_{\rm R} - \varphi_{\rm L})\ . \tag{28}$$

It follows that the π-junctions we discussed earlier carry a half unit of fermion number.

Next we shift the field φ by $\varphi = \varphi_0 + \phi$ to get

$$\begin{aligned} \mathcal{L} &= \frac{1}{2\pi}\epsilon^{\mu\nu}\partial_\nu\theta\, b_\mu - b_\mu j_k^\mu \\ &+ \frac{1}{8\pi}(\partial_\mu\phi)^2 - g\cos(\phi) + \frac{1}{2}j_k^\mu\epsilon_{\mu\nu}\partial^\nu\phi + \frac{1}{8\pi}(\partial_\mu\theta)^2 \end{aligned} \tag{29}$$

where b_μ is a multiplier field that imposes the condition (27). Since the ϕ-field is massive, it can be integrated, to yield the truly trivial topological theory,

$$\mathcal{L}_{\theta b} = \frac{1}{2\pi}\epsilon^{\mu\nu}\partial_\nu\theta\, b_\mu - b_\mu j_k^\mu. \tag{30}$$

C. Retaining the fermion bound states

The topological theory we just derived is however not always a good description of the low energy physics. This is most easily seen by considering the special case where the topological current describes widely separated narrow π-solitons. We learned in section IV A that these can support low energy fermionic bound states with energy $\epsilon_0 < \epsilon < \Delta$ inside the gap. Since we furthermore can fine tune so one of these modes occurs arbitrarily close to zero energy, the topological theory (30) can clearly not be universally correct. Moving away from the ϵ_0 point, but still having the bound state far below the bulk gap, *i.e.* $\epsilon_0 \ll g$, it would still be desirable to have a theory that describe these low-lying excitations. What went wrong in the derivation of (30) is that while the bosonic fluctuations with energy $\geq g$ were integrated, the more important fluctuations changing the fermion number were not taken into account. We will now remedy this and present a model that properly includes the dynamics of the low-lying fermionic bound states.

We shall first construct a model in the limit of widely separated point-like kinks. Any real function Δ that interpolates between $\pm|\Delta_0|$ at $x = \pm\infty$ supports a zero mode. The kink, $|\Delta|\eta(x)$, where η is the step function, can be thought of as a limit of such functions, and thus supports a zero mode. Also, as discussed above, we get an approximate zero mode for constant $|\Delta| = m$, and a rapid winding of the phase θ an odd number of π. In both these cases the topological current related to the kink can be be described by

$$j_k(x,t) = \sum_{a=1}^{N}\delta(x-x_a)\,(1,\dot x_a) \tag{31}$$

where we allowed for the kink at position x_a to move with velocity $\dot x_a$.

It is now straightforward to write a Lagrangian for the bound states residing on the kinks,

$$\begin{aligned} L &= \sum_{a=1}^{N}\xi_a^\dagger i\frac{d}{dt}\xi_a \\ &= \sum_{a=1}^{N}\xi_a^\dagger(t,x_a(t))i(\partial_t - \dot x_a(t)\partial_x)\xi_a(t,x_a(t)) \\ &= \int dx\, j_k^\mu\,\xi^\dagger(x,t)i\partial_\mu\xi(x,t)\,. \end{aligned} \tag{32}$$

Combining this with the term (30), yields

$$\mathcal{L}_{\xi\theta b} = \frac{1}{2\pi}\epsilon^{\mu\nu}\partial_\nu\theta\ \left[b_\mu + \xi^\dagger i\partial_\mu\xi\right] - \epsilon_0\xi^\dagger\xi - b_\mu j_k^\mu \tag{33}$$

where we also introduced a chemical potential ϵ_0 that fixes the energy of the bound state. We shall take ξ to be a complex fermionic field (otherwise it would not describe a single bound state), but note that it differs from a conventional Dirac fermion in being dimensionless.

The first term in Lagrangian (33) is closely related to the topological Lagrangian for a spin-less 2D chiral superconductor given in Ref. 33. The main difference is that in the 2D case the Dirac fermion $\xi(x,t)$ is replaced by a Majorana field $\gamma(x,t)$. In the present setting, that would be appropriate for a domain wall between a trivial and non-trivial phase of the wire. The second term $\sim \epsilon_0$ is not topological and is present only for a complex field. Note that the kinetic term $\sim \xi^\dagger\partial_0\xi$ in (33) has support only where the topological charge does not vanish, and thus there are no bulk degrees of freedom. The above analysis is, however, valid only for point like sources. The generalization to extended sources, that is the finite size kinks considered in the previous sections, is our next task.

D. Fermion bound states in extended kinks

Since for a static kink, the Hamiltonian in (33) is only a chemical potential, it can not describe the fermion modes on an extended kink, but instead gives a continuum of states at energy ϵ_0. To get a realistic low energy theory we must thus introduce more terms in the effective Hamiltonian. Following the usual logic of effective theories we shall retain the lowest derivative terms that ensure the correct symmetries. The crucial symmetry here is the broken global $U(1)$ symmetry related to the electric charge. In the linearized theory (19) this is the (global) chiral symmetry (22). Clearly terms like $\xi^\dagger\xi$, $\xi^\dagger\partial_x^2\xi$ *etc.,* are allowed, but also pairing terms like $e^{i\theta}\xi^\dagger\partial_x\xi^\dagger$ *etc.*. In fact it is necessary to include a pairing term in order to get the appropriate symmetry breaking. Putting the chemical potential ϵ_0 to zero, the simplest possible action for an extended kink is,

$$\mathcal{L}_{\xi\theta b} = \frac{1}{2\pi}\epsilon^{\mu\nu}\partial_\nu\theta\,\left[b_\mu + \xi^\dagger i\partial_\mu\xi\right] - \mathcal{H}_\xi - b_\mu j_k^\mu \qquad (34)$$

with

$$\mathcal{H}_\xi = \frac{1}{2\pi}\xi^\dagger\big(M^2-\partial_x^2\big)\xi + \frac{\delta M}{4\pi}\left[e^{i\theta}\xi i\partial_x\xi + e^{-i\theta}\xi^\dagger i\partial_x\xi^\dagger\right], \qquad (35)$$

where the mass parameter M and the pairing strength δ, are phenomenological parameters.

We can simplify this Hamiltonian by performing a rotation of the fields:

$$\xi \to e^{-i\theta/2}\xi \qquad\qquad \xi^\dagger \to e^{i\theta/2}\xi^\dagger\ . \qquad (36)$$

This will transform the Hamiltonian (35) to $\mathcal{H}_\xi = (\xi^\dagger,\xi)\bar{\mathcal{H}}(\xi,\xi^\dagger)^{\mathrm{T}}$ with

$$\bar{\mathcal{H}}_\xi = \begin{pmatrix} M^2-(\partial_x-\frac{i}{2}\partial_x\theta)^2 & \delta M i\partial_x \\ \delta M i\partial_x & -M^2+(\partial_x+\frac{i}{2}\partial_x\theta)^2 \end{pmatrix}. \qquad (37)$$

Next, we expand the quantum field as $\xi(x,t) = \sum_n(e^{-iEt}u_n^*(x)c_n^\dagger + e^{iEt}v_n^*(x)c_n)$, which yields the following BdG equations for the eigenfunctions $u(x)$ and $v(x)$,

$$\Big((\partial_x+\frac{i}{2}\partial_x\theta)^2 + E\partial_x\theta - M^2\Big)u(x) + \delta M i\partial_x v^*(x) = 0 \qquad (38)$$

$$\Big((\partial_x-\frac{i}{2}\partial_x\theta)^2 - E\partial_x\theta - M^2\Big)v^*(x) - \delta M i\partial_x u(x) = 0$$

In the limit $\delta \to 0$ and under the assumption that θ varies slowly (i.e, we assume $\partial_x^2\theta$ and $(\partial_x\theta)^2$ to be small) we obtain the following equation for $u(x)$

$$\left[\partial_x^2 + (\partial_x\theta)i\partial_x + E(\partial_x\theta) - M^2\right]u(x) = 0, \qquad (39)$$

which is (15) in the limit where the energy E is small compared to M. As expected there is no continuous component in the spectrum, and the low energy part of the spectrum compares well with the full model with suitable adjustment of the model parameters. In particular, we should set $M^2 = \xi_0^{-2} = 4\Delta^2/v_F^2$, $E = \tilde{\epsilon} = 2\epsilon/v_F$. The requirement that $E \ll M$ then translates to $\epsilon \ll \Delta$, that is, for energies well below the gap, which is consistent with a zero energy bound state.

To actually *derive* the effective Lagrangian (33) one should integrate out the high energy modes. This would not only give expressions for the effective parameters, but also provide an ultraviolet cutoff that would define the region of validity of the effective model. We have not been able to do this in a controlled way, but in Appendix C it is shown, by manipulating path integral expressions, how the crucial kinetic term $\frac{1}{2}\epsilon^{\mu\nu}\partial_\nu\theta\xi^\dagger i\partial_\mu\xi$ can arise from the microscopic description.

Finally we note that the extension of the topological theory (33) to the model Lagrangian (34) for the subgap regime, is reminiscent of the extension, proposed in Ref. 37. of the 2D topological theory in Ref. 33. In both cases the models are constructed using phenomenological and heuristic arguments, and it remains a theoretical challenge to find general methods to describe localized fermionic zero modes in the general context of topological field theory.

VII. CONCLUDING REMARKS

In this paper we studied several models for trivial and topological superconducting wires in one dimension. More specifically, we investigated the properties of π-junctions, and in particular those where the phase of the

order parameter winds an angle π over the junction, corresponding to a system in symmetry class D. For this more general case, we find that there is no topologically protected zero energy mode associated with a π-junction. Rather, local breaking of the PTRS by means of the complex winding of the order parameter can shift the energy of the bound state in the junction region away from zero energy. This symmetry breaking is not allowed in class BDI, where, as a consequence, the bound state is topologically pinned to zero energy. We demonstrated that the low energy bound states in some specific cases can be obtained analytically and showed that these results agree well with numerical calculations. Most importantly, we discussed how our results might be used to obtain a bulk probe - in contrast to the common method of probing the edges - to distinguish a topological wire from a trivial one, and suggested some experimental approaches to this end. Finally we constructed a low energy field theory with a topological term describing itinerant π-junctions, and discussed its relation to theories in two dimensions.

Acknowledgements. C.S. thanks S. Abay Gebrehiwot, M. Leijnse, H.Q. Xu and C. Yu for interesting discussions and hospitality. T.H.H. thanks F. von Oppen for a useful discussion. This research was sponsored, in part, by the Swedish research council. J.C.B. acknowledges funding from the ERC synergy grant UQUAM.

Appendix A: Topology of the p-wave superconductor modes.

Here, we discuss the topological properties of the various models we consider in this paper. To set the scene, we start by recalling the topological properties of the Kitaev chain, see Ref. [1].

Consider the model (2) and assume that t and Δ are both real, so that the Hamiltonian belongs to symmetry class BDI. The topological invariant takes the form of a winding number[2], and to show this in the present case, we write the k-space Hamiltonian (3) as

$$\mathcal{H}_K(k) = \vec{d}(k) \cdot \vec{\tau}\,, \tag{A1}$$

with $\vec{\tau} = (\tau_x, \tau_y, \tau_z)$. For models in class BDI, one can choose a basis such that one of the components of the vector $\vec{d}$ is zero, say $d_x = 0$. The energy is given by $\epsilon(k) = \pm|\vec{d}(k)|$, which means that for a gapped system, we have $\vec{d}^2(k) > 0$. Hence, the winding number ν around the origin of the curve in (τ_y, τ_z)-space (*i.e.*, the space of Hamiltonians) swept out by $\vec{d}(k)$ as k sweeps through the full Brillouin zone is well defined. This winding number is the topological invariant characterizing the different phases. For the Kitaev chain we have $\vec{d}(k) = (0, -\Delta\sin(k), -\mu/2 - t\cos(k))$, and in Fig. 7, we (schematically) show the curve $\vec{d}(k)$ in the trivial phase, with winding $\nu = 0$, and the two different topological phases, with winding $\nu = \pm 1$.

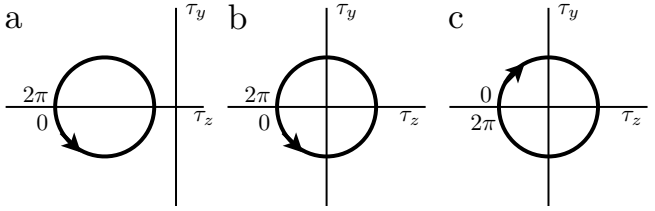

FIG. 7: Winding numbers ν of $\vec{d}(k)$ for the full Kitaev chain, in (a) trivial phase with $\nu = 0$, for $0 < t < \mu/2$, $\Delta > 0$, (b) topological phase with $\nu = 1$ for $\mu = 0$, $0 < t = \Delta$ and (c) topological phase with $\nu = -1$ for $\mu = 0$, $0 < t = -\Delta$. The arrows denote the direction in which k increases.

Next we turn to the linear model $\mathcal{H}_{\rm Lin}$ in Eq. (5). Assuming that Δ is real and constant, the momentum space version of the Hamiltonian (6) is again of the form (A1), with $\vec{d}(k) = (0, -2\Delta, v_F k)$.

Since the k-space is not compact, it is possible that the curve swept out by $\hat{d}(k) = \vec{d}(k)/|\vec{d}(k)|$ (the normalization is needed to obtain finite limits and is valid as long as the Hamiltonian is gapped) as k goes from $-\infty$ to ∞ is not closed. This is indeed what we find in Fig. 8, where we depict the two cases $\Delta = \pm 1$. Despite that we can not de-

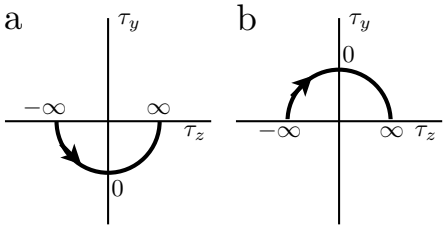

FIG. 8: 'Winding' of the vector $\hat{d}(k)$ for the linearized model (6), for (a) $\Delta > 0$ and (b) $\Delta < 0$.

fine a winding number for neither of the values $\pm\Delta$, we can still consider the *difference in winding number* $\delta\nu$ between the two cases, which gives $|\delta\nu| = 1$. Therefore, we expect a zero energy bound state at a boundary between two regions with $\Delta = \pm 1$ respectively, even in the linearized model. We stress, that although that this argument in not rigorous, it is nevertheless true, and in the main text we showed that the analytic form of the zero mode of the linearized model of Ref. 24 accurately describes the DZM in the junction of the full Kitaev chain.

We now turn to the alternative linearized model given by $\mathcal{H}_v$ in Eq. (9). Here the k-space is again not compact, and there is also a discontinuity at $k = 0$. The first issue is remedied by identifying the points at $\pm\infty$ (which amounts to considering the $a \to 0$ limit of the lattice model). To deal with the second, we note that for this model, $\vec{d}(k) = \frac{1}{2}(0, \Delta\mathrm{sgn}(k), -\bar{\mu} + v_F|k|)$, and in Fig. 9 we show the corresponding 'winding' of the vector $\hat{d}(k) = \vec{d}/|\vec{d}|$, in the case $\Delta > 0$. Even when identifying the points at $k = \pm\infty$, the curve is not continuous, but with a regularization that smoothens out the singu-

larity in the V-shaped band, by replacing the factor sgn by a continuous odd function that rapidly changes sign around $k = 0$, the d-vector will will be continuous, and the winding number will be well defined. This concludes the demonstration of the existence of a linearized continuum model with topological properties identical to that of the Kitaev chain.

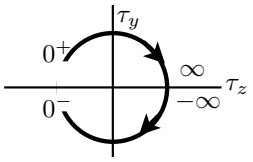

FIG. 9: The 'winding' of the $\hat{d}(k)$-vector corresponding to the linearized model $\mathcal{H}_v$ before the regularization which removes the discontinuity at $k = 0$. The arrows indicate the direction in which k increases. We have used $\Delta > 0$. As discussed in the text, the gap between the points 0^+ and 0^- is closed if the dispersion relation is smoothened at $k = 0$.

Appendix B: Topological aspects of the s-wave paired models

In this appendix, we discuss the topological properties of the full and linearized s-wave models. Due to the extra spin degree of freedom in these models, the winding arguments used for the p-wave superconductors are not directly applicable and another method of topological classification must be used. We will use the method outlined in Ref. 22.

We begin with the full s-wave model, given by (4). Assuming a real and constant order parameter, the corresponding k-space Hamiltonian can (in suitable units) be written as

$$H^S(k) = (k^2 - \bar{\mu})\tau_z s_0 - \Delta\tau_y s_y \tag{B1}$$

where the Pauli matrices τ_i and s_i act in particle-hole space and spin-space respectively. This Hamiltonian belongs to symmetry class BDI, meaning PTRS $\mathcal{T}^2 = +1$ and PHS $\mathcal{C}^2 = +1$. These operators are in our chosen basis given by $\mathcal{T} = \tau_0 s_0 K$ and $\mathcal{C} = \tau_x s_0 K$, with K denoting the complex conjugation operator.

To investigate the topological properties of this Hamiltonian, we write it in the form

$$H^S(k) = \begin{pmatrix} H_0(k) & \hat{\Delta} \\ \hat{\Delta}^{\mathrm{T}} & -H_0(k) \end{pmatrix}, \tag{B2}$$

where the matrix structure is in particle-hole space, $H_0(k) = (k^2 - \bar{\mu})s_0$ and $\hat{\Delta} = \Delta i s_y$. We note that the latter term is real and has the property $\hat{\Delta}^{\mathrm{T}} = -\hat{\Delta}$. By a unitary transformation with $U = \exp(-i(\pi/4)\tau_y s_0)$, the matrix in equation (B2) can be rotated into

$$UH^S(k)U^\dagger = \begin{pmatrix} 0 & A(k) \\ A(-k)^{\mathrm{T}} & 0 \end{pmatrix}, \tag{B3}$$

with $A(k) = H_0(k) + \hat{\Delta}$.

Next, we note that $\mathrm{Det}(H^S(k)) = \mathrm{Det}(UH^S(k)U^\dagger) = \mathrm{Det}(A(k))\mathrm{Det}(A(-k)^{\mathrm{T}})$ so that if $H^S(k)$ is gapped for all k, *i.e.* $\mathrm{Det}(H^S(k)) \neq 0$, the determinant of $A(k)$ can not vanish either. This allows us to define $z(k) = \exp(i\theta(k)) = \mathrm{Det}(A(k))/|\mathrm{Det}(A(k))|$ for gapped Hamiltonians $H^S(k)$. One may then show that

$$z(k) = \mathrm{sgn}(\Delta^2 + (k^2 - \bar{\mu})^2). \tag{B4}$$

For the s-wave Hamiltonian (B1), which is real and gapped for all k, $\bar{\mu}$ and finite Δ, the determinant is real and non-vanishing. Then $z(k)$ is well defined and is equal to $+1$, independently of any compactification of k-space (which is needed for any well defined topological invariant), rendering the model topologically trivial.

We next turn our attention to the linear s-wave model. To derive it, we apply the linearization scheme described in section II C to (4) and again assume a real order parameter which gives us the following Hamiltonian:

$$H^S_{\mathrm{Lin}} = \int dx \sum_\sigma ((-iv_F\varphi^\dagger_{\sigma,+}\partial_x\varphi_{\sigma,+} + iv_F\varphi^\dagger_{\sigma,-}\partial_x\varphi_{\sigma,-}) + \Delta(x)(\varphi_{\uparrow,+}\varphi_{\downarrow,-} + \varphi_{\uparrow,-}\varphi_{\downarrow,+} + \varphi^\dagger_{\downarrow,+}\varphi^\dagger_{\uparrow,-} + \varphi^\dagger_{\downarrow,-}\varphi^\dagger_{\uparrow,+}). \tag{B5}$$

We write this as

$$H^S_{\mathrm{Lin}} = \int dx \Psi^\dagger \mathcal{H}^{\mathcal{S}}{}_{\mathrm{Lin}}(x)\Psi \tag{B6}$$

with

$$\mathcal{H}^S_{\mathrm{Lin}} = \begin{pmatrix} -iv_F\partial_x & 0 & 0 & -\Delta \\ 0 & -iv_F\partial_x & \Delta & 0 \\ 0 & \Delta & iv_F\partial_x & 0 \\ -\Delta & 0 & 0 & iv_F\partial_x \end{pmatrix}, \tag{B7}$$

and the basis

$$\Psi = (\varphi_{\uparrow,+}, \varphi_{\downarrow,+}, \varphi^\dagger_{\uparrow,-}, \varphi^\dagger_{\downarrow,-})^{\mathrm{T}}. \tag{B8}$$

The matrix in equation (B7) looks very much like two separate blocks of the linear p-wave superconductor which seems a bit troublesome since we know that the linear p-wave model host zero modes. That would imply that the linear s-wave model *also* would host zero modes, which would contradict our findings in this paper.

One may suspect that the appearance of two p-wave models is incidental, and that by adding corrections to

the linearization this illusion is shattered. This suspicion is indeed justified since, as we now show, the linear s-wave superconductor in fact is topologically trivial.

The corresponding k-space Hamiltonian is given by

$$H^S_{\rm Lin}(k) = v_F k \tau_z s_0 + \Delta \tau_y s_y \tag{B9}$$

where the Pauli matrices τ_i and s_i now act in right-left space and spin-space respectively. This Hamiltonian also belongs to class BDI. In our basis the particle-hole (now right-left) symmetry operator is given by $\mathcal{C} = \tau_z s_0 K$ and the pseudo time reversal symmetry operator is $\mathcal{T} = \tau_x s_x K$. We rotate the Hamiltonian with the unitary matrix $U = \exp(-i(\pi/4)\tau_x s_x)$, giving us a structure like (B3) but now with $A(k) = iv_F k s_x + i\Delta s_y$. One may then, as above, define $z(k)$ which in this case turns out to be $z(k) = \mathrm{sgn}(v_F^2 k^2 + \Delta^2) = +1$ for all v_F, k and finite Δ. As was the case in Appendix A, k-space is not compact. Regardless of this issue, $z(k)$ can never wind.

Thus we can conclude that both the full and linear s-wave superconductors are trivial, and hence that the zero modes these models exhibit are not topologically protected.

Appendix C: Origin of the term $\epsilon^{\mu\nu}\partial_\nu\theta\xi^\dagger i\partial_\mu\xi$

Starting from the original Lagrangian (19), we present an argument for how the kinetic term $\frac{1}{2\pi}\epsilon^{\mu\nu}\partial_\nu\theta\xi^\dagger i\partial_\mu\xi$ can appear in an effective Lagrangian. Although, as already emphasized in the main text, several of the steps in the below derivations are based on unproven assumptions, the emergence of the kinetic term is far from obvious, and this indicates that a more rigorous proof along these lines might be possible.

The starting point is the partition function,

$$Z[\theta, g] = \int \mathcal{D}[\bar\psi, \psi] e^{i\int d^2x\, \mathcal{L}(\bar\psi,\psi,\theta)}. \tag{C1}$$

The strategy is to change fermionic variables in such a way that the high energy part of the spectrum can still be bosonized and integrated out, as in the previous section, while the the low lying fermion spectrum will be captured by a Lagrangian like (33). To this end, we shall use the following identity,

$$\begin{aligned}
&\int \mathcal{D}[a_\mu]\mathcal{D}[\xi^\dagger,\xi] e^{i\int d^2x \left[a^\mu(\xi^\dagger p_\mu \xi - \bar\psi\gamma_\mu\psi) - \mathcal{H}_\xi\right]} \\
&= \int \mathcal{D}[a_\mu] e^{i\int d^2x\, a^\mu j_\mu + \frac{1}{2}\mathrm{Tr}\ln(H + a^\mu p_\mu)} \\
&= e^{i\mathcal{F}[j_\mu]},
\end{aligned} \tag{C2}$$

where $p_x = -i\partial_x$, $j_\mu = \bar\psi\gamma_\mu\psi$ and $\mathcal{H}_\xi$ is an Hamiltonian that we shall assume to be quadratic in the fields and H is the corresponding operator acting on the Nambu spinors.

To derive the last line in (C2) we first calculate the lowest order by expanding the logarithm and evaluating the trace (which is over both space and Nambu indices). The resulting integrals are not convergent in the ultraviolet since there is no time derivative, so we must introduce a cutoff energy scale Λ. The resulting effective theory is only to be applied below this scale. Note that there is no gauge invariance related to the auxiliary field a since it does not couple to a conserved current. Taking for $\mathcal{H}_\xi$ the expression (35) a straight forward calculation gives $\mathrm{Tr}\ln(H + a^\mu p_\mu) = c_0 a_0^2 + c_1 a_1^2 + \dots$ where we omitted all higher derivative terms. The explicit expressions for the coefficients in terms of δ, M^2 and Λ are not particularly illuminating. Substituting this in the second line of (C2) and integrating over a, we retain the third line with

$$\mathcal{F}[j_\mu] = \tilde c_0\, j_0^2 + \tilde c_1\, j_1^2 + \dots . \tag{C3}$$

Before inserting the identity (C2) in the path integral (C1), we perform the chiral rotation,

$$\psi \to e^{\frac{i}{2}\vartheta(x)\gamma_5}\psi \tag{C4}$$

under which the Lagrangian (19) becomes,

$$\mathcal{L} = \bar\psi\left(i\partial\!\!\!/ - \pi \not{j}_k - g(x)\right)\psi\,. \tag{C5}$$

Putting this together, we get the following representation for the partition function,

$$Z[\theta, g] = \int \mathcal{D}[a_\mu]\mathcal{D}[\xi^\dagger,\xi]\mathcal{D}[\bar\psi,\psi] e^{iS[a,\xi^\dagger,\xi,\bar\psi,\psi;\theta]}\ , \tag{C6}$$

$$\begin{aligned}
S = \int d^2x\, [&\bar\psi\left(i\partial\!\!\!/ - \pi\not{j}_k - \not{a} - m\right)\psi \\
&+ \tilde c_0(\psi\gamma_0\psi)^2 + \tilde c_1(\psi\gamma_1\psi)^2 - a^\mu\xi^\dagger i\partial_\mu\xi - \mathcal{H}_\xi]\ ,
\end{aligned} \tag{C7}$$

where we put $g(x) = m$ to connect to the previous discussion about the kink solutions. Next we make a shift $a^\mu \to a^\mu - \pi j_k^\mu$, to rewrite the action as

$$S = \int d^2x\, [\mathcal{L}_f - a^\mu\xi^\dagger i\partial_\mu\xi + \pi j_k^\mu\, \xi^\dagger i\partial_\mu\xi - \mathcal{H}_\xi]\ , \tag{C8}$$

where

$$\mathcal{L}_f = \bar\psi\left(i\partial\!\!\!/ - \not{a} - m\right)\psi + \tilde c_0(\psi\gamma_0\psi)^2 + \tilde c_1(\psi\gamma_1\psi)^2 \tag{C9}$$

is very similar to the massive Thirring model. The ψ-field can now be integrated to give an effective Lagrangian, for the a_μ field. Using the gauge invariance of (C9) we get

$$\mathcal{L}_{eff}(a) = -\frac{1}{\tilde m^2}F^2 \dots \tag{C10}$$

where $F_{\mu\nu}$ is the field strength for the potential a_μ and $\tilde m$ a dimensional constant that depends both on m and, via the coefficients $\tilde c_0$ and $\tilde c_1$, on δ, M^2 and Λ. Finally, we can integrate the vector field a_μ to get the desired effective action for the ξ-field,

$$\mathcal{L}_{\xi\theta b} = \frac{1}{2}\epsilon^{\mu\nu}\partial_\nu\theta\,(b_\mu + \xi^\dagger i\partial_\mu\xi) - \mathcal{H}_\xi - b_\mu j_k^\mu + \dots \tag{C11}$$

where we also used the constraint (27) to express j_k^μ in terms of θ, and where the dots indicate both neglected higher derivative terms in the quadratic action, and interaction terms resulting from integrating the a_μ field. All the steps glossed over above can be performed, at least to low order in perturbation theory. The main question is however not technical, but rather what principle should be used to determine $\mathcal{H}_\xi$. A possible approach is to choose the parameters in $\mathcal{H}_\xi$ so to minimize the size of the leading corrections due to higher derivative terms and induced interactions.

[1] A. Kitaev, Physics-Uspekhi **44**, 131 (2001).
[2] A. P. Schnyder, S. Ryu, A. Furusaki, and A. W. W. Ludwig, Phys. Rev. B **78**, 195125 (2008).
[3] A. Kitaev, AIP Conference Proceedings **1134**, 22 (2009).
[4] S. Ryu, A. P. Schnyder, A. Furusaki, and A. W. W. Ludwig, New Journal of Physics **12**, 065010 (2010).
[5] A. Altland and M. R. Zirnbauer, Phys. Rev. B **55**, 1142 (1997).
[6] R. M. Lutchyn, J. D. Sau, and S. Das Sarma, Phys. Rev. Lett. **105**, 077001 (2010).
[7] Y. Oreg, G. Refael, and F. von Oppen, Phys. Rev. Lett. **105**, 177002 (2010).
[8] T.-P. Choy, J. M. Edge, A. R. Akhmerov, and C. W. J. Beenakker, Phys. Rev. B **84**, 195442 (2011).
[9] S. Nadj-Perge, I. K. Drozdov, B. A. Bernevig, and A. Yazdani, Phys. Rev. B **88**, 020407 (2013).
[10] F. Pientka, L. I. Glazman, and F. von Oppen, Phys. Rev. B **89**, 180505 (2014).
[11] S. Nadj-Perge, I. K. Drozdov, J. Li, H. Chen, S. Jeon, J. Seo, A. H. MacDonald, B. A. Bernevig, and A. Yazdani, Science **346**, 602 (2014).
[12] V. Mourik, K. Zuo, S. M. Frolov, S. R. Plissard, E. P. A. M. Bakkers, and L. P. Kouwenhoven, Science **336**, 1003 (2012).
[13] M. T. Deng, C. L. Yu, G. Y. Huang, M. Larsson, P. Caroff, and H. Q. Xu, Nano Lett. **12**, 6414 (2012).
[14] A. Das, Y. Ronen, Y. Most, Y. Oreg, M. Heiblum, and H. Shtrikman, Nature Physics **8**, 887 (2012).
[15] D. Bagrets and A. Altland, Phys. Rev. Lett. **109**, 227005 (2012).
[16] J. Liu, A. C. Potter, K. T. Law, and P. A. Lee, Phys. Rev. Lett. **109**, 267002 (2012).
[17] T. Ojanen, Phys. Rev. B **87**, 100506 (2013).
[18] P. Lucignano, F. Tafuri, and A. Tagliacozzo, Phys. Rev. B **88**, 184512 (2013).
[19] R. Wakatsuki, M. Ezawa, Y. Tanaka, and N. Nagaosa, Phys. Rev. B **90**, 014505 (2014).
[20] L. Fu and C. L. Kane, Phys. Rev. B **79**, 161408 (2009).
[21] S. Ryu and Y. Hatsugai, Phys. Rev. Lett. **89**, 077002 (2002).
[22] S. Tewari and J. D. Sau, Phys. Rev. Lett. **109**, 150408 (2012).
[23] W. Su, J. Schrieffer, and A. Heeger, Phys. Rev. Lett. **42**, 1698 (1979).
[24] H. Takayama, Y. Lin-Liu, and K. Maki, Phys. Rev. B **21**, 2388 (1980).
[25] X.-G. Wen, Advances in Physics **44**, 405 (1995).
[26] T. Hansson, V. Oganesyan, and S. Sondhi, Annals of Physics **313**, 497 (2004).
[27] G. Y. Cho and J. E. Moore, Annals of Physics **326**, 1515 (2011).
[28] A. Chan, T. L. Hughes, S. Ryu, and E. Fradkin, Physical Review B **87**, 085132 (2013).
[29] J. Goldstone and F. Wilczek, Physical Review Letters **47**, 986 (1981).
[30] C. L. M. Wong and K. T. Law, Phys. Rev. B **86**, 184516 (2012).
[31] S. Nakosai, J. C. Budich, Y. Tanaka, B. Trauzettel, and N. Nagaosa, Phys. Rev. Lett. **110**, 117002 (2013).
[32] E. Fradkin, C. Nayak, A. Tsvelik, and F. Wilczek, Nuclear Physics B **516**, 704 (1998).
[33] T. H. Hansson, A. Karlhede, and M. Sato, New Journal of Physics **14**, 063017 (2012).
[34] M. Stone and F. Gaitan, Annals of Physics **178**, 89 (1987).
[35] E. Fradkin, *Field theories of condensed matter physics; 2nd ed.* (Cambridge Univ. Press, Cambridge, 2013).
[36] R. Jackiw and C. Rebbi, Phys. Rev. D **13**, 3398 (1976).
[37] T. H. Hansson, T. Kvorning, V. P. Nair, and G. J. Sreejith, Phys. Rev. B **91**, 075116 (2015).